

MSURJ

MCGILL SCIENCE UNDERGRADUATE RESEARCH JOURNAL

VOLUME 18 | ISSUE 1 | MARCH 2023



ON THE COVER

Volcanoes connect the depths of planet Earth with the “supra-crustal” world in which we live. They spew gases and particulate matter into the atmosphere, build new islands, and reset ecological succession. Near and beneath water, volcanic eruptions may result in the formation of pumice rafts which float in the aqueous environment by or in which they were made. On page B19, Redick reviews existing knowledge and case studies on the formation of pumice rafts as well as their geological and biological implications. Pumice rafts are carriers of life and proof of a dynamic and powerful Earth that both facilitates and impedes human activities.

The digital painting on the cover depicts a stylized life of a pumice raft, beginning with the volcanic eruption, to being quenched by water, to carrying an array of organisms as it drifts.

Graphic Designer: David Derish

BOARD 2022-2023

Editors-in-Chief

John Ni
Biochemistry
Sofia Reynoso
Biology

Managing Editors

Aelis Spiller
Earth Systems Science
Ryan Huang
Neuroscience
Shafaq Nami
Bioengineering
Tiffany Spector
Pharmacology
Laura Reumont
Computer Science
Autumn Pereira
Biology and Mathematics

Senior Editors

David Derish
Medicine
Mina Mahdi
Cognitive Science
Muhammad Shahzad
Microbiology and Immunology
Ines Durant
Physiology
Javeria Rizwan
Physics

Editors

Anita Allikmets
*Natural Sciences, University
College London*
Armance Volta
Physics
Benjamin Herfray
Mechanical Engineering
Mackenzie Pereira
Physics
Megan Katz
Biochemistry
Patrick Hallaert
Biology
Xinchen Wang
Finance and Mathematics

Layout Designers

David Derish
Shafaq Nami
Sofia Reynoso
Aelis Spiller
Armance Volta
Benjamin Herfray
Mackenzie Pereira
John Ni

805 Sherbrooke St. West, Room 1B22
Montreal, Quebec, H3A 2K6 Canada
Phone: (514) 398-6979
Fax: (514) 398-6766
Email: msurj.sus@mail.mcgill.ca
Website: msurjonline.mcgill.ca

TABLE OF CONTENTS

vii Foreword

ix Acknowledgements

A. RESEARCH ARTICLES

1 Description and Exploration of Mean-Gauss Surfaces
Alexander Nazeer

11 Rho GTPase Regulatory Proteins Contribute to Podocyte Morphology and Function
Emily Foxman, Sajida Ibrahim, Tomoko Takano

18 Comparison of Small Molecule-Responsive RNA Aptazymes for Applications in Gene Control
Janeva Shahi & Maureen McKeague

B. REVIEW ARTICLES

1 Uncovering the Regulators of CRISPR-Cas Immunity
Idia Boncheva

6 The Role of Iron in Epidermal Healing and Infection
Idia Boncheva

10 At Once Friends and Foes: Myeloid-Derived Suppressor Cells in Human Tuberculosis
Angela Nelson

15 Bacterial Interactions Affecting Chemotherapy Effectiveness
Jenni M. Chambers & Thomas A. Ilingworth

19 A Review of Pumice Raft Formation Environments, Saturation, and Dispersal Mechanisms
Nathalie R. Redick

26 An Enduring Controversial Story in the Human Brain: Adult Hippocampal Neurogenesis in the Dentate Gyrus
Zhipeng Niu & Tanya Capolicchio

FOREWORD

Dear Reader,

As we near two decades of publication, we continue to be amazed by the hard work and impressive findings of our undergraduate peers. We are proud of our continued mission to advocate for undergraduate research and publishing embodied by the work of authors, editors, and peer reviewers.

Among the articles enclosed is a review on CRISPR-Cas, a technology developed in part by Nobel Laureate in Chemistry Jennifer Doudna. Doudna emphasises the importance of early exposure to research in a scientific career, as it fosters “natural curiosity.” The authors included in this issue exemplify this “natural curiosity” so vital to scientific inquiry and progress.

We would like to present the 18th volume of the *McGill Science Undergraduate Research Journal*, which includes nine research and review articles, a culmination of these students’ hard work and perseverance. Within these articles, topics range from pumice rafts to tuberculosis to mean-Gauss surfaces. We hope that the passion and effort displayed by these authors remain evident throughout this issue.

On behalf of our entire editorial board, thank you.

John Ni & Sofia Reynoso
Editors-in-Chief

ACKNOWLEDGEMENTS

The McGill Science Undergraduate Research Journal would like to thank its generous contributors without whom this journal would not have been possible.

We thank the librarians of McGill University for their guidance. We thank the Office for Science Education for their continued support of both undergraduate research at McGill and the MSURJ. Furthermore, we thank our advisors Dr. Armin Yazdani, Michael Shamash, and Dr. Véronique Brulée for their continued support.

We thank all our financial supporters in the McGill community for their generous support:

Faculty of Medicine and Health Sciences
Centre de recherche en biologie structurale
Faculty of Science
Department of Pharmacology and Therapeutics
Department of Mathematics and Statistics
Science Undergraduate Society of McGill University

Finally, we thank the peer reviewers, including Dr. Kostas Pantopoulos, Dr. Pradipta Banerjee, Dr. Antonio Inserra, Dr. Michael Manga, Dr. Owen McCarty, Deepak Saini, Brenda Lynn Koborsy, Mohammad Reza Naghdi, and the anonymous peer-reviewers. Their careful revision of the articles is critical to the success of the 18th issue of the *MSURJ*.

Description and Exploration of Mean-Gauss Surfaces

Research Article

¹Department of Mathematics and Statistics, Concordia University, Montreal, QC, Canada

Keywords

Curvature, Gaussian, differential geometry, surfaces, equivalence relation

Email Correspondence

a.naazee@hrc.concordia.ca

<https://doi.org/10.26443/msurj.v18i1.192>

©The Author. This article is published under a CC-BY license: <https://creativecommons.org/licenses/by/4.0/>

Abstract

In this paper we explore solving the prescribed mean curvature equation for surfaces meeting a new relation given by $H_S = \lambda K_S$, where H_S and K_S are the mean and Gaussian curvatures, respectively. We prove several existence theorems for various families of surfaces and state a conjecture for surfaces of revolution. To conclude, we state a weak existence theorem, and a strong conjecture concerning possible solutions. The intention is that by using differential geometry tools which would have likely been seen at the undergraduate level, the paper and its results are more accessible. My hope is that these new theorems find applications in the classification of surfaces in the future, or at the very least serves as an interesting curiosity.

Introduction

We will be exploring the existence of surfaces for which a proportionality relationship between the mean and Gaussian curvatures exist. More specifically those for which the following holds:

$$H_S = \lambda K_S \quad (1)$$

where S is a smooth surface, H_S the mean curvature of S , K_S the Gaussian curvature, and λ a scalar. It would seem that solutions to this problem have not yet been researched, and as such, I will assign the name of Mean-Gauss surfaces to them.

To begin, we define the two curvatures and give explicit formulas for their computations. Then we proceed to show that there exists at least one Mean-Gauss surface (the sphere). Following which, we will work toward proving several results concerning the existence of other such surfaces, yielding several new theorems and conjectures.

The main body of exploration will be dealing with surfaces in \mathbb{R}^3 as these will allow for visualizations. Furthermore, since this problem does not seem to have been explored, beginning with the “simplest” case is likely a good place to start.

Throughout the paper, we assume only a surface level knowledge of differential geometry in the hopes that this work provides insights and inspiration to those not so far along their mathematical journey. Another thing to note is that this paper is an excerpt of a larger work that was submitted as my honours research project under the supervision of Dr. A. Stancu of Concordia University.

Mean-Gauss Surfaces

The prescribed mean curvature equation is given by:

$$\operatorname{div} \left(\frac{\nabla u}{\sqrt{1 + \|\nabla u\|^2}} \right) + f(u) = 0$$

where ∇ represents the gradient, and $u(x)$ is a function defining a surface. Furthermore, we have that:

$$\operatorname{div} \left(\frac{\nabla u}{\sqrt{1 + \|\nabla u\|^2}} \right)$$

is a scaled version of the mean curvature of an n dimensional manifold embedded in \mathbb{R}^{n+1} defined as the graph $S = (x_1, x_2, \dots, x_n, u(x_1, x_2, \dots, x_n))$, hence its namesake. The proof of this fact is quite mechanical, but every part falls into place in a most satisfying manner; as such, I encourage the reader to attempt it. The inclusion of the divergence form here serves only to give an idea of what problem led me to investigating relationship (1), and will not be used past this section.

Possible solutions to the divergence equation is a topic with a large body of research behind it. Generally these take a differential equation approach, applying known techniques to find possible solutions, or prove the existence of solutions of specific forms.

For this paper, we will investigate whether there exist solutions when $f(u)$ is the Gaussian curvature of our surface or some scaled version of it. More specifically, we remove the requirement that our surface writes as a graph, and consider the more general relation $H_S = \lambda K_S$ instead.

Definition 1. Define a Mean-Gauss surface to be a smooth surface S such that globally,

$$H_S = \lambda K_S,$$

where K_S is the Gaussian curvature, H_S is the mean curvature, and $\lambda \in \mathbb{R}$. □

As for the question of why restrict λ to scalar values, we can consider the following:

Let S be a surface defined by $(x(u, v), y(u, v), z(u, v))$; then for $\lambda(u, v)$

we want

$$H_S = \lambda(u, v)K_S,$$

but if we allow λ to be a function, then we can simply choose

$$\lambda = \frac{H_S}{K_S}$$

which is a solution for all surfaces having $K_S \neq 0$ for any u, v in its domain. As such, this question does not require much investigating.

Even if $K_S = 0$ at some set of points $\{p_i\} \in S$, the relation still holds everywhere else on the surface. Furthermore, we have local satisfaction everywhere but on neighborhoods of the surface which are developable.

That being said, it would be interesting to ask for $\lambda(u, v)$ satisfying (1) and such that

$$T(\lambda(u, v)) \neq \frac{H_S}{K_S}$$

for any elementary or "simple" transformation T . This is a question not covered here, but which could prove to be an interesting avenue of future research.

Defining the Curvatures

We begin by giving a relation between the Weingarten map and the fundamental forms, from which we will define the curvatures to be used in the following sections. Going forward, we are dealing with surfaces embedded in \mathbb{R}^3 unless stated otherwise.

Weingarten Map

For a surface S embedded in \mathbb{R}^3 we define the Weingarten map as

$$\mathcal{W}_{p,S} = (I)^{-1}(II)$$

where I is the matrix of the first fundamental form and II that of the second.

$$I = \begin{pmatrix} E & F \\ F & G \end{pmatrix},$$

$$II = \begin{pmatrix} L & M \\ M & N \end{pmatrix}.$$

Principal Curvatures

We define the principal curvatures of a surface S at a point $p \in S$ to be the minimum and maximum of the normal curvatures of all curves passing through p . They can be found using the following:

For principal curvatures k_1, k_2 of S at p , and tangent vectors $t_1, t_2 \in T_p S$ corresponding to the principal curvatures we have

$$\mathcal{W}_p(t_i) = k_i t_i.$$

In other words, the principal curvatures are the eigenvalues of the Weingarten map. Furthermore, we call the eigenvectors t_1, t_2 the principal directions of S at p . \square

Gaussian Curvature

We can compute the Gaussian curvature K in several ways, one of which is

$$K = k_1 k_2.$$

Another one that is useful for computation is

$$K = \text{Det}(\mathcal{W}_{p,S}),$$

or equivalently

$$K = \frac{\text{Det}(II)}{\text{Det}(I)}.$$

Mean Curvature

Similar to the Gaussian curvature we can find the mean curvature in several ways:

$$H = \frac{k_1 + k_2}{2},$$

another one being

$$H = \frac{1}{2} \text{Trace}(\mathcal{W}_{p,S}),$$

or equivalently

$$H = \frac{LG - 2MF + NE}{2\text{Det}(I)}.$$

Higher Dimensional

If S is a manifold embedded in \mathbb{R}^{n+1} , then the Weingarten map is an n dimensional square matrix, and we can use the following definitions:

$$K = \prod_{i=1}^n k_i,$$

$$H = \frac{1}{n} \sum_{i=1}^n k_i. \quad \square$$

\square Weingarten Surfaces

Mean-Gauss surfaces as defined by (1) are a particular case of Weingarten Surfaces. A class of surfaces whose mean and Gaussian curvatures are connected by a function f in the sense that¹

$$f(H, K) = 0. \quad (2)$$

For Mean-Gauss surfaces we have:

$$\frac{k_1 + k_2}{2} = \lambda' k_1 k_2,$$

$$k_1 = \lambda k_1 k_2 - k_2,$$

$$k_1 - \lambda k_1 k_2 = -k_2,$$

$$k_1(1 - \lambda k_2) = -k_2,$$

$$k_1 = \frac{-k_2}{(1 - \lambda k_2)},$$

$$k_1 = \frac{k_2}{k_2 \lambda - 1}.$$

So we define f to be

$$f(H, K) = W(k_1, k_2) = k_1 - \frac{k_2}{k_2\lambda - 1}. \quad (3)$$

The set of solutions to (2) are called the curvature diagram, or W-diagram of a surface.

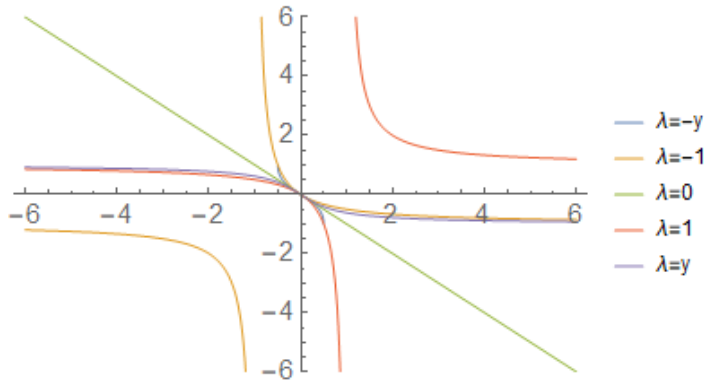


Figure 1. W-diagram of $[x - \frac{y}{\lambda-1}]$ (2) for various λ .

We have Theorem 1 giving relations concerning said diagrams:

Theorem 1 (Interpretation of Principal Curvatures¹). *If the curvature diagram of a surface S*

- i) *degenerates to exactly one point, then S has two constant principal curvatures and is part of a plane, sphere, or circular cylinder.*
- ii) *is contained in one of the coordinate axes through the origin, then S is developable.*
- iii) *is contained in the main diagonal $k_1 = k_2$, then the surface S is part of a plane or sphere, as every point is umbilic.*

We also have the following bi-directional statements:

- i) *The curvature diagram is contained in a straight line parallel to the diagonal $k_1 = -k_2$ if and only if the mean curvature is constant.*
- ii) *The curvature diagram is contained in a standard hyperbola $k_1 = \frac{c}{k_2}$ for $c \in \mathbb{R}$ if and only if the Gaussian curvature is constant. \square*

Spheres and Hyperspheres

One family of surfaces for which the Mean-Gauss relation is satisfied are spheres and hyperspheres.

Consider the sphere $S = \{(x, y, z) | x^2 + y^2 + z^2 = \rho^2\}$, which has the parametric equation

$$S(\rho, \theta, \phi) = (\rho \cos \theta \sin \phi, \rho \sin \theta \sin \phi, \rho \cos \phi)$$

where $\theta \in [0, 2\pi]$ is the azimuthal angle (longitude), $\phi \in [0, \pi]$ is the polar angle (co-latitude), and ρ the radius of S .

Then S has the following Gaussian and mean curvatures.

$$K = \frac{1}{\rho^2},$$

$$H = \frac{1}{\rho}.$$

An important remark is that both quantities are constant based on the radius of our sphere.

Now, by the above we see that the unit sphere satisfies the condition with $\lambda = 1$, and for $\lambda \neq 1$ we have

$$H_S = \lambda K_S,$$

$$\frac{1}{\rho} = \lambda \frac{1}{\rho^2},$$

$$\lambda = \rho.$$

For hyperspheres of radius ρ , we take a different approach by using the Gauss and Weingarten map.

Recall that the Gauss map $\mathcal{G} : S \rightarrow \mathbb{S}^n$, takes our surface to the unit ball for \mathbb{R}^n . But here our surface is already a sphere, so we simply scale it.

Note that we are taking the geometer's approach; using n to denote the dimension of the sphere.

So if $S = \{x \in \mathbb{R}^{n+1} | \sum_{i=1}^{n+1} x_i^2 = \rho^2\}$ is a sphere of radius ρ embedded in \mathbb{R}^{n+1} , then for $x \in S$, the unit normals and by extension the Gauss map will be

$$\mathcal{G}(S) = -\left(\frac{S}{\rho}\right)$$

which maps every $x \in S$ to $-\frac{x}{\rho}$, giving us that for every $x \in S$ we have

$$\sum_{i=1}^{n+1} \left(-\frac{x_i}{\rho}\right)^2 = \frac{1}{\rho^2} \sum_{i=1}^{n+1} x_i^2$$

$$= \frac{1}{\rho^2} \rho^2$$

$$= 1,$$

which describes the unit sphere \mathbb{S}^n . Remark that we chose the negative normal direction; the reasoning becomes apparent in the next step.

Now,

$$\mathcal{W} = -D\mathcal{G},$$

the negative of the Jacobian of the Gauss map, which is given by

$$\mathcal{W} = \left(\frac{1}{\rho}\right)\mathcal{I}$$

where \mathcal{I} is the identity matrix for \mathbb{R}^n , since $D : T_p\mathbb{S}^n \rightarrow T_p\mathbb{S}^n$.

The curvatures are then given by the trace of \mathcal{W} over n and its determinant for the other.

$$H_S = \frac{1}{n} \text{Trace}(\mathcal{W}) = \frac{1}{\rho}$$

$$K_S = \text{Det}(\mathcal{W}) = \frac{1}{\rho^n}$$

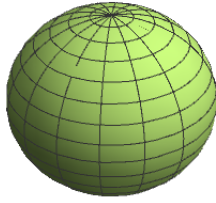
We see that the Mean-Gauss relation is satisfied for $\lambda = \rho^{n-1}$.

Thus, we have proven Theorem 2 as follows:

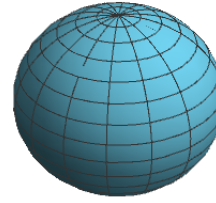
Theorem 2 (n -Sphere). *For any n -sphere S of radius ρ , the Mean-Gauss relation*

$$H_S = \lambda K_S$$

is satisfied by $\lambda = \rho^{n-1}$. \blacksquare



(a) Gaussian Curvature



(b) Mean Curvature

Figure 2. Sphere coloured according to curvature.

If we compare this result with the standard case of $n = 2$, we can see that it is consistent.

$$E = \|(1, 0, f_x)\|^2 = 1 + f_x^2 \quad F = (1, 0, f_x)(0, 1, f_y) = f_x f_y \quad G = \|(0, 1, f_y)\|^2 = 1 + f_y^2$$

And we have a unit normal to S ,

$$\begin{aligned} \vec{n} &= \frac{(1, 0, f_x) \times (0, 1, f_y)}{\|(1, 0, f_x) \times (0, 1, f_y)\|} \\ &= \frac{(-f_x, -f_y, 1)}{\sqrt{1 + f_x^2 + f_y^2}} \\ &= \frac{(-f_x, -f_y, 1)}{d}, \end{aligned}$$

where $d = \sqrt{1 + f_x^2 + f_y^2}$. Now, the coefficients of the second fundamental form are

$$\begin{aligned} L &= (0, 0, f_{xx}) \cdot \vec{n} = \frac{f_{xx}}{d}, & M &= (0, 0, f_{xy}) \cdot \vec{n} = \frac{f_{xy}}{d}, & N &= (0, 0, f_{yy}) \cdot \vec{n} = \frac{f_{yy}}{d}. \end{aligned}$$

Using the definition of the Weingarten map

$$\mathcal{W}_{p,S} = (I)^{-1}(II),$$

we have

$$\mathcal{W}_{p,S} = \frac{1}{EG - F^2} \begin{pmatrix} GL - FM & GM - FN \\ ME - FL & NE - FM \end{pmatrix},$$

yielding the curvatures

$$H_S = \frac{1}{2} \frac{GL - 2FM + NE}{EG - F^2}$$

Trivial Cases

It should be mentioned that there are trivial cases of this problem. First, if the surface S is a plane which has 0 Gaussian and mean curvature, then $H = \lambda K$ is trivially satisfied.

Another case which can be considered trivial or rather one we can immediately rule out is that of non-planar developable surfaces. In this case, one of the principal curvatures will be 0, giving

$$H = \lambda(0)$$

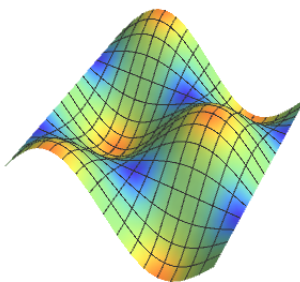
which lacks a solution for λ in the non-extended reals.

The last trivial case to be considered is that of minimal surfaces with $H_S = 0$ satisfied by $\lambda = 0$. Therefore, we restrict $\lambda \in \mathbb{R} \setminus \{0\}$.

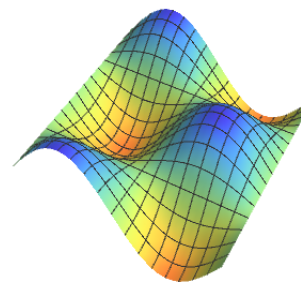
Graphs of Functions

Let $S \subset \mathbb{R}^3$ be a graph; that is, $S = \{(x, y, z) \in \mathbb{R}^3 | f(x, y) = z\}$ for some function f which is continuous and well defined.

Then, the coefficients of the first fundamental form of S are given by



(a) Gaussian Curvature



(b) Mean Curvature

Figure 3. Graph of $f(x, y) = \sin(x) \cos(y)$ coloured according to curvature.

$$\begin{aligned}
&= \frac{1}{2} \frac{(1+f_y^2)(f_{xx})}{d} - 2 \frac{f_x f_y f_{xy}}{d} + \frac{(1+f_x^2)(f_{yy})}{d} \\
&= \frac{1}{2d} \frac{(1+f_y^2)(f_{xx}) - 2f_x f_y f_{xy} + (1+f_x^2)(f_{yy})}{1+f_x^2+f_y^2} \\
&= \frac{1}{2d^3} [(1+f_y^2)(f_{xx}) - 2f_x f_y f_{xy} + (1+f_x^2)(f_{yy})],
\end{aligned}$$

and

$$\begin{aligned}
K_S &= \frac{LN - M^2}{EG - F^2} \\
&= \frac{\frac{f_{xx}f_{yy}}{d^2} - \frac{f_{xy}^2}{d^2}}{d^2} \\
&= \frac{f_{xx}f_{yy} - f_{xy}^2}{d^4}.
\end{aligned}$$

Now we want to meet the relation $H_S = \lambda K_S$ for λ a non-zero constant. As such, we can leave out the $\frac{1}{2}$ scalar from the mean curvature, giving us

$$\begin{aligned}
\frac{1}{d^3} [(1+f_y^2)(f_{xx}) - 2f_x f_y f_{xy} + (1+f_x^2)(f_{yy})] &= \lambda \frac{f_{xx}f_{yy} - f_{xy}^2}{d^4}, \\
d[(1+f_y^2)(f_{xx}) - 2f_x f_y f_{xy} + (1+f_x^2)(f_{yy})] &= \lambda [f_{xx}f_{yy} - f_{xy}^2]
\end{aligned}$$

Immediately, we note a trivial solution to this equation which we covered in the *Trivial Cases* section: flat surfaces where the second order partials are 0, giving $0 = 0$.

So assume $f_{xx}f_{yy} - f_{xy}^2 \neq 0$ which rules out said trivial case, giving

$$d \frac{[(1+f_y^2)(f_{xx}) + (1+f_x^2)(f_{yy})]}{[f_{xx}f_{yy} - f_{xy}^2]} = \lambda.$$

Then for λ to be a constant, either both d and $\frac{[(1+f_y^2)(f_{xx}) + (1+f_x^2)(f_{yy})]}{[f_{xx}f_{yy} - f_{xy}^2]}$ are constants, or they are reciprocals of each other as functions.

Case I: Let d be a constant; that is, $\sqrt{1+f_x^2+f_y^2} = c$ for some $c \in \mathbb{R}$. Then clearly, f_x^2 and f_y^2 must be constants or $f_x^2 + f_y^2 = \hat{c}$, a constant.

If both are constant, then f is a plane which is the trivial case and not being considered here.

If not both constant, then $f_x^2 + f_y^2 = \hat{c}$, for some $\hat{c} \in \mathbb{R}$. Then f can be of the forms

$$f_- = c_1 + yc_2 - x\sqrt{\hat{c} - c_2^2}$$

and

$$f_+ = c_1 + yc_2 + x\sqrt{\hat{c} - c_2^2}$$

for constant c_1 and c_2 . But then $f_{xx} = f_{yy} = f_{xy} = 0 \Rightarrow$ we have a contradiction to $f_{xx}f_{yy} - f_{xy}^2 \neq 0$. Note that this is equivalent to the second fundamental form being a 0 matrix.

Therefore, d is not a constant, and we are in the case that they are reciprocals of each other.

Case II: We have

$$\begin{aligned}
\frac{[(1+f_y^2)(f_{xx}) + (1+f_x^2)(f_{yy})]}{[f_{xx}f_{yy} - f_{xy}^2]} &= \frac{\lambda}{d}, \\
\frac{GdL + EdN}{dLdN - d^2M^2} &= \frac{\lambda}{d},
\end{aligned}$$

$$\begin{aligned}
\frac{d}{d^2} \frac{GL + EN}{LN - M^2} &= \frac{\lambda}{d}, \\
\frac{1}{d} \frac{GL + EN}{LN - M^2} &= \frac{\lambda}{d}, \\
\frac{GL + EN}{LN - M^2} &= \lambda.
\end{aligned}$$

To continue, we will need a few definitions and propositions:

Definition 2 (Umbilical Points^{2 (p178)}). We say that a point p is umbilical if

$$k_1(p) = k_2(p)$$

for principal curvatures k_1, k_2 . \square

Proposition 1 (Spheres are totally umbilic). Every point p on a sphere S is umbilic.

The proof of which is immediate from a calculation which yields $k_{1,2} = \frac{1}{\rho}$ where ρ is the radius of the sphere. Furthermore, spheres are the only totally umbilic surfaces with non-zero curvatures. \square

Proposition 2 (Diagonal Fundamental Forms^{2 (p201)}). Let p be a point of a surface S , and suppose that p is not an umbilic. Then, there is a surface patch $\sigma(u, v)$ of S containing p whose first and second fundamental forms are

$$Edu^2 + Gdv^2 \quad \text{and} \quad Ldu^2 + Ndv^2,$$

respectively, for some smooth functions E, G, L, N . \square

Now assume that S is not totally umbilic; then, there exists a point p of S for which locally the equation in case II becomes

$$\frac{GL + EN}{LN} = \frac{G}{N} + \frac{E}{L} = \lambda. \quad (4)$$

Furthermore, by the same proposition we have that

$$\begin{aligned}
F &= 0, \\
f_x f_y &= 0
\end{aligned}$$

which implies either $f_x = 0$ or $f_y = 0$ in a neighborhood of p . Without loss of generality, let $f_y = 0$, then $N = \frac{f_{yy}}{d} = 0$, and from (4),

$$\frac{G}{N} + \frac{E}{L} = \frac{1}{0} + \frac{E}{L}$$

is undefined.

Therefore, for S satisfying the mean Gauss relation there are no such points p , and we have that S is totally umbilic. Since the sphere is the only surface with non-zero curvatures and which is totally umbilic, we have that S must be part of a sphere.

Thus we have proven the following Theorem 3:

Theorem 3 (Mean-Gauss Graphs). Let $S = \{(x, y, z) \in \mathbb{R}^3 | z = f(x, y)\}$, for a function f which is smooth and well defined, be the graph of a function such that $H_S = \lambda K_S$ for $\lambda \in \mathbb{R} \setminus \{0\}$ and such that $f_{xx}f_{yy} - f_{xy}^2 \neq 0$. Then, S is a part of or a whole sphere.

We note that for S to be the graph of a function and a whole sphere, we will require more than one chart. \blacksquare

Surfaces of Revolution

Let $C = (x(s), y(s))$ be a regular smooth curve parameterized by arc length, which generates a surface of revolution S in the following way:

$$S = \{(x(s), y(s) \cos(t), y(s) \sin(t))\}.$$

We call C the profile curve of S . For brevity going forward, we will omit s when writing such that $S = \{(x, y \cos(t), y \sin(t))\}$.

We have first order partial derivatives

$$S_s = (x', y' \cos(t), y' \sin(t)), \quad S_t = (0, -y \sin(t), y \cos(t)),$$

and second

$$S_{ss} = (x'', y'' \cos(t), y'' \sin(t)), \quad S_{tt} = (0, -y \cos(t), -y \sin(t)), \\ S_{st} = (0, -y' \sin(t), y' \cos(t)).$$

Then the first fundamental form of S has the components

$$E = \|S_s\|^2 = x'^2 + y'^2 \cos^2(t) + y'^2 \sin^2(t) = x'^2 + y'^2(\cos^2(t) + \sin^2(t)) = x'^2 + y'^2 \\ = \|C\|^2 = 1, \\ F = -y' y \sin(t) \cos(t) + y y' \sin(t) \cos(t) = 0,$$

In matrix form,

$$\mathcal{I} = \begin{pmatrix} 1 & 0 \\ 0 & y^2 \end{pmatrix}.$$

In order to compute the second fundamental form, we start with the unit normal:

$$\vec{n} = \frac{S_s \times S_t}{\|S_s \times S_t\|} \\ = \frac{\begin{bmatrix} x' & y' \cos(t) & y' \sin(t) \\ 0 & -y \sin(t) & y \cos(t) \end{bmatrix}}{d} \\ = \frac{[(y' y \cos^2(t) + y' y \sin^2(t)), -(x' y \cos(t)), -(x' y \sin(t))]}{d} \\ = \frac{[y' y, -x' y \cos(t), -x' y \sin(t)]}{[y'^2 y^2 + x'^2 y^2 \cos^2(t) + x'^2 y^2 \sin^2(t)]^{\frac{1}{2}}} \\ = \frac{[y' y, -x' y \cos(t), -x' y \sin(t)]}{y[y'^2 + x'^2(\cos^2(t) + \sin^2(t))]^{\frac{1}{2}}} \\ = \frac{[y' y, -x' y \cos(t), -x' y \sin(t)]}{y} \\ = (y', -x' \cos(t), -x' \sin(t)).$$

Now the components of the second fundamental form are:

$$L = S_{ss} \cdot \vec{n} \\ = (x'', y'' \cos(t), y'' \sin(t))(y', -x' \cos(t), -x' \sin(t)) \\ = x'' y' - y'' x' \cos^2(t) - y'' x' \sin^2(t) \\ = x'' y' - y'' x',$$

$$M = S_{st} \cdot \vec{n} \\ = (0, -y' \sin(t), y' \cos(t))(y', -x' \cos(t), -x' \sin(t)) \\ = x' y' \sin(t) \cos(t) - x' y' \sin(t) \cos(t) \\ = 0, \\ N = S_{tt} \cdot \vec{n} \\ = (0, -y \cos(t), -y \sin(t))(y', -x' \cos(t), -x' \sin(t)) \\ = y x' \cos^2(t) + y x' \sin^2(t) \\ = y x',$$

giving the matrix form

$$\mathcal{II} = \begin{pmatrix} x'' y' - y'' x' & 0 \\ 0 & y x' \end{pmatrix},$$

with mean and Gaussian curvature

$$H_S = \frac{1}{2} \frac{GL - 2FM + NE}{EG - F^2} \\ = \frac{1}{2} \frac{y^2(x'' y' - y'' x') + y x'}{y^2} \\ = \frac{1}{2} \frac{y(x'' y' - y'' x') + x'}{y}, \\ K_S = \frac{LN - M^2}{EG - F^2} \\ = \frac{(x'' y' - y'' x') y x'}{y^2} \\ = \frac{(x'' y' - y'' x') x'}{y}.$$

Now putting it in the form of the relation (1), we get:

$$H_S = \lambda' K_S, \\ \frac{y(x'' y' - y'' x') + x'}{y} = \lambda' \frac{(x'' y' - y'' x') x'}{y}, \\ y(x'' y' - y'' x') + x' = \lambda'(x'' y' - y'' x') x', \\ y(x'' y' - y'' x') + x' - \lambda'(x'' y' - y'' x') x' = 0, \\ (x'' y' - y'' x')(y - \lambda x') + x' = 0.$$

Case I: $(x'' y' - y'' x') = 0$

Then $x' = 0 \Rightarrow x = c$, for some constant c , and either S degenerates to a single point or is a yz -plane passing through $x = c$.

Case II: $(y - \lambda x') = 0$

Then $x' = 0 \Rightarrow y = 0$ and S is given by $S = \{(c, 0, 0)\}$ a single point.

Case III: $(x'' y' - y'' x')(y - \lambda x') = -x'$

For case III, we take a different approach. Let $(x'' y' - y'' x')$, $(y - \lambda x')$, and x' be non-zero and recall we parameterized C by arc length, so we have $x'^2 + y'^2 = 1$ giving several relations. For the moment we are interested in

$$x'^2 + y'^2 = 1 \Rightarrow 2x' x'' + 2y' y'' = 0, \\ x'' = \frac{-y' y''}{x'}.$$

Then from above, we recalculate the mean and Gaussian curvatures

$$\begin{aligned}
H_S &= \frac{1}{2} \frac{y(x''y' - y''x') + x'}{y} \\
&= \frac{1}{2} \frac{y([\frac{-y'y''}{x'}]y' - y''x') + x'}{y} \\
&= \frac{1}{2} \left(\frac{-y'^2y'' - y''x'^2}{x'} + \frac{x'}{y} \right) \\
&= \frac{1}{2} \left(\frac{-y''}{x'}(y'^2 + x'^2) - \frac{x'}{y} \right) \\
&= \frac{1}{2} \left(\frac{x'}{y} - \frac{y''}{x'} \right), \\
K_S &= \frac{(x''y' - y''x')x'}{y} \\
&= \frac{x'([\frac{-y'y''}{x'}]y' - y''x')}{y} \\
&= \frac{-y'^2y'' - y''x'^2}{y} \\
&= \frac{-y''(y'^2 + x'^2)}{y} \\
&= \frac{-y''}{y},
\end{aligned}$$

giving the new relation

$$\begin{aligned}
H &= \hat{\lambda}K, \\
\frac{1}{2} \left(\frac{x'}{y} - \frac{y''}{x'} \right) &= \hat{\lambda} \frac{-y''}{y}, \\
\left(\frac{x'}{y} - \frac{y''}{x'} \right) &= \lambda \frac{y''}{y}, \quad \lambda = -2\hat{\lambda}.
\end{aligned}$$

Now we once again refer to the parameterization by arc length which gives that for $x, y \in [0, 1]$ we have the expression $x' = \pm\sqrt{1 - y'^2}$. We keep in mind the symmetry of surfaces of revolution and consider only the positive case:

$$\begin{aligned}
\left(\frac{\sqrt{1 - y'^2}}{y} - \frac{y''}{\sqrt{1 - y'^2}} \right) &= \lambda \frac{y''}{y}, \\
\left(\frac{1 - y'^2 - yy''}{y\sqrt{1 - y'^2}} \right) \left(\frac{y}{y''} \right) &= \lambda, \\
\left(\frac{1 - y'^2 - yy''}{y''\sqrt{1 - y'^2}} \right) &= \lambda, \\
(1 - y'^2 - yy'') &= \lambda(y''\sqrt{1 - y'^2}).
\end{aligned}$$

From here, recall that our original profile curve was given by $(x(s), y(s))$, a function of s . Make the substitution $z = y' = \frac{dy}{ds}$. This gives

$$\begin{aligned}
y'' &= \frac{dz}{ds} = \frac{dz}{dy} \cdot \frac{dy}{ds} \\
&= z \frac{dz}{dy}.
\end{aligned}$$

Then,

$$\begin{aligned}
(1 - z^2 - yz \frac{dz}{dy}) &= \lambda(z \frac{dz}{dy} \sqrt{1 - z^2}), \\
1 - z^2 &= \lambda z \frac{dz}{dy} \sqrt{1 - z^2} + yz \frac{dz}{dy},
\end{aligned}$$

$$\begin{aligned}
1 - z^2 &= \frac{dz}{dy} \left(\lambda z \sqrt{1 - z^2} + yz \right), \\
\frac{dy}{dz} &= \frac{\lambda z}{\sqrt{1 - z^2}} + \frac{yz}{(1 - z^2)}. \tag{*}
\end{aligned}$$

Equation (*) is a non-homogeneous linear differential equation in y , so we begin by solving the homogeneous case:

$$\begin{aligned}
\frac{dy}{dz} &= \frac{yz}{(1 - z^2)}, \\
\frac{1}{y} dy &= \frac{z}{(1 - z^2)} dz, \\
\ln(y) &= \frac{-1}{2} \ln(1 - z^2) + C, \\
\ln(y) &= \ln\left(\frac{1}{\sqrt{1 - z^2}}\right) + C, \\
e^{\ln(y)} &= e^{\ln\left(\frac{1}{\sqrt{1 - z^2}}\right) + C}, \\
e^{\ln(y)} &= e^{\ln\left(\frac{1}{\sqrt{1 - z^2}}\right)} e^C, \\
y &= \frac{D(z)}{\sqrt{1 - z^2}}. \tag{**}
\end{aligned}$$

Then differentiating with respect to z gives us:

$$\begin{aligned}
y' &= \frac{D'[\sqrt{1 - z^2}] - D\left[\frac{-z}{\sqrt{1 - z^2}}\right]}{(1 - z^2)} \\
&= \frac{D'}{\sqrt{1 - z^2}} + \frac{Dz}{(1 - z^2)^{\frac{3}{2}}} \\
&= \frac{D'}{\sqrt{1 - z^2}} + \frac{yz}{(1 - z^2)}.
\end{aligned}$$

Returning to (*), the non-homogeneous case, by plugging in our found homogeneous solution, we obtain

$$\begin{aligned}
\frac{\lambda z}{\sqrt{1 - z^2}} + \frac{yz}{(1 - z^2)} &= \frac{D'}{\sqrt{1 - z^2}} + \frac{yz}{(1 - z^2)}, \\
\lambda z &= D'.
\end{aligned}$$

Therefore, D' is a linear function giving

$$D = \lambda \frac{z^2}{2} + R$$

where R is a constant. Then from (**) and using $\lambda = -2\hat{\lambda}$,

$$\begin{aligned}
y &= \frac{-\hat{\lambda}z^2 + R}{\sqrt{1 - z^2}} \\
&= \frac{R - \hat{\lambda}z^2}{\sqrt{1 - z^2}}.
\end{aligned}$$

Case IIIa: If $\hat{\lambda} \neq R$, a computer algebra system³ (the process of which can be seen in reference) gives the results:

$$\begin{aligned}
c_1 - \frac{s}{\sqrt{2}} &= \int_1^{y(s)} \frac{1}{\sqrt{-\frac{\xi^2(-4ab+4b^2+\xi^2)+2ab-\xi^2}{b^2}}} d\xi, \\
c_1 + \frac{s}{\sqrt{2}} &= \int_1^{y(s)} \frac{1}{\sqrt{-\frac{\xi^2(-4ab+4b^2+\xi^2)+2ab-\xi^2}{b^2}}} d\xi,
\end{aligned}$$

$$c_1 - \frac{s}{\sqrt{2}} = \int_1^{y(s)} \frac{1}{\sqrt{\frac{\vartheta^2(-4ab+4b^2+\vartheta^2)+2ab-\vartheta^2}{b^2}}} d\vartheta,$$

$$c_1 + \frac{s}{\sqrt{2}} = \int_1^{y(s)} \frac{1}{\sqrt{\frac{\varphi^2(-4ab+4b^2+\varphi^2)+2ab-\varphi^2}{b^2}}} d\varphi.$$

At first glance, the linearity of the left hand side leads to a contradiction of the assumption that we are in a non-trivial case; however, further research into the implications of the solution are required.

For the this paper we will focus on the more immediate case:

Case IIIb: Now if $\hat{\lambda} = R$, we get:

$$\begin{aligned} y &= \hat{\lambda} \frac{1-z^2}{\sqrt{1-z^2}} \\ &= \hat{\lambda} \sqrt{1-z^2}, \\ y^2 &= \hat{\lambda}^2 (1-z^2) \\ &= \hat{\lambda}^2 - \hat{\lambda}^2 z^2, \\ y^2 - \hat{\lambda}^2 &= -\hat{\lambda}^2 z^2, \\ \frac{\hat{\lambda}^2 - y^2}{\hat{\lambda}^2} &= z^2, \\ \frac{\sqrt{\hat{\lambda}^2 - y^2}}{\hat{\lambda}} &= z, \\ \frac{1}{\hat{\lambda}} &= \frac{z}{\sqrt{\hat{\lambda}^2 - y^2}}. \end{aligned}$$

Then, by definition we have $z = y'$, giving:

$$\begin{aligned} \int \frac{1}{\hat{\lambda}} ds &= \int \frac{y'}{\hat{\lambda} \sqrt{1 - (\frac{y}{\hat{\lambda}})^2}} ds, \\ \frac{s}{\hat{\lambda}} + \phi &= \arcsin\left(\frac{y}{\hat{\lambda}}\right). \end{aligned}$$

Note that we used the substitution $u = \frac{y}{\hat{\lambda}}$ to integrate. Finally, we get an expression for the component function $y(s)$:

$$y(s) = \hat{\lambda} \sin\left(\frac{s}{\hat{\lambda}} + \phi\right).$$

We remark here that the constant ϕ represents a phase shift on the input angle of our function. Now from the arc-length parameterization:

$$\begin{aligned} x'^2 + y'^2 &= 1, \\ x'^2 + \left(\hat{\lambda} \cos\left(\frac{s}{\hat{\lambda}} + \phi\right) \frac{1}{\hat{\lambda}}\right)^2 &= 1, \\ x'^2 &= 1 - \left(\cos\left(\frac{s}{\hat{\lambda}} + \phi\right)\right)^2, \\ x' &= \pm \sin\left(\frac{s}{\hat{\lambda}} + \phi\right), \\ x(s) &= \mp \hat{\lambda} \cos\left(\frac{s}{\hat{\lambda}} + \phi\right) + \gamma. \end{aligned}$$

So $x(s)$ takes the form of a general sinusoidal function; we have reflections along the x -axis given by \mp , amplitude control via $\hat{\lambda}$, phase shifts from ϕ , and finally translations along x handled by γ .

So the profile curve C of S meeting the criteria is given by

$$C = \left(\mp \hat{\lambda} \cos\left(\frac{s}{\hat{\lambda}} + \phi\right) + \gamma, \hat{\lambda} \sin\left(\frac{s}{\hat{\lambda}} + \phi\right)\right),$$

which is a circle centered on the x axis at $x = \gamma$ of radius $\hat{\lambda}$. Then the surface of revolution S is

$$S = \left\{\mp \hat{\lambda} \cos\left(\frac{s}{\hat{\lambda}} + \phi\right), \hat{\lambda} \sin\left(\frac{s}{\hat{\lambda}} + \phi\right) \cos(t), \hat{\lambda} \sin\left(\frac{s}{\hat{\lambda}} + \phi\right) \sin(t)\right\},$$

which is a sphere of radius $\hat{\lambda}$, centered at $(\gamma, 0, 0)$.

A fascinating result is that depending on our definition of the domain of s , namely if $|\text{Dom}(s)| < |2\hat{\lambda}\pi|$ where $|\cdot|$ represents the standard Lebesgue measure, we obtain part of a sphere which still meets the criteria. So we can extend our hypothesis to include:

If $H = \lambda K$ for a surface S as above and non-zero λ , then S is part of a sphere.

Which gives a solid basis for the following conjecture:

Conjecture 1 (Mean-Gauss Surfaces of Revolution). *Given $C = (x(s), y(s))$, a complete smooth curve parameterized by arc length, which generates a surface of revolution S in the following way:*

$$S = \{(x(s), y(s) \cos(t), y(s) \sin(t))\}$$

for which we have $H_S = \lambda K_S$ for $\lambda \in \mathbb{R} \setminus \{0\}$ and $K_S \neq 0$ globally.

Then S is a sphere, or part of a sphere with profile curve:

$$\begin{aligned} x(s) &= \mp \hat{\lambda} \cos\left(\frac{s}{\hat{\lambda}} + \phi\right) + \gamma, \\ y(s) &= \hat{\lambda} \sin\left(\frac{s}{\hat{\lambda}} + \phi\right). \end{aligned} \quad \square$$

An important remark is that if we were instead to chose to rotate about the y axis, we would obtain a similar result but having instead:

$$\begin{aligned} y(s) &= \mp \hat{\lambda} \cos\left(\frac{s}{\hat{\lambda}} + \phi\right) + \gamma, \\ x(s) &= \hat{\lambda} \sin\left(\frac{s}{\hat{\lambda}} + \phi\right). \end{aligned}$$

And since the phase shift can be chosen as required to fit our initial conditions we can put the equations in standard form for \mathbb{R}^2 namely:

$$\begin{aligned} y(s) &= \mp \hat{\lambda} \sin\left(\frac{s}{\hat{\lambda}} + \phi'\right) + \gamma, \\ x(s) &= \hat{\lambda} \cos\left(\frac{s}{\hat{\lambda}} + \phi'\right). \end{aligned}$$

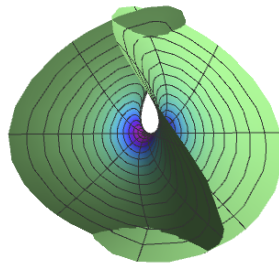
Surfaces of Constant Curvature

For surfaces of constant curvature, there are three possible cases. One and two are relatively uninteresting in our context, but they will be briefly covered.

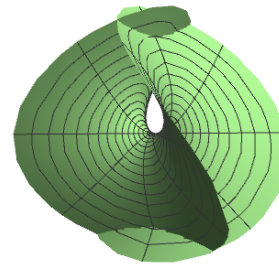
- i) Constant mean curvature surfaces
- ii) Constant Gaussian curvature surfaces
- iii) Both mean and Gaussian curvatures are constant

Case I: Constant Mean Curvature

If $H = 0$, then we have the trivial case of a plane or a minimal surface



(a) Gaussian Curvature



(b) Mean Curvature

Figure 4. Enneper's Minimal Surface coloured according to curvature.

which is satisfied by $\lambda = 0$. As previously mentioned, it is excluded from the general case of our relation.

And if $H = \gamma$ for some $\gamma \in \mathbb{R}$, but $K = f(x)$ is non constant for $x \in \mathbb{R}^3$, then there is clearly no λ constant which will satisfy

$$\gamma = \lambda f(x)$$

for every x on the surface.

Case II: Constant Gaussian Curvature

In this case, if $K = 0$ then our relation is not satisfied for any $\lambda \in \mathbb{R}$, as discussed in *Trivial Cases*.

And as in Case I, if $H = f(x)$ and $K = \gamma$ then

$$f(x) = \lambda \gamma$$

has no solutions which hold for every x on the surface. ■

Case III: Constant Mean and Gaussian Curvature

To handle case III, we need a theorem and its corollary from Montiel and Ros⁴.

Theorem 4 (Classification of Surfaces with Parallel Second Fundamental Form). *An orientable surface whose principal curvatures are constant, or equivalently, whose Gauss and mean curvatures are constant, is necessarily an open subset of a plane, a sphere, or of a right circular cylinder.* □

Corollary 1. *The only connected surfaces closed as subsets of \mathbb{R}^3 having constant principal curvatures are planes, sphere and right circular cylinders.* □

From the above corollary, we need only consider the 3 surfaces. If we have a right circular cylinder we are in the case that $K = 0$ and the relation is not satisfied. The plane is once again the trivial case, leaving us with the sphere which we have shown satisfies our relation.

Thus we have proven the following Theorem 5:

Theorem 5 (Mean-Gauss Surface of Constant Curvature). *The only orientable surfaces of constant curvature (mean or Gaussian) which satisfies $H = \lambda K$ non-trivially are spheres.* ■

Mean-Gauss Theorems

Collected Relation Theorems

For ease of reference, find the collected theorems from the previous sections below.

Spheres

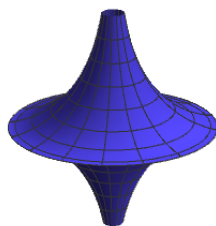
For any n -sphere S of radius ρ , the Mean-Gauss relation

$$H_S = \lambda K_S$$

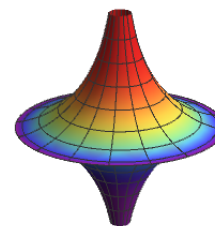
is satisfied by $\lambda = \rho^{n-1}$. ■

Graphs

Let $S = \{(x, y, z) \in \mathbb{R}^3 | z = f(x, y)\}$, for a function f which is smooth and well defined, be the graph of a function such that $H_S = \lambda K_S$ for $\lambda \in \mathbb{R} \setminus \{0\}$ and such that $f_{xx}f_{yy} - f_{xy}^2 \neq 0$. Then S is a part of or a whole



(a) Gaussian Curvature



(b) Mean Curvature

Figure 5. Pseudo-Sphere has $K_S = -1$ globally.

sphere.

Surfaces of Revolution (Conjecture)

Given $C = (x(s), y(s))$, a complete smooth curve parameterized by arc length, which generates a surface of revolution S in the following way:

$$S = \{(x(s), y(s) \cos(t), y(s) \sin(t))\}$$

for which we have $H_S = \lambda K_S$ for $\lambda \in \mathbb{R} \setminus \{0\}$ and $K_S \neq 0$ globally.

Then

$$\begin{aligned} x(s) &= \mp \hat{\lambda} \cos\left(\frac{s}{\lambda} + \phi\right) + \gamma, \\ y(s) &= \hat{\lambda} \sin\left(\frac{s}{\lambda} + \phi\right), \end{aligned}$$

and S is a sphere, or part of a sphere. □

Surfaces of Constant Curvature

The only orientable surfaces of constant curvature (mean or Gaussian) which satisfies $H = \lambda K$ non-trivially are spheres. ■

We also state a version of the Implicit function theorem from Lang⁵ which refers to it as “The Implicit Mapping Theorem.” Note that some of the statements of the theorem in our version have been made more specific as Serge Lang is dealing with general Banach spaces.

Theorem 6 (Implicit Function Theorem). Let $f : \mathbb{R}^{m+n} \rightarrow \mathbb{R}^m$ where $(x, y) \mapsto f(x, y)$ be a continuously differentiable function. Then for a fixed point $(a, b) \in \mathbb{R}^{m+n}$ with $f(a, b) = 0$, if the Jacobian matrix

$$J_{f,y}(a, b) = \begin{bmatrix} \frac{\partial f_1}{\partial y_1}(a, b) & \dots & \frac{\partial f_1}{\partial y_m}(a, b) \\ \vdots & \ddots & \vdots \\ \frac{\partial f_m}{\partial y_1}(a, b) & \dots & \frac{\partial f_m}{\partial y_n}(a, b) \end{bmatrix}$$

is invertible, then there exists an open set $U \subset \mathbb{R}^n$ containing (a) such that there exists a unique continuously differentiable function $g : U \rightarrow \mathbb{R}^m$ for which $g(a) = b$ and $f(x, g(x)) = 0$ for all $x \in U$. □

In essence, the implicit function theorem tells us that for any surface S , there exist points p_i for which in a neighborhood of the image of p_i we can describe the surfaces as the graph of a function.

Theorem 7 (Weak Mean-Gauss Theorem). The only embedded smooth non-developable surfaces $S \subset \mathbb{R}^3$ containing at least one point (a, b) satisfying the condition $J_{f,y}(a, b)$ is invertible, and which globally satisfies $H_S = \lambda K_S$ where $\lambda \in \mathbb{R}$ are part of or a complete sphere.

Proof. The proof by contradiction is immediate from the relation for graphs of functions (Theorem 3) and the implicit function theorem.

Let S be a surface as described and not part of a sphere, then locally there would be a patch for which the surface writes as the graph of function which is not locally spherical, hence it fails the relation. ■

Conjecture 2 (Strong Mean-Gauss Conjecture). The only smooth non-developable surfaces $S \subset \mathbb{R}^3$ satisfying the Mean-Gauss relation $H_S = \lambda K_S$ for $\lambda \in \mathbb{R}$ are part of or a whole sphere. □

While the proven theorems in this paper point towards the strong conjecture holding, more research is needed in order to prove it concretely, and

■ even further work needs to be done in order to prove an n dimensional version of the theorems.

Another interesting question is that if we relax the global requirement for smoothness, what types of surfaces can we build which satisfy the relation?

One simple example is if we have two spheres of equal radii, we can take two parts and glue them together. Then the relation is satisfied everywhere but along the glued boundary where the classical notion of curvature fails to exist.

Acknowledgements

I would like to thank Dr. Alina Stancu for her guidance throughout this process, without which none of this would have been possible.

□ Her passion, and excitement towards differential geometry directly inspired my own. Furthermore, I want to thank her for the framework to the solution of the partial differential equation in Case III of *Surfaces of Revolution*. It was a critical step that I suspect I would not have been able to solve on my own, or at least not without great struggle and frustration.

Also, thank you to all of my classmates, and the math department as a whole. The sheer brilliance of my peers and mentors and their spirit of cooperation serves as a constant source of inspiration.

References

1. Krivoshapko, S. & Ivanov, V. *Encyclopedia of Analytical Surfaces* (Springer International Publishing Switzerland, 2015). p. 471. <http://doi.org/10.1007/978-3-319-11773-7>.
2. Pressley, A. *Elementary Differential Geometry* (Springer London Dordrecht Heidelberg New York, 2010). <http://doi.org/10.1007/978-1-84882-891-9>.
3. Wolfram Research, Inc. *Wolfram | Alpha*, Champaign, IL, (2022), https://www.wolframalpha.com/input?i=y%28t%29%5E2-a%5E2+%3D+y%28t%29%5E2*y%27%28t%29%5E2-2*a*b*y%27%28t%29%5E2%2Bb%5E2y%27%28t%29%5E4.
4. Montiel, S. & Ros, A. *Curves and Surfaces* (American Mathematical Society, 2009). p. 263.
5. Lang, S. *Fundamental of Differential Geometry* (Springer-Verlag, New York, Berlin, Heidelberg, 1999). p. 19. <https://doi.org/10.1007/978-1-4612-0541-8>.

¹Department of Anatomy & Cell Biology, McGill University, Montreal, QC, Canada

²Research Institute, McGill University Health Centre, Montreal, QC, Canada

³Division of Nephrology, McGill University Health Centre, Montreal, QC, Canada

Keywords

CRISPR/Cas9, Podocyte, GTPase-Activating Proteins

Email Correspondence

emily.foxman@mail.mcgill.ca

<https://doi.org/10.26443/msurj.v18i1.193>

©The Author. This article is published under a CC-BY license: <https://creativecommons.org/licenses/by/4.0/>

Emily Foxman¹, Sajida Ibrahim², and Tomoko Takano^{2,3}

Rho GTPase Regulatory Proteins Contribute to Podocyte Morphology and Function

Abstract

Podocytes are a critical cellular component of the glomerular filtration barrier, whose strict permselectivity prohibits the passage of large proteins and charged species into the urine. Phenotypic variability or injury of these highly specialized cells can lead to proteinuria and has been linked with altered activity of Rho GTPases, which are strongly associated with the actin cytoskeleton. Notable regulators of these intracellular molecular switches are called guanine nucleotide exchange factors (GEFs), GTPase-activating proteins (GAPs), and guanine nucleotide dissociation inhibitors (GDIs). In this study, the roles of several GEFs in podocyte morphology and activity were investigated, including ECT2, ARHGEF2, ARHGEF26, and ARHGEF40. Results from RhoA and Rac1 G-LISA Activation Assays indicated that the absence of ARHGEF40 impairs epidermal growth factor (EGF)-stimulated RhoA and Rac1 activation, whereas knockout of ARHGEF2 and ARHGEF26 may selectively diminish RhoA activation. Furthermore, filopodia formation was hindered for the ARHGEF40 knockout. There are a number of additional investigations underway to understand Rho GTPase regulatory proteins, including the elimination of new sets of GEFs and GAPs *in vivo*. It is hopeful that these studies can provide insights into potential novel therapeutic strategies for proteinuria.

Introduction

Proteinuria is a commonly recognized manifestation and possible contributor to renal disease. This phenomenon, the leakage of proteins into the urine, is a result of kidney dysfunction in the glomerulus. The glomerulus is responsible for the filtration of blood and is composed of a network of capillaries contained within a structure called the Bowman's capsule, surrounded by a three-layered glomerular filtration barrier. After exiting the capillary endothelium, the filtrate passes through the glomerular endothelium, basement membrane, and the filtration slits established by podocytes and various proteins¹. These layers prevent the passage of high molecular weight and negatively charged species into the urinary space. The origin of proteinuria can be described as the loss of selective permeability of the glomerular filtration barrier to plasma proteins in the kidney².

Podocytes are an essential component of the glomerular filtration barrier. They are highly differentiated epithelial cells with a polarized organization consisting of a cell body and a series of extensions called foot processes³. The basal side is fused to the glomerular basement membrane and the foot processes of neighbouring podocytes form an interdigitating structure called the slit diaphragm. This specialized cell-cell contact point contributes to the size selectivity of the glomerular filtration barrier⁴. Phenotypic variability or injury of podocytes can result in alterations of the slit diaphragm framework and ultimately the disruption of the filtration barrier. Consequently, the loss of permselectivity allows the transglomerular leakage of proteins into the urine.

The specialized cellular morphology of podocytes is reliant on an extensive actin cytoskeletal architecture. Foot processes contain a cortical network of actin filaments and bundles which provide mechanical support, shape, and a foundation for cell motility⁵. An undesirable reorganization of the actin cytoskeleton leads to foot process effacement, characterized by a simplification of the interdigitation pattern and detachment from the glomerular basement membrane⁶. Since the integrity of the slit diaphragm and glomerular filtration barrier is largely dependent on foot process configuration, the regulation of the podocyte actin skeleton is crucial for maintaining kidney function.

The Rho family of small GTPases have been established as skillful regulators of the actin cytoskeleton and are therefore relevant in the understanding of podocyte dysfunction and proteinuria. They are a subdivision of the Ras superfamily of small GTPases and exist as molecular switches, binding to various effectors and regulating downstream signalling pathways. Rho

GTPases alternate between two distinct conformational states: an active GTP-bound state, during which they recognize target proteins and generate dynamic responses, and an inactive GDP-bound state. While the conversion between conformations involves a simple hydrolysis reaction, the activity of Rho GTPases is carefully regulated for homeostatic signalling cascades. There are three classes of proteins that regulate the activity of Rho GTPases. Guanine nucleotide exchange factors (GEFs) activate Rho GTPases by promoting the dissociation of bound GDP and facilitating the binding of GTP. Conversely, GTPase-activator proteins (GAPs) inactivate Rho GTPases by increasing their intrinsic activity, causing them to return to 'off' states after interacting with effectors. Guanine nucleotide dissociation inhibitors (GDIs) sequester the inactive GDP-bound Rho GTPases, preventing the exchange for GTP⁷. While there are only 20 members of the Rho GTPase family⁸, the human genome encodes over 80 GEFs and over 60 GAPs^{9,20}.

Three prototypical Rho GTPases are RhoA, Rac1, and Cdc42, all of which likely play a role in the regulation of the actin skeleton, and consequently podocyte morphology. In particular, RhoA is implicated in the production of stress fibers, a contractile actomyosin structure of the cytoskeleton¹². Rac1 is responsible for lamellipodia formation and extension, which are protrusions at the leading edge of migrating cells driven by a network of polymerizing actin filaments¹¹. Finally, Cdc42 is known to contribute to the development of finger-like projections called filopodia, which emerge from lamellipodia. These also contain bundles of actin and may act as sensory probes during cell migration¹⁰.

Past experimentation established the foundation of a protein-protein interaction network for Rho GTPases and their aforementioned regulatory proteins in podocytes. A proximity-based biotinylation assay (BioID) using baits of RhoA, Cdc42, and Rac1 coupled with proteomic analysis identified 20 GEFs as players in the Rho GTPase environment (Figure 1). From this preliminary interactome, four GEFs were chosen to further investigate the role of Rho GTPase regulatory proteins in cytoskeletal dynamics and podocyte biology: ECT2, ARHGEF2, ARHGEF26, and ARHGEF40.

Epithelial cell-transforming sequence 2 (ECT2) acts as a specific regulator of RhoA in podocytes. Past studies have implicated this gene in the proliferation and invasion of non-small cell lung cancer tumours¹³, as well as the progression of gastric carcinogenesis¹⁴. Furthermore, gene analyses of two nephrotic syndrome patients suggest that a non-functioning ECT2 gene may lead to renal tubulointerstitial injury and eventual glomerular sclerosis¹⁵.



Figure 1. A protein-protein interaction network for Rho GTPases in podocytes. Each regulatory protein (GEF) is shown to affiliate with at least one Rho GTPase. Eight are specific for RhoA, four are specific for Rac1, and two are specific for Cdc42. The scaled WD-score indicates the confidence of the interaction. Unpublished data from Takano Lab.

ARHGEF2, similarly to ECT2, interacts with RhoA. It has been reported that, in Madin-Darby canine kidney (MDCKII) cells, ARHGEF2 overexpression promotes the activation of RhoA and induces the formation of stress fibers as well as focal adhesions, leading to a slow rate of wound healing¹⁶. Similarly, in HeLa cells, upregulation of GEF-H1 (encoded by the ARHGEF2 gene) resulted in increased actomyosin contractility, increased cell adhesion, and decreased cell migration, due to downstream pathways involving RhoA¹⁷.

ARHGEF26 is an extensive regulator of Rho GTPases, shown through the BioID analysis to interact with RhoA, Cdc42, and Rac1 in podocytes. However, the contribution of ARHGEF26 in cytoskeletal dynamics has not yet been defined. A study has shown that decreased levels of ARHGEF26 lead to increased invadopodia formation in cancer cells¹⁸. Resembling filopodia and lamellipodia, invadopodia are actin-rich membrane protrusion structures that participate in the degradation of extracellular matrix during metastatic cancer. ARHGEF40, also known as Solo, is of particular interest due to its association with Cdc42. While this affiliation is not characterized in podocytes, reports have described that ARHGEF40 knock-downs accelerate the migration of collective MDCK cells with visible finger-like projections¹⁹. Furthermore, ARHGEF40-depleted cells showed the absence and thinning of stress fibers²⁰. In this study, light microscopy, G-LISA Small GTPase Activation Assays, and actin assembly assays were used to investigate the functional interactions of these regulators (ARHGEF2, ARHGEF26, ARHGEF40, ECT2) at the cellular and molecular level. These findings are pertinent in the elucidation of the mechanisms of podocyte injury and proteinuric renal disease, so may prove to be potential therapeutic targets.

Methods

Cell Culture and Transfection

All procedures using cell lines were performed using immortalized human podocytes. Conditions of culture include maintenance at 33 °C with 5% CO₂ in RPMI1640 medium containing 10% FBS and 1% penicillin/streptomycin (PS). Cell lines were transfected at a density of 350k cells per well in 6-well tissue culture plates. Using the backbone vector PX-459-V2

encoding the Cas9 protein, a cloned sgRNA sequence, and the Lipofectamine 3000 Reagent (ThermoFisher), a CRISPR sequence targeted for the knockout (KO) of each GEF was integrated. Furthermore, the plasmid contained a puromycin resistance gene as a selective marker. Following an incubation period (~18 hours) with the transfection reagents, cells were provided with antibiotic-free medium, then subjected to puromycin (2 µg/mL) treatment for 48 hours. After returning to normal RPMI-supplemented media, cells were kept under 33 °C incubation until confluent.

CRISPR/Cas9 Knockout System

The CRISPR-Cas9 system is reliant on two major components: a guide RNA sequence (Table 1) and a CRISPR-associated nuclease (Cas9). For the GEF KO cell lines, a single guide CRISPR strategy was implemented, in which the complementary sequence to the target DNA and the tracrRNA (important for target recognition) are fused together. This allowed the CRISPR/Cas9 system to generate inactivating mutations in the protein-coding genes by creating frameshift insertion-deletions (indels) in exonic sequences. Notably, an additional scrambled sequence was created that does not recognize the human genome, so the Cas9 protein would not perform an incision/excision.

ECT2 guide	5' TATTAACATCCACTACTGGG 3'
ARHGEF2 (assembly 2) guide	5' AAGAGAAACGGACTGCAAGG 3'
ARHGEF26 guide	5' GAGTGAGGTCGATAACGACG 3'
ARHGEF40 (assembly 1) guide	5' GGTGGAGAGGACTTATCGGG 3'
Scrambled guide	5' GCACTACCAGAGCTAACTCA 3'

Table 1. sgRNA sequences used in conjunction with the CRISPR-Cas9 system to achieve gene knockouts of four different GEFs in human podocytes.

The validation of CRISPR/Cas9 editing was accomplished using Tracking of Indels by Decomposition (TIDE) analyses, which were preceded by genomic DNA (gDNA) extraction of KO cell lines and polymerase chain reaction (PCR) to amplify the targeted region. The demonstration of the presence of an indel mutation at the guide RNA cut site is sufficient evidence for the gene knockout²¹.

Human podocyte GEF KO cell lines were maintained in 6 cm tissue culture plates and allowed to reach full confluency before trypsinization and preparation for gDNA extraction. The extraction was performed according to the Qiagen Genomic DNA Handbook and the Qiagen Blood & Cell Culture DNA Kit. PCR primers (Table 2) were designed to amplify a 400 to 700 base-pair region around the target cut site. The genomic DNA was amplified using the Q5 High-Fidelity PCR Kit (New England Biolabs: Product No. M0491S) according to the manufacturer's instructions. The amplified DNA for each GEF KO cell line, grouped with a scrambled sample, was sent for conventional Sanger sequencing by Genome Québec. The resulting chromatograms were input into the TIDE Analysis software²². Comparing the scrambled DNA and potential knockout DNA produced information about the quality of sequence data, verification of the expected cut site, relative abundance of aberrant nucleotides over the sequence trace, and overall gene editing efficiency.

Rho GTPase Activity Assay (G-LISA)

The intracellular amounts of Rac1-GTP and RhoA-GTP (active forms) in each GEF KO human podocyte cell line were determined using the G-protein linked immunosorbent assay (G-LISA) (Cytoskeleton Inc.). Kit and lysate preparation were performed per the manufacturer's protocol.

Transcript	Primer Pair
ECT2	5' ACTTACTTTTGCCCAATGACCA 3' (forward)
	5' GCTAGACCGCCCTCACATAC 3' (reverse)
ARHGEF2 (assembly 2)	5' TACCAACACTCCCGAAATGC 3' (forward)
	5' CACCCTGATCCCCTTAACCA 3' (reverse)
ARHGEF26 (assembly 3)	5' TTCCGCTTAGTGAATGGCGT 3' (forward)
	5' GCTCCTCGAGAATCCTTCG 3' (reverse)
ARHGEF40 (assembly 1)	5' GGGATCTGTAGCCTGGTCCT 3' (forward)
	5' GCAGAATAGTGATGCACGGC 3' (reverse)
Scrambled	5' CACCGCACTACCAGGCTAACTCA 3' (forward)
	5' aaacTGAGTTAGCTCTGGTAGTGC 3' (reverse)

Table 2. PCR Primers designed for each GEF genomic sequence targeted by sgRNA.

Cell Morphology Assessment

A basal cell morphology assessment was completed using fluorescence staining and confocal microscopy. The condition groups included ECT2

KO, ARHGEF2 KO, ARHGEF26 KO, ARHGEF40 KO, and scrambled. Coverslips were prepared in a 12-well plate. All steps were performed at room temperature unless otherwise stated. Wells were filled with ethanol for 10 minutes, washed with PBS, and exposed to a 1/200 dilution of collagen type I (Sigma) in PBS for 1 hour at 37 °C. A final wash with PBS was performed before adding 1 mL of RPMI and 60k human podocyte cells from a pre-existing culture line. Podocytes were serum-starved in RPMI containing 1% FBS for 18 hours before experimentation.

To achieve a fixed cell-staining environment, each well containing cells and a coverslip were washed with PBS, then 500 µL of a 4% paraformaldehyde (PFA) in PBS solution was added for 15 minutes. After washing once again with PBS, permeabilization was accomplished by exposing the wells to 500 µL of a 0.5% triton (Sigma-Aldrich) in PBS solution for 5 minutes. Two dyes were used to visualize the target structures of podocytes: PromoFluor-488-Phalloidin (PromoKine, Cedarlane) in a 1/100 dilution and DAPI (ThermoFisher) in a 1/1000 dilution. The former detects polymerized actin in the cytoskeleton and the latter stains nuclei. The wells were simultaneously incubated with phalloidin and DAPI for 20 minutes. Finally, the coverslips were mounted on a slide using Aqua Mount (Epre-dia, ThermoFisher) and kept at 4 °C until microscopy was performed on a Zeiss LSM780 Laser Scanning Confocal Microscope at 20x magnification.

Micrographs were analyzed on ImageJ using only the phalloidin overlay. Individual podocytes were identified and the relevant metrics of inquiry included cell area, cell perimeter, cell aspect ratio, and integrated density. The aspect ratio was calculated as a fraction of the minor axis (shortest distance between cell boundaries crossing the center) to the major axis (longest distance between cell boundaries).

Filopodia Assay

In a 12-well plate, 75k cells were plated for each human podocyte GEF KO cohort and treated with epidermal growth factor (EGF) at a concentration of 100 ng/mL in order to stimulate Rho GTPase activity. These wells contained a modified liquid medium: RPMI1640 with 1% FBS. The plate was placed in a 37 °C incubator, which promotes cell differentiation, and snapshots were taken using the IncuCyte S3 (Essen Bioscience) instrument and software every 2 hours over a 24-hour period.

Analysis of filopodia involved the manual counting of characteristic sharp and thin projections from podocytes, followed by normalization to cell confluency. Photographs from the 10-hour time point were chosen, as EGF stimulation was in effect, but not the sole player in filopodia formation. Rather, phenotypic variability in cell shape and the degree of Rho GTPase responses to stimulation would be more potent contributors. For each well containing either a GEF KO, scrambled, or parental cohort, sixteen snapshots were analyzed to ensure precision.

Results

Knockout Validation

TIDE determined the indel spectrum plot for each treated pool, which explains the composite sequence trace in the sample in comparison to the control (scrambled). Furthermore, TIDE provided an aberrant sequence signal plot, depicting the percentage of irregularity along the sequence trace of the control and experimental samples. As shown in Figure 2, the CRISPR/Cas9 system generated a considerable amount of indels in each GEF group, indicating a high degree of gene disruption and knockout efficiency.

Rho GTPase Activity

The G-LISA colorimetric assays provided variable evidence for the effects of Rho GTPase GEFs on stimulation from EGF (Figure 3). As a baseline control, the parental podocyte cell line showed an approximate 27% increase in activated RhoA (GTP-RhoA) and an approximate 37% increase

in activated Rac1 after treatment with EGF. In the ECT2 KO, there was an ~20% increase in GTP-RhoA and ~53% increase in GTP-Rac1 following EGF treatment. Under the same conditions, ARHGEF2 KO tended to increase to a similar degree in GTP-Rac1 (~27%); however, a difference in GTP-RhoA was not apparent after treatment. A similar tendency was observed for the ARHGEF26 KO; a ~19% increase in GTP-Rac1, but no

Effect of Knockout on Cell Morphology

For basal morphological analysis using fluorescence staining, phalloidin was employed to measure cell area, perimeter, and to label actin filaments in podocytes. DAPI served to confirm the viability of nuclei and cell life (Figure 4). There was no significant effect of the knockout GEFs on cell

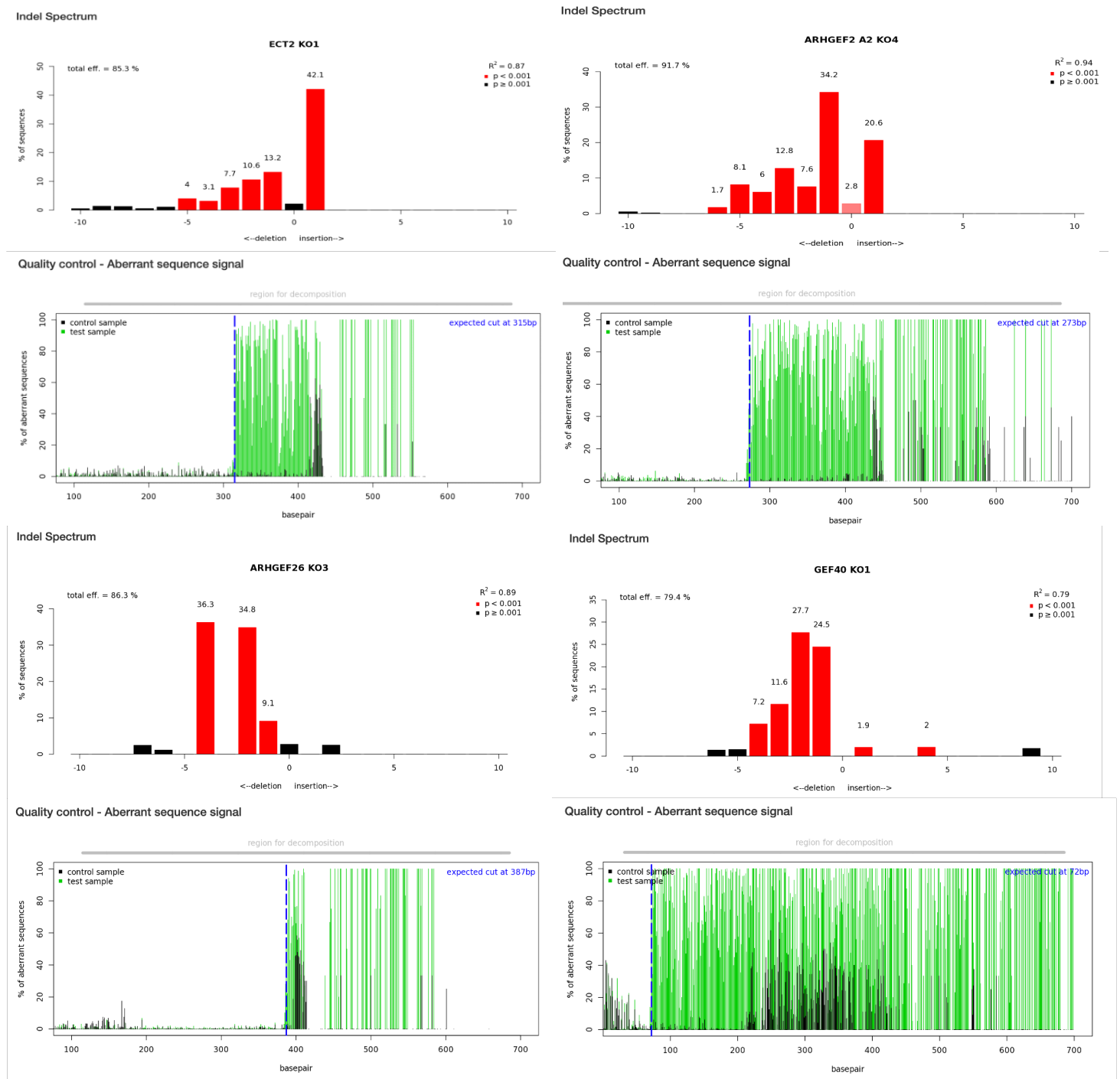


Figure 2. TIDE Analyses for each GEF knockout in human podocytes. The indel spectrum indicates the type of insertion/deletion and efficiency of gene editing. The aberrant sequence signal plot describes the amount of deviation in the genome sequence of knockout pools to the scrambled, unedited pool.

change in GTP-RhoA. Finally, the ARHGEF40 KO1 group showed neither an increase nor decrease of GTP-RhoA or GTP-Rac1 following EGF treatment. This suggests that the absence of ARHGEF40 impairs EGF-stimulated RhoA and Rac1 activation, whereas knockout of ARHGEF2 and ARHGEF26 may selectively impair RhoA activation.

surface area or cell aspect ratio (shape elongation) in human podocytes. However, an ARHGEF2 knockout resulted in a decrease in intensity of phalloidin staining, as shown in Figure 5. This indicates a decreased presence of actin filaments and provides more evidence that ARHGEF2 plays a role in the development and maintenance of the actin skeleton via RhoA activation.

Gene Target	Percentage Total Efficiency
ECT2	85.3
ARHGEF2 (assembly 2)	91.7
ARHGEF26	86.3
ARHGEF40 (assembly 1)	79.4

Table 3. TIDE determined the percentage of sequences in each transfected podocyte condition that carried an indel. A high degree of efficiency indicates the success of gene disruption (knockout) for the Rho GTPase GEF.

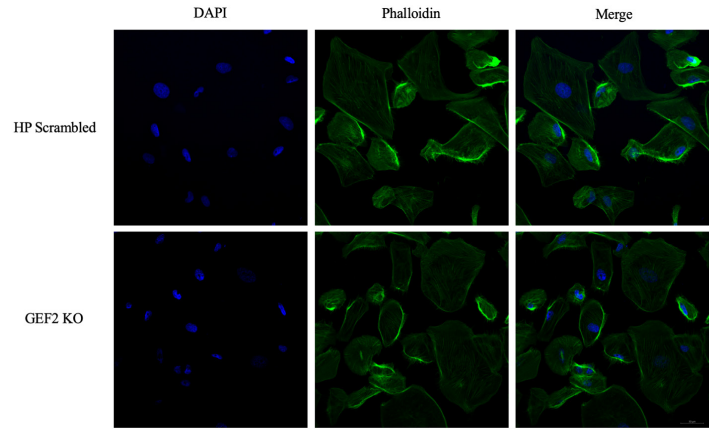


Figure 4. Representative images of the fluorescence staining for DAPI (blue) and Phalloidin (green) in human podocytes.

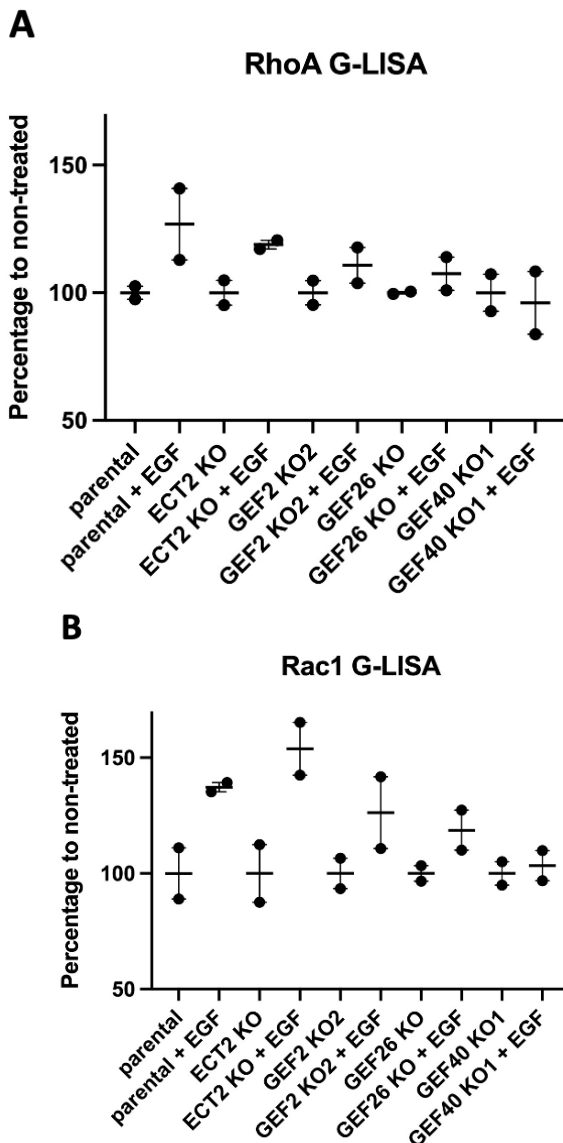


Figure 3. G-LISA experiments measure the activation of specific Rho GTPases using a colorimetric assay. When cells are treated with EGF, an increase in Rho GTPase activity is expected. The effects of GEF knockouts with respect to this activation rate are depicted as the percentage change to non-treated cells. Note that $n=1$ and each set of points represent duplicates. (A) The activity of RhoA in a parental human podocyte line, compared to podocytes with knockouts of each GEF (ECT2, ARHGEF2, ARHGEF26, ARHGEF40). Cells treated with EGF help to decipher the inhibition or facilitation of each GEF in Rho GTPase activation. (B) The activity of Rac1 in each of the same knockout and treatment groups.

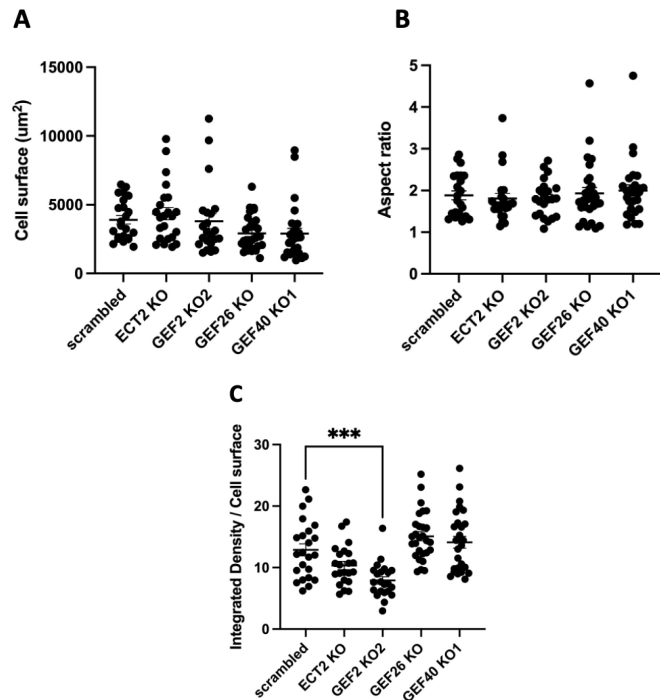


Figure 5. Morphological analyses of human podocytes for GEF knockouts from fluorescence staining, $n>20$ for each group. (A) Cell surface area showed no significant change between cohorts. (B) Fit ellipse showed no significant differences. (C) Density of phalloidin staining normalized to cell surface area. A noticeable decrease was present in the ARHGEF2 KO2 group, compared to the scrambled control.

The filopodia assay indicated that an ARHGEF40 knockout impairs filopodia formation in human podocytes. As shown in Figure 6, the number of cellular projections detected, when normalized to cell confluence, was decreased by approximately 40%. Such an effect indicates that ARHGEF40 may be a facilitator of cell migration and sensory activities. This result was not observed for any other knockout (ECT2, ARHGEF2, ARHGEF26).

Discussion

While it is well-known that Rho GTPase proteins play a critical role in the maintenance of the actin cellular framework and podocyte function, the underlying mechanisms of their regulatory proteins' behaviour have yet to be fully understood. This is likely due to the complex interaction networks that comprise cytoskeletal dynamics and the difficulty in targeting distinct signalling pathways. In this study, an attempt was made at deciphering the ways in which four guanine nucleotide exchange factors of Rho GTPases

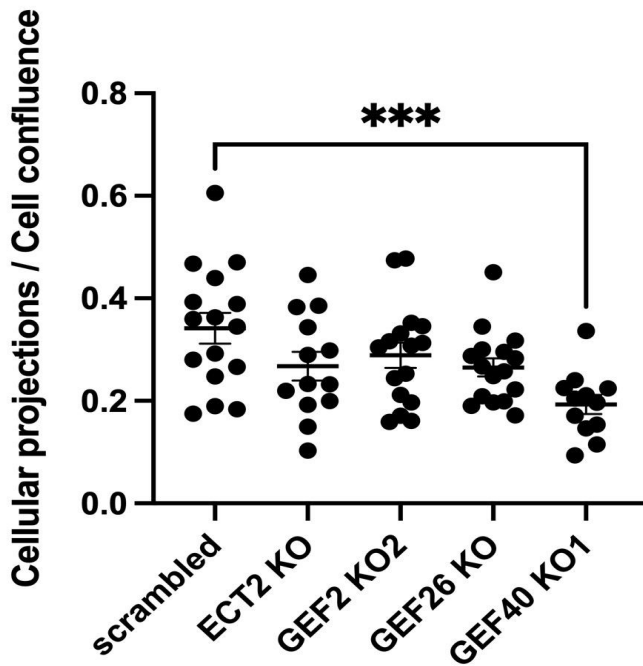


Figure 6. Filopodia formation in human podocytes 10 hours after treatment with EGF. The number of cellular projections in n=16 photographs of each treatment group were counted and normalized to the cell confluence.

(ECT2, ARHGEF2, ARHGEF26, and ARHGEF40) affect podocyte biology. Such information could provide valuable insights on the progression of foot process effacement, glomerular filtration barrier dysfunction, and proteinuria.

The G-LISA experiments provided preliminary clues into how GEFs allow Rho GTPases to be stimulated and activated by EGF. While a tendency to maintain activation with EGF treatment was detected for most GEF KO pools, the reliability of these results are limited by the lack of substantial sample sizes. Knockout of each GEF appears to have an impact on distinct Rho GTPases in duplicates; however, further experimentation will be performed to confirm the results.

The morphological analysis using fluorescence staining did not administer conclusive evidence of the role of particular GEFs on podocyte architecture. With no visible changes in cell surface area and shape (elongation), it is possible that there are more potent contributors to these features of podocytes than the Rho GTPase regulatory proteins. Furthermore, there may be multifactorial cooperation between complexes that contribute to podocyte appearance. However, since this was an elementary basal phenotype screening, the logical next step is to ascertain any morphological differences in these knockout groups following stimulation with a substance such as EGF.

The decrease in integrated density of phalloidin staining in the ARHGEF2 knockout cohort is an intriguing outcome. As previously mentioned, phalloidin detects actin filaments/stress fibers in the cytoskeleton. Since it was established that RhoA participates in the formation of stress fibers, and ARHGEF2 is a regulator of RhoA, it is sensible that the absence of ARHGEF2 would alter the architecture of these thread-like structures within podocytes. To validate this outcome, the cell morphology assessment investigations are being repeated on differentiated podocytes. This will provide further insight the true *in vivo* phenotypic state of these cells.

The filopodia assay produced robust evidence for the role of ARHGEF40 in cell migration and sensory performance. It is expected that the absence of ARHGEF40 would lead to decreased activation of Cdc42, consequently impairing the formation of filopodia. This was confirmed by a significant 40% decrease in the number of fibers projecting from podocytes after stimulation by EGF. This phenomenon suggests that ARHGEF40 affects the actin cytoskeleton via interactions with Rho GTPases (Cdc42), and its

elimination from the kidney could generate considerable functional modifications.

One unforeseen complication arose in the TIDE analysis of ARHGEF40. The software gave an alert indicating there was no good alignment found between the control (scrambled) and test (ARHGEF40 KO) samples. This means that the alignment window may have been too small or the sequence read was of poor quality and could negatively skew the TIDE estimation. To ameliorate this, the left boundary of the alignment window was set 10 base pairs lower. In doing so, the control and test samples appeared better aligned and the TIDE analysis continued. To ensure accuracy of these results, the protocols for gDNA extraction, PCR, and sequencing could be repeated.

As previously mentioned, there is much work to be done to understand the mechanisms of Rho GTPase regulatory proteins. The potential future directions of these studies are manifold and are a significant undertaking. Firstly, a large portion of the Rho GTPase interactome discovered in podocytes has yet to be analyzed in this manner. Fortunately, the same methods of gene knockouts and analyses for ~20 other GEFs, as well as some GAPs, are in progress.

Secondly, it may be advantageous to explore other functional assays involved in actin dynamics. They may provide additional insights into the alterations in cell behaviour induced by the absence of regulatory proteins. Finally, on a broader scale, the investigation of renal phenotypes in systemic or conditional gene knockout mice could produce compelling evidence for the role of these proteins.

Conclusion

Collectively, the present study attempts to provide further rationale for the relevance of Rho GTPase regulatory proteins in podocyte architecture and function. In this way, an understanding of the mechanisms of the glomerular filtration barrier and its associated pathological variations are improved. Together with previous work into the Rho GTPase interactome in podocytes, there is clearly much to be determined about such crosstalk and signalling. Further experimentation should reveal concrete evidence for the impact of GEFs and GAPs on actin cytoskeletal dynamics, cell migration, and Rho GTPase activity. There are also expanding opportunities using these Rho GTPase regulatory proteins for the identification and development of novel therapeutic agents against proteinuria.

Acknowledgments

This research was conducted as part of a PHGY396: Undergraduate Research Project at the Research Institute of McGill University Health Centre. The author would like to thank Sajida Ibrahim for her continuous support, instruction, and insight. Additionally, the author thanks Tomoko Takano for her guidance and encouragement throughout the course of the project.

References

1. D'Amico, G. & Bazzi, C. Pathophysiology of proteinuria. *Kidney Int.* **63**, 809–825 (2003). <https://doi.org/10.1046/j.1523-1755.2003.00840.x>
2. Cravedi, P. & Remuzzi, G. Pathophysiology of proteinuria and its value as an outcome measure in CKD: Proteinuria in CKD. *Br. J. Clin. Pharmacol.* **76**, 516–523 (2013) <https://doi.org/10.1111/bcp.12104>

3. Greka, A. & Mundel, P. Cell Biology and Pathology of Podocytes. *Annu. Rev. Physiol.* **74**, 299–323 (2012). <https://doi.org/10.1146/annurev-physiol-020911-153238>
4. Grahammer, F., Schell, C. & Huber, T. B. The podocyte slit diaphragm—from a thin grey line to a complex signalling hub. *Nat. Rev. Nephrol.* **9**, 587–598 (2013). <https://doi.org/10.1038/nrneph.2013.169>
5. Welsh, G. I. & Saleem, M. A. The podocyte cytoskeleton—key to a functioning glomerulus in health and disease. *Nat. Rev. Nephrol.* **8**, 14–21 (2012). <https://doi.org/10.1038/nrneph.2011.151>
6. Greka, A. & Mundel, P. Cell Biology and Pathology of Podocytes. *Annu. Rev. Physiol.* **74**, 299–323 (2012). <https://doi.org/10.1146/annurev-physiol-020911-153238>
7. Moon, S. Rho GTPase-activating proteins in cell regulation. *Trends Cell Biol.* **13**, 13–22 (2003). [https://doi.org/10.1016/s0962-8924\(02\)00004-1](https://doi.org/10.1016/s0962-8924(02)00004-1)
8. Asano-Matsuda, K., Ibrahim, S., Takano, T. & Matsuda, J. Role of Rho GTPase Interacting Proteins in Subcellular Compartments of Podocytes. *Int. J. Mol. Sci.* **22**, 3656 (2021). <https://doi.org/10.3390/ijms22073656>
9. Matsuda, J., Maier, M., Aoudjit, L., Baldwin, C. & Takano, T. ARHGEF7 (β-PIX) Is Required for the Maintenance of Podocyte Architecture and Glomerular Function. *J. Am. Soc. Nephrol.* **31**, 996–1008 (2020). <https://doi.org/10.1681/asn.2019090982>
10. Heasman, S. J. & Ridley, A. J. Mammalian Rho GTPases: new insights into their functions from in vivo studies. *Nat. Rev. Mol. Cell Biol.* **9**, 690–701 (2008). <https://doi.org/10.1038/nrm2476>
11. Villalonga, P., Ridley, A. J. & Verma, V. in *Encyclopedia of Biological Chemistry III* (eds Lennarz, W. J. & Lane, M. D.) 268–273 (Elsevier, 2021). <https://doi.org/10.1016/B978-0-12-819460-7.00195-X>
12. Jiu, Y. et al. Vimentin intermediate filaments control actin stress fiber assembly through GEF-H1 and RhoA. *J. Cell Sci.* **130**, 892–902 (2017). <https://doi.org/10.1242/jcs.196881>
13. Justilien, V. & Fields, A. P. Ect2 links the PKC ϵ -Par6 α complex to Rac1 activation and cellular transformation. *Oncogene* **28**, 3597–3607 (2009). <https://doi.org/10.1038/onc.2009.217>
14. Jin, Y. et al. Up-regulation of ECT2 is associated with poor prognosis in gastric cancer patients. *Int. J. Clin. Exp. Pathol.* **7**, 8724–8731 (2014).
15. Izu, A. et al. Nonfunction of the ECT2 gene may cause renal tubulointerstitial injury leading to focal segmental glomerulosclerosis. *Clin. Exp. Nephrol.* **16**, 875–882 (2012). <https://doi.org/10.1007/s10157-012-0636-0>
16. Sandí, M.-J. et al. MARK3-mediated phosphorylation of ARHGEF2 couples microtubules to the actin cytoskeleton to establish cell polarity. *Sci. Signal.* **10**, 32–86 (2017). <https://doi.org/10.1126/scisignal.aan3286>
17. Siesser, P. F. et al. FAM123A Binds to Microtubules and Inhibits the Guanine Nucleotide Exchange Factor ARHGEF2 to Decrease Actomyosin Contractility. *Sci. Signal.* **5**, ra64 (2012). <https://doi.org/10.1126/scisignal.2002871>
18. Goicoechea, S. M., Zinn, A., Awadia, S. S., Snyder, K. & Garcia-Mata, R. A RhoG-mediated signaling pathway that modulates invadopodia dynamics in breast cancer cells. *J. Cell Sci.* **130**, 1064–1077 (2017). <https://doi.org/10.1242/jcs.195552>
19. Isozaki, Y. et al. The Rho-guanine nucleotide exchange factor Solo decelerates collective cell migration by modulating the Rho-ROCK pathway and keratin networks. *Mol. Biol. Cell* **31**, 741–752 (2020). <https://doi.org/10.1091/mbc.e19-07-0357>
20. Fujiwara, S., Ohashi, K., Mashiko, T., Kondo, H. & Mizuno, K. Interplay between Solo and keratin filaments is crucial for mechanical force-induced stress fiber reinforcement. *Mol. Biol. Cell* **27**, 954–966 (2016). <https://doi.org/10.1091/mbc.e15-06-0417>
21. Giuliano, C. J., Lin, A., Girish, V. & Sheltzer, J. M. Generating Single Cell-Derived Knockout Clones in Mammalian Cells with CRISPR/Cas9. *Curr. Protoc. Mol. Biol.* **128**, e100 (2019). <https://doi.org/10.1002/cpmb.100>
22. Brinkman, E. K., Chen, T., Amendola, M. & van Steensel, B. Easy quantitative assessment of genome editing by sequence trace decomposition. *Nucleic Acids Res.* **42**, 168–168 (2014). <https://doi.org/10.1093/nar%2F-nar%2F42ku936>

Research Article

¹Department of Pharmacology & Therapeutics, McGill University, Montreal, QC, Canada

²Department of Chemistry, McGill University, Montreal, QC, Canada

Keywords

Nucleic acid, RNA ribozyme, Small molecule, Gene expression, Aptamer

Email Correspondence

janeva.shahi@mail.mcgill.ca

<https://doi.org/10.26443/msurj.v18i1.191>

©The Author. This article is published under a CC-BY license: <https://creativecommons.org/licenses/by/4.0/>

Janeva Shahi¹, Maureen McKeague^{1,2}

Comparison of Small Molecule-Responsive RNA Aptazymes for Applications in Gene Control

Abstract

Modelling how genes act in both space and time is critical to understand animal development, which can potentially drive intervention in gene expression. Gene regulation is examined using many techniques; however, challenges such as cell delivery, invasiveness, toxicity, and efficacy limit our ability to fully probe gene networks. Recent advances have led to the development of tunable, titratable, and reversible tools that can be genetically-encoded into animal model systems to modulate genes with temporal and spatial control. This study compares such tools, testing several aptazyme-based switches that can be expressed inside cells and controlled through the addition of non-toxic small molecules. Three switches responsive to different small molecules were compared for switching activity in mammalian cells. The most efficient switches in terms of activity gauged by their modulation of gene expression were then further assayed. Finally, the specificity of the hypoxanthine switch was tested based on chemical structure and classification. The comparisons revealed the importance of both timing and small molecule concentrations on switch activity, while the specificity testing demonstrated switch activity inside the cell correlated to the aptamer binding properties that were measured biochemically. This work demonstrates the suitability of aptazyme-based switches for application in diverse genetic environments, and in controlling and studying gene networks in animals.

Introduction

Measuring how genes act in both space and time is critical to understand animal developmental processes. Strategies such as gene knockouts¹, CRISPR mutations², tissue-specific promoters³, and inducible and transcriptional activators⁴ have been developed to allow for temporal regulation of gene expression. However, these tools are often limited by their delivery into cells, or do not result in long-term function^{1,2,3,4}. Additionally, many of these strategies cannot be easily regulated, thus limiting their use to later developmental timepoints in animal studies. To address these limitations, we are testing nucleic acid tools known as RNA aptazymes that can be genetically-encoded into cells and organisms to control expression of a specific gene at any desired timepoint in any specific tissue.

Aptazyme switches precisely regulate the expression level of a desired gene through the activity of a natural self-cleaving ribozyme, which in our case is a hammerhead ribozyme isolated from the satellite tobacco ringspot virus (sTRSV)⁵. Ribozymes are catalytic RNA that, when placed in the 3' untranslated region (UTR) of a gene, are capable of cleaving and destabilizing mRNAs by removing the poly A tail, ultimately preventing protein translation^{6,7,8}. To produce an RNA switch, the ribozyme is coupled to an aptamer⁹. Aptamers are synthetic oligonucleotides of DNA or RNA molecules that can tightly bind to a specific target molecule and change conformation¹⁰. Specifically, RNA aptamers upon conformational change can be incorporated into RNA aptazymes where target binding induces to destabilization of ribozyme activity^{6,7,9,10}. These aptamer molecules can be effective in improving control of gene expression due to their high specificity, high affinity, and relatively small size¹⁰. In the switch system, when the aptamer's target molecule binds, it blocks ribozyme activity by interfering with the tertiary loop interactions required for ribozyme self-cleavage (Figure 1). More specifically, in an "ON" aptazyme switch, binding of the ligand to the aptamer prevents ribozyme cleavage, thus permitting translation – so the gene turns 'ON' in the presence of the molecule. Conversely, in the absence of the molecular input, the activity of the ribozyme results in mRNA degradation and the suppression of gene expression.

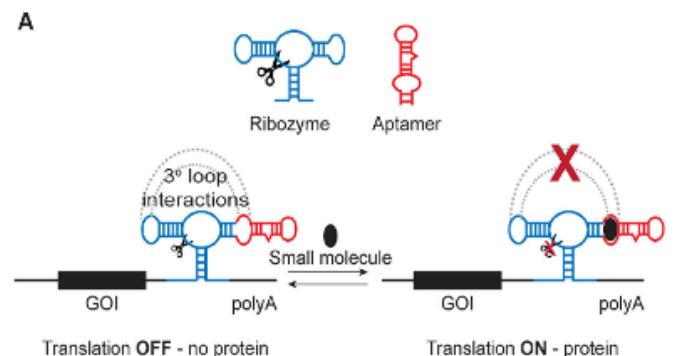


Figure 1. Aptazyme switch for gene expression control. The figure shows that RNA switches can control gene translation via mRNA degradation. In this study particularly, an "ON" aptazyme-based switch is applied. The full-length ribozyme has self-cleaving activity mediated by tertiary loop interactions at its catalytic core which leaves mRNA susceptible to degradation and preventing protein translation. Binding of the target to the aptamer inactivates the ribozyme catalytic activity, allowing for protein production. GOI = gene of interest

The goal of this work is to develop and test aptazyme-based switches within a genetic construct that can easily be ported into animal models. To date, RNA aptazymes have been tested in yeast and mammalian cells^{9,11,12,13,14}. We hypothesize that RNA aptazymes will be useful tools in animals due to 1) the compact RNA-based composition avoids the use of immunogenic protein components¹⁰; 2) there is no molecular dependence of species-specific transcription factors ideally making them applicable to a wide range of animal species^{10,12}, and 3) the fast and direct action of the switches can allow for concise gene pathways to be tested^{13,14}.

Here, we examine the function of three small-molecule responsive aptazyme switches in a plasmid system in a common mammalian cell model. Two of the switches that demonstrated turn-on activity in the presence of their respective target molecules, hypoxanthine and folinic acid, were then tested with pre-treatment of increasing concentrations of small molecule under a range of incubation times post-transfection. Finally, the specificity of the hypoxanthine switch was tested by challenging the switch with similar purine molecules, adenine and guanine. This work demonstrates the portability of the switches in different genetic contexts and highlights the potential for applying these switches as tools in animal models.

Methods

2.1 Materials

DMEM growth media was supplied from Thermo Fisher (Canada), derivative of human embryonic kidney (HEK293T) cells were generously provided by the Hébert lab at McGill University, all chemicals are from Sigma Aldrich, and kits used for assays are from New England Biolabs (NEB) unless otherwise noted. Oligonucleotides were purchased from Integrated DNA Technologies (Coralville, IA). All sequences (**Figure 2a**) are available from the McKeague lab upon request.

Oligo Name	Sequences
PGP #10	CCTTAGATTCTGCAGCCCTATAGCTAATCATAAATATACAACAAACAAACAAAGCTGTCCACC
PGP #11	TGTATCTTATCATGTCTGTGATCAGCGGGTTTCCCGGTTTTTATTTTTCTTTTTGCTGT
PS #46	ATTCTGCAGCCCTATAGCTAATCA
PS #47	ATCTTATCATGTCTGTGATCAGC
Neo-UGUAGCGG	AAACAAACAAAGCTGTACCAGGAGCTTGTCTTAAATGGTCCTCCGGTCTGATGAGTCTGTAGCGGGGACGAAACAGCAAAAAGAAAAATAAAA
Fol-UGGAG	AAACAAACAAAGCTGTACCAGGAGTGTGGTACGTTATATTCAGCCGGTCTGATGAGTCTGTAGAGAGACGAAACAGCAAAAAGAAAAATAAAA
Xan-ACGAG	AAACAAACAAAGCTGTACCAGGAGTGTATACCTAGTGGTCGACCCGGTCTGATGAGTCTACGAGAGACGAAACAGCAAAAAGAAAAATAAAA

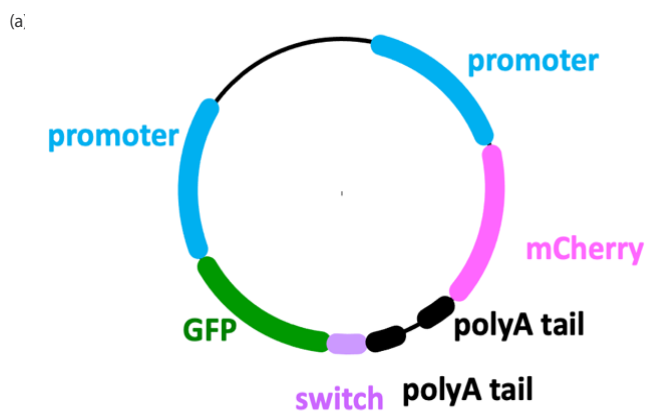


Figure 2. (a) Table listing the oligonucleotide sequences of primers and plasmids used in this work. (b) Backbone plasmid (pMM100) is illustrated with reporter proteins and indicated location of switch insertion.

2.2 Switch Insertion Design

The two reporter genes are GFP and mCherry. Each switch sequence was inserted into the 3' UTR region of GFP in plasmid pMM100 (available from McKeague lab upon request) (**Figure 2b**). Thus, GFP expression is dependent on switch activity, while mCherry expression should remain constant (to normalize for transfection efficiency).

2.3 Cloning RNA switches into the Plasmid

The backbone plasmid pMM100 was grown via overnight TOP10 culture, at 37°C for 16-18 hours. Following the overnight culture, the plasmid was prepped using Qiagen QIAprep Spin Miniprep Kit (250), quantified using a Thermo Scientific Nanodrop and stored at -20°C. PCR was performed using the forward primer PGP #10, reverse primer PGP #11, and the Phusion HF (high fidelity) enzyme from NEB as described by the manufacturer. PCR product was confirmed via 2% agarose gel electrophoresis, purified using the Monarch PCR Cleanup Kit according to manufacturer instructions, and quantified using Nanodrop. The backbone plasmid (pMM100) was digested using XmaI from NEB in CutSmart buffer. Following treatment with Quick-CIP, the cut plasmid was purified via 0.8% gel electrophoresis, then purified using the NEB Monarch Gel Extraction Kit according to the manufacturer instructions. Gibson assembly¹⁵ was performed by incubating the digested pMM100 backbone plasmid and the PCR switch insert as previously described. The plasmid was plated on E. coli and ampicillin plates. Colonies were selected and tested via colony PCR using the forward primer PS #46, reverse primer PS #47, and enzyme Taq DNA polymerase^{16,17}. Following the colony PCR, products underwent 2.5% agarose gel electrophoresis for 45 minutes and were purified using the Monarch PCR and DNA Cleanup Kit. Purified colony plasmids were sent for Sanger sequencing. Once sequences were confirmed, freezer stocks of the plasmid were made and stored at -80°C.

2.4 Target Molecules

Stock solutions of target small molecules for cell treatment were made prior to transfection. The various concentrations of small molecule tested in-vitro were serial-diluted down from their stocks: for a 10 mM neomycin stock, 0.5 g was dissolved into 10.0 mL of DNase/RNase nuclease free water; for the 10 mM folinic acid stock, 47.3 mg was dissolved into 10.0 mL of DMEM media; and for the 220 mM hypoxanthine stock, 2.99 g was dissolved into 99.8 mL of DMSO.

2.5 HEK-293 Cell Maintenance

HEK-293 cells were maintained by incubation at 37°C, 5% CO₂, and DMEM media with 5% Fetal Bovine Serum (FBS) and 1% Antibiotic-Antimycotic (AB/AM). These cells were passaged every 72-96 hours and discarded following 25-30 passages after initial thaw.

2.6 Mammalian Cell Transfection with Plasmid

A 24-well plate was seeded with 500 µL of cells at roughly 70% confluency, with an aim of 110,000 cells per well; at the time of transfection, cells were close to 100% confluency. For small molecule assays, cells were pre-treated with 500 µL of designated concentration of small molecule 1 hour prior to transfection. For transfection, OptiMEM, Lipofectamine 3000, and P3000 reagent from the Lipofectamine 3000 Kit from Sigma Aldrich were added to the plasmid and this suspension was transfected into the plated HEK-293 cells. In a 24-well plate, 50 µL of DNA-lipid complex was attained, in addition to 500 ng of DNA per well.

2.7 Measuring Fluorescence

At each designated time point post-transfection, or following an incubation period, cells were treated with Glo-Lysis 1X buffer from Promega, left to lyse for 5-7 minutes at room temperature, and quantified for GFP and mCherry fluorescence using the BioTek Cytation 5 plate reader by 24 well and 96 well plate readings.

Results and Discussion

3.1 Preliminary comparison of xanthine, neomycin, and folinic acid switches.

Numerous aptazyme switches^{10,12} developed and tested in mammalian cells^{9,11,12,13,14} have been reported to date. Small molecule-based aptazymes

are ideal since small molecules can be more easily delivered to cells and animals to modulate and turn on genes of interest. As such, we first tested switches developed to respond to small molecules that are expected to show no or little *in vivo* toxicity. Namely, we compared switches that interact with the FDA approved drug folic acid¹⁸; the antibiotic neomycin¹⁹; and a purine found in cells, hypoxanthine²⁰. Notably, each of these switches have previously demonstrated the ability to function in eukaryotes and show high “turn on” activity^{13,14}. Each switch was cloned in a zebrafish-compatible plasmid to control GFP expression. Specifically, GFP is controlled by the Ubi-promoter which shows high function in zebrafish²¹. On the same plasmid, mCherry was included to serve as a transfection control.

The control called sTRSV represents the ribozyme lacking the aptamer that allows for constant self-cleavage of the GFP RNA transcript and thus should result in very little expression. In all experiments, sTRSV showed excellent negative control (off) activity (**Figure 3**). Conversely, sTRSVi is a positive control in that the ribozyme cannot function. As such, GFP should be constitutively expressed. Indeed, sTRSVi in all experiments showed high gene expression (**Figure 3**). For each molecule, we tested the switches by incubating high concentrations of the target molecule for 72 hours (**Figure 3b**). Following incubation, switch activity was compared by measuring GFP fluorescence normalized to mCherry. Importantly, when comparing these three aptazyme switch designs head-to-head, the hypoxanthine switch showed the most switching activity, turning on 2-fold in the presence of 2 mM of target molecule compared to in its absence (**Figure 3b**). The neomycin switch showed no switching activity, and folic acid showed a small increase in gene expression with 2 mM target molecule. Considering K_d for each of the switches^{13,14}, the hypoxanthine aptamer exhibits micromolar binding affinity to its ligand while that of folic acid is nanomolar. Given these results, we focused on further characterizing the hypoxanthine and folic acid switches.

3.2 Testing the hypoxanthine-responsive switch under various parameters

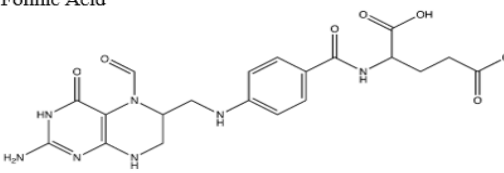
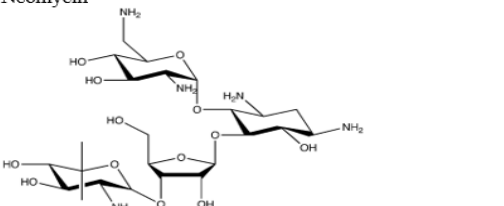
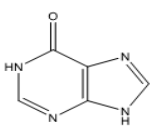
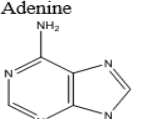
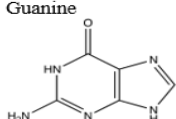
To further investigate the hypoxanthine-responsive switch, we conducted experiments testing activity of the switch using high concentrations over various time points post-transfection, as well as a large concentration study. Since cells had to be lysed, one 24 well plate was transfected per timepoint. To minimize uncertainties associated with different results for gene expression, fluorescence was normalized to sTRSV and sTRSVi control switch activity.

We tested the hypoxanthine switch at concentrations with 0 mM, 1 mM, and 2 mM at eight different timepoints post-transfection ranging from 18-96 hours (**Figure 4a**). Following the various incubation times (post-transfection), switch activity was compared by measuring GFP fluorescence normalized to mCherry. Comparing the switch activity over the various timepoints, incubation periods between 18 to 24 hours showed the highest “turn on” activity, but later timepoints (36-72 hours) resulted in reduced variability. Given these results, we confirmed that shorter than 72-hour transfection incubation periods for our given switch are indeed enough time to allow for gene expression, though periods within this range closer to 72 hours may be more useful for future comparisons.

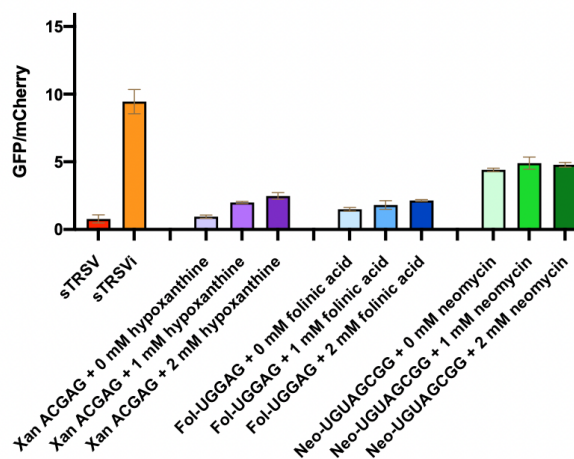
We next performed a concentration gradient experiment using concentrations of hypoxanthine ranging from 100 μ M to 10 mM (**Figure 4b**). Following the incubation time (post-transfection), switch activity of the switches treated with various concentration of molecule was compared by measuring GFP fluorescence normalized to mCherry. Comparing the switch activity, increasing “turn on” activity was observed across increasing concentrations of small molecule, where the largest change in gene expression was noted between 500 μ M and 10 mM concentration.

3.3 Testing the folic-acid responsive switch under various parameters

While the folic acid switch showed less activity than the hypoxanthine switch in the initial experiments (3.1), we nevertheless sought to measure the importance of incubation time (post-transfection time points) and concentration of folic acid switch activity. As per control switch confirmation, sTRSVi showed a higher normalized GFP/mCherry relative expression while sTRSV remains low as expected (**Figure 5**). We tested the

Switch Name	Small Molecule
Fol-UGGAG (folic acid aptamer inserted into sTRSV)	Folic Acid 
Neo-UGUAGCGG (neomycin aptamer inserted into sTRSV)	Neomycin 
Xan-ACGAG (xanthine aptamer inserted into sTRSV)	Original Molecule Hypoxanthine 
Derivative Molecules for Specificity Testing	
	Adenine 
	Guanine 

(a)



(b)

Figure 3. (a) Table outlining the switches and their associated target small molecule(s) tested in this work. (b) Preliminary *in-vitro* testing of hypoxanthine, folic acid, and neomycin switches to detect the highest measure of fluorescence. The plot (**Figure 3b**) shows the change in normalized GFP/mCherry fluorescence upon addition of small molecule target to the three distinct switches at 72 hours post-transfection. For the control switches, sTRSV (red) and sTRSVi (orange), three and six replicates were prepared, respectively. Control switch sTRSVi was treated with different concentration of respective small molecule in duplicate. Our control switch sTRSV was not treated with any molecule as it acts as our negative control. For each switch tested, different concentrations of the molecules were used in duplicates. Results are the mean and standard deviation of the number of replicates described: hypoxanthine data is in purple, folic acid in blue, and neomycin in green.

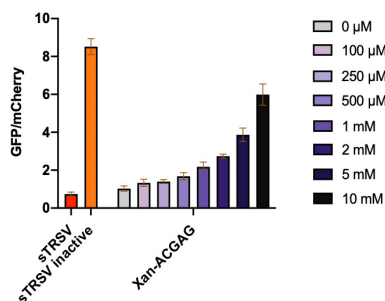
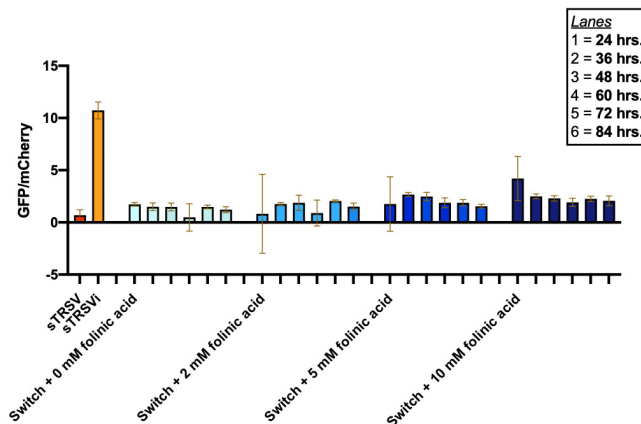
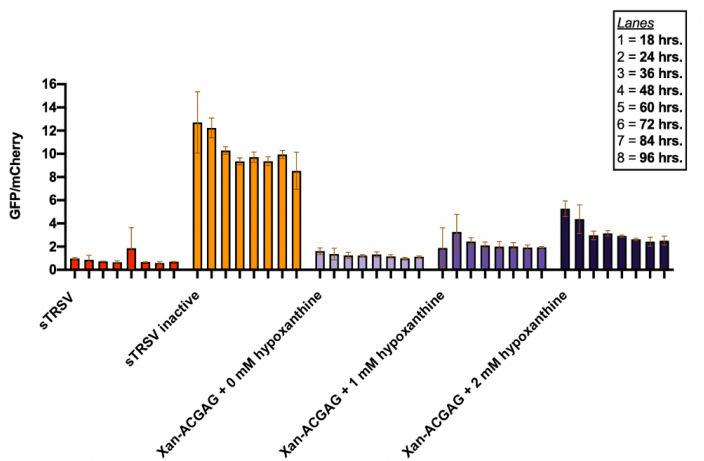


Figure 5. Folic acid-responsive switch results in increased GFP/mCherry relative expression in presence of folic acid in vitro with increasing time post-transfection. The plot shows the change in fluorescence with increasing concentrations of folic acid at six distinct time points post-transfection. For the control switches, sTRSV (red) and sTRSVi (orange), three and eight replicates were prepared respectively. Control switch sTRSVi was treated with different concentration of folic acid in duplicate. Our control switch sTRSV was not treated with any molecule as it acts as our negative control. All other conditions represent the mean and standard deviation of four replicates.

of low affinity) while guanine had a very small K_d (indicative of high affinity) for XBA. As such, we tested these two molecules for the ability to activate the hypoxanthine-responsive aptazyme switch.

We tested the hypoxanthine switch with 0 mM, 1 mM, and 2 mM of hypoxanthine, guanine, or adenine at a constant incubation time of 72 hours post-transfection. Similar to the aptamer binding experiments, the switch was activated in the presence of guanine but not adenine. Interestingly, even though guanine has a similar affinity to the aptamer as xanthine, the switching activity was less than with hypoxanthine. Nevertheless, these results confirm that the selectivity of the aptamer is maintained despite it being incorporated into a switch and expressed inside a cell.

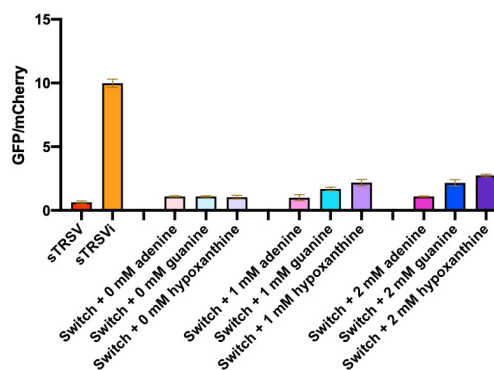


Figure 6. Hypoxanthine-responsive switch specificity in the presence of guanine and adenine. The plot shows the change in fluorescence with addition of derivative small molecule to Xan-ACGAG at 72 hours post-transfection. For the control switches, sTRSV (red) and sTRSVi (orange), three and six replicates were prepared, respectively. Control switch sTRSVi was treated with different concentration of respective small molecule in duplicate. Our control switch sTRSV was not treated with any molecule as it acts as our negative control. All other conditions are the mean and standard deviation of four replicates.

Figure 4. (a) Hypoxanthine-responsive switch demonstrated increased GFP/mCherry relative expression in the presence of hypoxanthine in vitro at early time points post-transfection. For the control switches, sTRSV (red) and sTRSVi (orange), three and six replicates were prepared respectively. Control switch sTRSVi was treated with different concentration of hypoxanthine in duplicate. Our control switch sTRSV was not treated with any molecule as it acts as our negative control. Each other condition represents the mean and standard deviation of four replicates. Results show that the switch activity occurs rapidly in the first 18-24 hours, and then later likely starts to be reduced with time due to cell division. (b) The hypoxanthine-responsive switch shows an increased GFP/mCherry relative expression in vitro with increasing concentrations of hypoxanthine. For the control switches, sTRSV (red) and sTRSVi (orange), four and eight replicates were prepared respectively. Control switch sTRSVi was treated with different concentration of hypoxanthine in duplicate. Our control switch sTRSV was not treated with any molecule as it acts as our negative control. Each other condition represents the mean and standard deviation of four replicates.

folic acid switch with 0 mM, 2 mM, 5 mM, and 10 mM at six different time points post-transfection ranging from 24-84 hours. Following the various incubation times (post-transfection), switch activity was compared by measuring GFP fluorescence normalized to mCherry. “Turn on” activity was shown across increasing concentrations. However, there was no increased switching observed at time points later than 24 hours.

3.4 Specificity testing of the hypoxanthine-responsive switch

Aptamers are typically highly selective for their cognate targets but, nevertheless, can bind similar derivatives in some cases. As an example, the xanthine aptamer, which was tested in vitro with small molecule hypoxanthine (and used in our platform as a “hypoxanthine switch”) is a derivative of the original target ligand xanthine. Indeed, Kiga et al.³ demonstrated that the aptamer, which they refer to as XBA (xanthine-binding aptamer), could also target purines with several modifications to the ring structure. Here, we wanted to assess whether the selectivity demonstrated directly on the aptamer was maintained when incorporated into our aptazyme switch. In particular, adenine was bound to the aptamer with a large K_d (indica-

Conclusion

Several small-molecule responsive aptazyme-based switches were compared²². The hypoxanthine switch displayed robust “turn on” activity in the presence of low concentrations of molecule relatively quickly following transfection. Interestingly, the hypoxanthine-responsive switch specificity was demonstrated and is comparable to biochemical aptamer affinity studies. Future work will examine additional early switch time points as well as other possibly confounding molecules found inside cells. The long-term goal of this work is to generate a suite of switches that can be easily incorporated into animal models and integrated into the genome to study genes relevant to development.

Acknowledgments

We thank Lucia Wang for her support in cloning the various aptazyme switches tested in this work. We also thank Dr. Eiman Osman for her collaboration and support with the in-vitro experimentation done for this work. This work is a pilot sub-project under a collaboration between Prof. Maureen McKeague at McGill University and Dr. Karen Mruk at the University of Wyoming. We thank Dr. Mruk and her lab for their support and suggestions on the work.

Funding Sources

A Natural Sciences and Engineering Research Council of Canada (NSERC) Undergraduate Student Research Award (USRA) in the Faculty of Medicine and Health Sciences at McGill University to J.S. NIH (R21GM143565), NSERC Discovery, and Canada Research Chairs Grants to M.M., and funding from the Centre in Green Chemistry and Catalysis.

Author Contributions

J.S. conducted the experiments. J.S. and M.M. analyzed data and wrote the manuscript.

References

1. Akerberg, A. A., Stewart, S. & Stankunas, K. Spatial and temporal control of transgene expression in zebrafish. *PLoS One* **9**, e92217 (2014). <https://doi.org/10.1371/journal.pone.0092217>
2. Zhen, S., Takahashi, Y., Narita, S., Yang, Y. & Li, X. Targeted delivery of CRISPR/Cas9 to prostate cancer by modified gRNA using a flexible aptamer-cationic liposome. *Oncotarget* **8**, 9375-9387 (2017). <https://doi.org/10.18632/oncotarget.14072>
3. Knopf, F. et al. Dually inducible TetON systems for tissue-specific conditional gene expression in zebrafish. *Proc. Natl. Acad. Sci. USA* **107**, 19933-19938 (2010). <https://doi.org/10.1073/pnas.1007799107>
4. Gerety, S. S. et al. An inducible transgene expression system for zebrafish and chick. *Development* **140**, 2235-2243 (2013). <https://doi.org/10.1242/dev.091520>
5. Nelson, J. A., Shepotinovskaya, I. & Uhlenbeck, O. C. Hammerheads Derived from sTRSV Show Enhanced Cleavage and Ligation Rate Constants. *Biochemistry* **44**, 14577-14585 (2005). <https://doi.org/10.1021/bi051130t>
6. Zhou, J., Bobbin, M., Burnett, J. C. & Rossi, J. J. Current progress of RNA aptamer-based therapeutics. *Front. Genet.* **3**, 234 (2012). <https://doi.org/10.3389/fgene.2012.00234>
7. Hutchins, C. J., Rathjen, P. D., Forster, A. C. & Symons, R. H. Self-cleavage of plus and minus RNA transcripts of avocado sunblotch viroid. *Nucleic Acids Res.* **14**, 3627-3640 (1986). <https://doi.org/10.1093/nar/14.9.3627>

8. Prody, G. A., Bakos, J. T., Buzayan, J. M., Schneider, I. R. & Bruening, G. Autolytic processing of dimeric plant virus satellite RNA. *Science* **231**, 1577-1580 (1986). <https://doi.org/10.1126/science.231.4745.1577>
9. Altman, S. Nobel lecture. Enzymatic cleavage of RNA by RNA. *Biosci. Rep.* **10**, 317-337 (1990). <https://doi.org/10.1007/BF01117232>
10. Kiga, D., Futamura, Y., Sakamoto, K. & Yokoyama, S. An RNA aptamer to the xanthine/guanine base with a distinctive mode of purine recognition. *Nucleic Acids Res.* **26**, 1755-1760 (1998). <https://doi.org/10.1093/nar/26.7.1755>
11. McKeague, M. & DeRosa, M.C. Challenges and opportunities for small molecule aptamer development. *J. Nucleic Acids*, 748913 (2012). <https://doi.org/10.1155/2012/748913>
12. Townshend, B., Kennedy, A., Xiang, J. & Smolke C. D. High-throughput cellular RNA device engineering. *Nat. Methods* **12**, 989-994 (2015). <https://doi.org/10.1038/nmeth.3486>
13. Beilstein, K., Wittmann, A., Grez, M. & Suess, B. Conditional Control of Mammalian Gene Expression by Tetracycline-Dependent Hammerhead Ribozymes. *ACS Synth. Biol.* **4**, 526-534 (2015). <https://doi.org/10.1021/sb500270h>
14. Xiang, J.S. et al. Massively parallel RNA device engineering in mammalian cells with RNA-Seq. *Nat. Commun.* **10**, 4327 (2019). <https://doi.org/10.1038/s41467-019-12334-y>
15. Gibson, D. G. et al. Enzymatic assembly of DNA molecules up to several hundred kilobases. *Nat. Methods* **6**, 343-345 (2009). <https://doi.org/10.1038/nmeth.1318>
16. Denomme, G. A., Rios, M. & Reid, M. E. *Molecular Protocols in Transfusion Medicine* (Elsevier, 2000). <https://doi.org/10.1016/B978-0-12-209370-8.X5000-4>
17. Mülhardt, C. & Beese, E. W. *Molecular Biology and Genomics* (Elsevier, 2007). <https://doi.org/10.1016/B978-0-12-088546-6.X5000-3>
18. Bedford Laboratories. Leucovorin Calcium Injection (2011); https://www.accessdata.fda.gov/drugsatfda_docs/label/2012/040347s010lbl.pdf
19. Veirup, N. & Kyriakopoulos, C. *Neomycin* (StatPearls, 2022). <https://www.ncbi.nlm.nih.gov/books/NBK560603/>
20. Hayman, J. & Oxenham, M. *Human Body Decomposition* (eds Hayman, J. & Oxenham, M.) 53-90 (Elsevier, 2016). <https://doi.org/10.1016/C2015-0-00038-7>
21. Mosimann, C. et al. Ubiquitous transgene expression and Cre-based recombination driven by the ubiquitin promoter in zebrafish. *Development* **138**, 169-77 (2011). <https://doi.org/10.1242/dev.059345>
22. Mruk, K., Ciepla, P., Piza, P. A., Alnaqib, M. A. & Chen, J. K. Targeted cell ablation in zebrafish using optogenetic transcriptional control. *Development* **147**, dev183640 (2020). <https://doi.org/10.1242/dev.183640>

Uncovering the Regulators of CRISPR-Cas Immunity

Abstract

The clustered regularly interspaced short palindromic repeats (CRISPR) system and the CRISPR-associated proteins (Cas) make up an adaptive immune mechanism used by many bacteria and archaea to protect themselves from invading genetic material. Despite the immense evolutionary advantage of the CRISPR-Cas system, it must be meticulously regulated as it has the potential to target endogenous genes and damage the host organism. Identifying the main regulators involved in this process and how they are influenced by distinct conditions are of great clinical interest, since this prokaryotic defense system can be exploited for genome editing and therapy development. This review aims to elucidate the regulation of the CRISPR system in bacterial communities—upon quorum sensing and alginate production in biofilms—and in stressed conditions—upon antibiotic treatment or induction of the Rcs response. Despite the intrinsic contradictions of the results gathered in this review, growth rate is identified as a potential unifying regulator of CRISPR immunity. Overall, the regulation of the CRISPR-Cas system is shown to be multi-dimensional and cross-sectional, to greatly vary amongst lineages, and to be highly sensitive to conditional changes.

Keywords

CRISPR, bacteria, quorum sensing, antibiotics, biofilm

Email Correspondence

idia.boncheva@mail.mcgill.ca

<https://doi.org/10.26443/msurj.v18i1.195>

©The Author. This article is published under a CC-BY license: <https://creativecommons.org/licenses/by/4.0/>

Introduction

One of the reasons why bacteria remain such prominent and persistent invaders of the human body is their ability to quickly adapt and evolve through acquisition of novel genetic material. This can both provide significant evolutionary advantage and threaten bacteria survival. Microorganisms have evolved many mechanisms to protect themselves from parasitic DNA. The clustered regularly interspaced short palindromic repeats (CRISPR) system and its associated proteins (Cas) make up the only known adaptive and heritable defense mechanism in bacteria against bacteriophage invaders and other mobile genetic elements¹.

It was first discovered in *Escherichia coli* in 1987, but it has now been identified in around 50% of bacteria, and growing interest for this system has bloomed a new field of microbial and genetic studies^{2,3}. Although the CRISPR-Cas system has been identified in numerous bacteria, its distribution does not align with bacterial phylogenies⁴.

It has been predicted that factors such as oxygen prevalence, temperature, and the abundance of viral threats in the environment influence the distribution of this system but the ecological factors involved remain unclear⁵. This is further complicated by the fact that the defense system can readily be transferred through horizontal gene transfer⁴.

The CRISPR-Cas system functions as an intracellular patrolling complex that will recognize incoming foreign nucleic acid sequences and induce their degradation. There are two main components to this system: the CRISPR array and the Cas proteins. The former is a genomic locus where a series of identical repeats sequences and unique spacer sequences are alternately distributed downstream of a leader sequence. While the short repeats are intrinsic to the bacteria, the spacers are integrated into the host genome from previously encountered foreign DNA.

During the adaptation phase, the Cas1 and Cas2 proteins will scan foreign DNA that has entered the bacterial cell and capture a protospacer fragment from this invading genetic material. In most bacteria, this capture is dependent on the presence of a protospacer adjacent motif (PAM) which allows the host to differentiate between self and foreign genetic material.

The protospacer can then be integrated at the 5' end of the spacer array, adjacent to the leader sequence. For this reason, the CRISPR array represents a physical memory of past infections. Subsequently, in the biogenesis phase, also known as the maturation or expression phase, the spacers are transcribed and processed by host enzymes into CRISPR RNA (crRNA) which will be bound by Cas proteins and adaptor sequences, such as the transactivating noncoding CRISPR RNA (tracrRNA), to generate a mature antiviral complex.

Lastly, during the interference phase, the mature antiviral complex will once again scan the intracellular environment. The crRNA will mediate the recognition of foreign genetic material via sequence complementarity, and the accessory proteins of the mature system will induce targeted sequence damage to protect the bacterial cells (**Figure 1**). The Cas proteins are required at each step and they carry specialized functions: Csy proteins will generate a multi-protein surveillance complex that is essential for the adaptation phase, whereas the Csm proteins generate complexes that mediate interference.

The three steps described above are ubiquitous to all CRISPR-Cas systems, but there is still great variability amongst the proteins encoded, the specificity of the CRISPR-Cas system, and the mechanisms of protection adopted by this defense mechanism. There are 2 large classes, 6 types, and over 20 subtypes of bacterial CRISPR-Cas systems that are functionally distinct⁶. In this review, we will focus on two model bacterial strains and their corresponding CRISPR-Cas defenses: *Pseudomonas aeruginosa* PA14 which carry the Type I-F system and *Serratia* species 39006 which carries Type III-A, Type I-E, and Type I-F CRISPR-Cas systems. Type I and Type III systems are both members of class 1 systems which encode multi-protein effector complexes, but they have additional unique characteristics that distinguish them⁷. Type I systems recognize double-strand DNA which are degraded via Cas3 upon recognition of a PAM and the short neighboring 'seed' sequence⁷. Type III systems target foreign RNA transcripts to activate the Cas10 nuclease and induce non-specific RNA degradation, independently of canonical PAM requirements⁷.

Overall, there is a great understanding of the functional requirements for the activity of CRISPR-Cas. However, much remains unclear regarding the regulation of this system in different conditions. Constitutively active

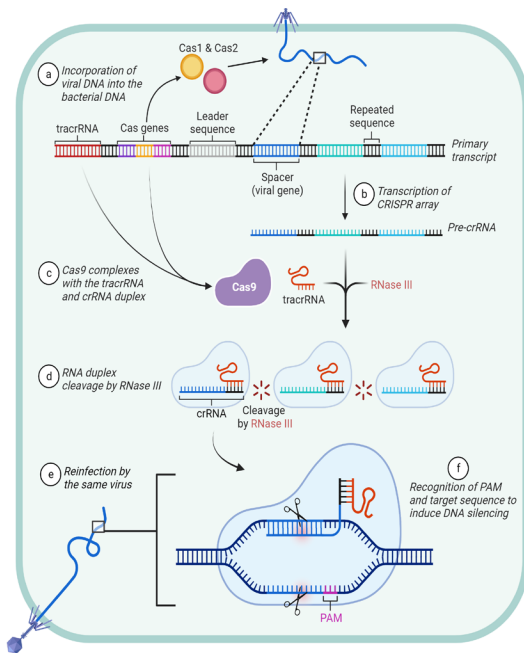


Figure 1⁹. Summary diagram of CRISPR-Cas system. Schematic showing the different steps of the adaptive immune response upon exposure to bacteriophage genetic material. Step A illustrates the adaptation phase. Steps B-D summarize the biogenesis phase, which is also known as the

CRISPR-Cas systems pose a significant evolutionary cost as they predispose the bacteria to self-targeting and to degradation of genetic material⁸. Thus, this defense mechanism must be tightly regulated. Additionally, there is a great interest in understanding the factors controlling the acquisition, biogenesis, and interference phases of the CRISPR-Cas system as this knowledge can be applied to very precise genome editing techniques and phage therapies. Consequently, this review aims to uncover the key regulators of the CRISPR-Cas system, the importance of each sensor, and the regulatory fluctuations that arise upon changes in conditions (Figure 2). To this effect, various intracellular pathways and intercellular signals will be analyzed: quorum sensing, biofilm formation, alginate biosynthesis, and the regulator of capsule synthesis (Rcs) response induced upon antibiotic treatment.

Methodology

Quorum Sensing: the more you seek, the less you know

Quorum sensing (QS) is a system of coordinated chemical signals that allow bacteria to communicate with one-another in order to detect population density, transfer genetic material with proximal cells, modulate cellular functions, control motility and synthesize structural and signaling metabolites¹⁰. There are three general types of QS systems: the acyl homoserine lactone (AHL) system, the autoinducing peptide (AIP) system, and the autoinducer-2 (AI-2) system¹⁰. The AHL system is expressed by Gram-negative bacteria exclusively and it functions via the release of signaling molecules with a common homoserine lactone ring¹⁰. The AIP QS system is found in Gram-positive bacteria and it is characterized by short peptides and a two-component regulatory system¹⁰. The AI-2 system is distributed amongst both Gram-positive and Gram-negative bacteria, and it confers interspecies communication abilities via a collection of inter-convertible molecules¹¹.

The AHL system will be explored here as it is the one held by both *P. aeruginosa* and *Serratia* model strains¹². In these bacteria, the LasI, RhII, and SmaI autoinducers will signal through their corresponding receptors which results in the expression of QS genes¹³ (Figure 2). One downstream

target of QS signals is the upregulation of type I-E and type I-F cas genes¹³. Indeed, *P. aeruginosa* PA14 mutants lacking autoinducer genes have been shown to exhibit attenuated efficacy in all three phases of the CRISPR-Cas system, and complementation restored function to wild-type (WT) levels for all steps of the immune process¹³. This suggests that the engagement of the QS system positively upregulates CRISPR-Cas immunity. This is in agreement with other studies, which have shown that QS-deficient mutants of either bacterial model were found to be less adaptable to invading nucleic acids¹². However, it is critical to acknowledge the limitations of these findings, as these results were obtained from studying only one of the three QS systems. Thus, it is possible that the regulation of CRISPR-Cas immunity by QS molecules and condition varies in other species that communicate via the AIP or the AI-2 systems. Additionally, the regulation of CRISPR-Cas immunity is likely more complex in bacteria that encode more than one QS system.

Certain groups that have attempted to modulate the expression of cas genes via quorum quenching (QQ)—a process of QS disruption—have obtained varying efficacy. Mion et al. measured the expression levels of *cas1*, *cas3*, and *csy1-4* in the presence or absence of the lactonase SsoPox-W263I to test the effects of QQ in the *P. aeruginosa* PA14 laboratory model and in 6 other clinically isolated strains of this species. The lactonase SsoPox-W263I is known to degrade acyl-homoserine lactones which are essential for QS in proteobacteria. Upon treatment with the enzyme, all *cas* & *csy* gene expression was abolished in PA14. However, clinically isolated strains showed variable results with some having a decreased *cas* and *csy* gene expression, while other showed no change or an increase in gene expression¹². This demonstrates that regulation of the CRISPR-Cas system can vary greatly between strains of a single species despite significant genetic homology. Additionally, these results highlight that laboratory studies with model organisms in controlled settings do not necessarily translate to clinical cases. This is particularly relevant as there are strong initiatives that aim to treat certain diseases through the genome editing power of the CRISPR-Cas system.

Other groups have studied the modulation of CRISPR-Cas using QS inhibitors. It has been reported that the chemical baicalein can increase survival of phage-sensitive bacteria such as *P. aeruginosa*. This QS inhibitor has been found to reduce DMS3vir phage absorption, delay lysis of bacterial culture, and favor the action of CRISPR immunity¹⁴. This sharply opposes previously published data, which proposes that QS inhibitors limit

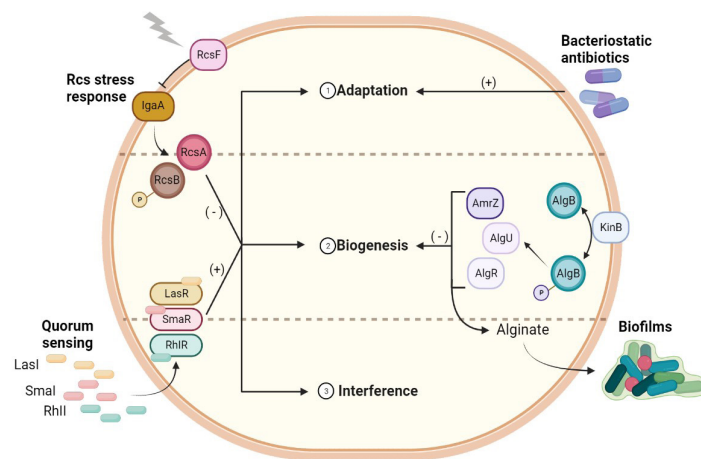


Figure 2¹⁵. The effects of various cellular signaling pathways on CRISPR-Cas regulation. The Rcs stress response pathway has been shown to downregulate all three phases of the CRISPR-Cas immune system, whereas quorum sensing upregulates these same phases. Some of the autoinducers (LasI & RhII) directly induce these effects, while others (SmaI) are repressors of the CRISPR-Cas system that are inhibited by AHL molecules upon quorum sensing¹. Bacteriostatic antibiotics positively regulate the adaptation phase, and the bacterial alginate synthesis pathway negatively regulates the biogenesis phase. The KinB membrane protein can act either as a phosphatase in acute virulence conditions, or as a phosphatase in chronic virulent conditions².

CRISPR-based immunity. Upon further analysis, these effects were attributed to the fact that the DMS3vir phage receptor—the type-4 pili—is regulated by QS genes¹⁴. Inhibiting QS proportionally downregulated the phage receptor which reduced viral intracellular propagation and provided the host cells with sufficient time to mount an immune response¹⁴. Thus, when evaluating the effects of QS systems on immunity, we must also take into consideration the downstream genes affected, as they have the potential to alter sensitivity to invaders through indirect actions on infection parameters.

There are clear contradictions between the effects of quorum sensing, quorum quenching, and quorum sensing-inhibitors on the regulation of CRISPR-Cas. This becomes further convoluted when multiple variables are investigated simultaneously. For example, to assess the relationship between temperature changes and QS on the rate of spacer acquisition in the CRISPR-Cas system, Høyland-Kroghsbo et al. constructed a *P. aeruginosa* PA14 strain lacking autoinducer genes, and then measured adaptation rates at various temperatures in bacteria that were supplemented or deprived of autoinducers. As quorum sensing molecules are upregulated at high temperatures and are known to activate the CRISPR-Cas system, it was hypothesized that a strong and effective adaptive immune response would be induced at high temperatures in bacteria. However, the relationship between temperature and QS seems to be slightly more complex. Overall, adaptation rates were highest at low temperatures. Supplementation of mutants with autoinducers had no effect at 15°C, indicating that QS does not affect the rate of spacer acquisition at low temperatures. On the other hand, supplementation significantly increased new spacer acquisition at 30°C and 23°C, but only moderately at 37°C. To rationalize these results, the research group hypothesized that low temperature stabilized CRISPR-Cas complexes and crRNA binding to foreign sequences¹³. This has recently gained further relevance as reports emerge of the temperature-dependent binding and release of Cas proteins to target DNA¹⁶. Regardless, these results demonstrate that even slight changes in conditions such as temperature can alter the potency of sensors in modulating CRISPR-Cas adaptation.

Biofilm formation and alginate synthesis: Strength in numbers

One of the main functions of QS is to induce microbial biofilms and increase virulence in high-density bacterial populations¹⁰. In certain favorable environments, bacteria are able to communicate with each other and adhere to surfaces to build a highly structured and complex three-dimensional community that is much harder to eradicate than populations of single cells¹⁰. This is a multi-step process that involves the synthesis of numerous polymeric extracellular substances such as the alginate polysaccharide. Alginate production has been associated with adherence enhancement, increased persistence, and protection from the extracellular environment¹⁷. The biosynthesis of alginate is controlled by the KinB-AlgB two-component system¹⁸. Upon inactivation of the cognate histidine kinase KinB, phosphorylated AlgB will accumulate in the cell and signal through various intermediate protein such as algR, algU, and amrZ to up-regulate alginate synthesis genes¹⁸ (**Figure 2**).

To measure the effects of the alginate biosynthesis pathway on CRISPR-Cas immunity, Borges et al. measured the levels of Cas and Csy protein expression in WT, $\Delta kinB$, $\Delta algR$, and $\Delta algU$ strains of *P. aeruginosa* after growth in liquid culture. They found that in the $\Delta kinB$ strain the levels of Cas and Csy proteins decreased relative to WT, whereas this expression was greatly increased in $\Delta algR$ and $\Delta algU$ strains. In other words, it was found that KinB promotes CRISPR-Cas protein expression, whereas AlgR and AlgU repress it. Thus, alginate biosynthesis inhibits CRISPR-Cas protein expression¹⁹. This directly opposes proposed trends about bacterial adaptive immunity in high-density populations and in biofilms. It has been previously suggested that since biofilm communities are more susceptible to phage infections due to high cell density and slow growth, these bacteria would exhibit exceptionally high levels of adaptive immunity^{13,19}. However, the alginate synthesis pathway, which is induced during biofilm formation, inhibits CRISPR systems. This discrepancy could be partially rationalized by the fact that alginate is not absolutely required for the formation of nonmucoid biofilms in *P. aeruginosa*¹⁷. Still, with very few studies comparing CRISPR-Cas activity in free-growing bacteria and biofilm communities, the effects of biofilm-related factors on the immune system's

regulation remains controversial. The research group tried to tackle this question and they showed in subsequent experiments that the effects of alginate synthesis molecules on adaptive immunity seem to partially depend on the organization of the bacterial community. It was reported that the downstream signaling molecule AmrZ can only control CRISPR-Cas immunity during surface-association and has no effect during planktonic growth. The group hypothesized that his state-dependent regulation could be an attempt at minimizing self-toxicity in bacteria during lifestyle transition¹⁸. Additionally, there is some data that suggests the possibility of regulatory feedback loops between CRISPR-Cas systems and biofilm-associated genes, as studies of the *Salmonella enterica* species have revealed that mutation of the cas3 gene resulted in reduced biofilm formation and virulence²⁰. Overall, the regulation of the CRISPR-Cas system in biofilms has not been completely characterized, but the research presented above demonstrates that networks of proteins can have distinct opposing or additive effects on bacterial immunity.

Antibiotics and the Rcs response: Stress less and live longer

As previously mentioned, viruses are not the only source of foreign genetic elements that bacteria are exposed to—they also frequently encounter plasmids that encode a variety of properties that can confer selective advantages. Antibiotic resistance genes are typically transferred between species via plasmids, thus at times it can be advantageous for the bacteria to repress its immune defenses. There are two general classes of antibiotics distinguished by their mechanisms of action and their effect on bacterial metabolism. Bacteriostatic antibiotics target a protein that is indispensable for cellular replication which results in growth arrest. Bactericidal antibiotics interfere with a process required for cell survival and subsequently cause cell death.

To evaluate how immunity evolves in bacterial populations when exposed to antibiotics, Dimitriu et al. infected *P. aeruginosa* PA14 strain with phage DMS3vir in nutrient-rich media supplemented with sub-inhibitory concentrations of 4 bacteriostatic and 4 bactericidal antibiotics. Bactericidal antibiotics exerted minimal effects on CRISPR-Cas immunity, whereas a significant proportion of the population upregulated this defense mechanism upon treatment with bacteriostatic antibiotics. To determine which phase of the CRISPR-Cas immunity was enhanced upon bacteriostatic antibiotic treatment, short-term infection assays in the presence or absence of antibiotics were carried out. None of the antibiotics caused an increase in Cas protein abundance. However, it was found that bacteriostatic antibiotics increased the rate of spacer acquisition, whereas bactericidal antibiotics had no effect. To test if the increased spacer acquisition was due to increased DNA damage, the research group quantified the expression of the DNA-repair SOS stress response. There was no correlation between SOS induction and the evolution of CRISPR immunity. Alternatively, an interesting pattern emerged between bacteriostatic antibiotics and slow growth. It was found that bacteria treated with bacteriostatic antibiotics released less phages upon infection, compared to cells treated with bactericidal antibiotics. Since the replication and spread of phages depends on host machinery, the reduced phage production was attributed to slower growth rate. Thus, bacteriostatic antibiotics increase CRISPR immunity via slowed cellular growth rather than stresses induced by the drug on the bacteria²¹ (**Figure 2**).

However, different stress responses can exert distinct effects on CRISPR-Cas regulation. When networks of genes that regulate CRISPR-Cas adaptive immunity in *Serratia* were screened, components of the Rcs stress response were identified. The regulator of capsular polysaccharide synthesis (Rcs) is a stress response to a variety of factors such as bactericidal β -lactam antibiotics²². Upon interaction between a stressor and the outer membrane lipoprotein RcsF, the inhibitory activity of IgaA on the signal phosphorelay will be lifted and allow downstream proteins RcsA and RcsB to positively regulate *rsc* genes²² (**Figure 2**). A mutagenesis analysis found that $\Delta igaA$ resulted in the greatest fold decrease of *csm* gene expression amongst all regulators screened²². Subsequent deletion of the *rscA* or the *rscB* genes in the $\Delta igaA$ mutant background restored *csm* expression levels by abolishing signaling through the Rcs response. Additionally, IgaA mutation abolished CRISPR-Cas immunity, induced minimal array expansion, and resulted in acquisition of antibiotic resistance genes. Upon deletion of downstream *rscA* or *rscB* genes, CRISPR-Cas immunity was restored²².

Similarly, a genome-wide analysis of Rcs-regulated genes in the plant-pathogenic bacterium *Erwinia amylovora* found that mutation of RcsC resulted in decreased expression of type I-E CRISPR-Cas system²³. Overall, adaptive immunity is disfavored by the Rcs response upon membrane stress. The induction of the Rcs response results in decreased expression of Cas proteins, adaptation, and interference of both type I and type III CRISPR systems in *Serratia*. Smith et al. suggested that the downregulation of CRISPR-Cas immunity upon antibiotic-induced surface membrane stress might be an evolutionary advantageous technique that can favor genetic sampling and the acquisition of antibiotic-resistance genes²². This explanation remains incomplete, as other sensors of cell envelope disruption such as BaeR in *E. coli* have been shown to promote Cas expression²⁴. Nevertheless, the experiments studying the Rcs phosphorelay pathway underpin a stress-dependent regulation pattern of the CRISPR-Cas system.

Comparing the available data regarding the effects of antibiotics on CRISPR-Cas regulation reveals a sharp contradiction amongst published results. On one hand, bacteriostatic antibiotics were shown to promote spacer acquisition and the evolution of CRISPR immunity²¹. In contrast, stress responses induced by antibiotic treatment demonstrated an inhibition of the CRISPR-Cas adaptation, interference, and effector proteins expression²². These results could be accounted for by the differential metabolic and signaling effects of bacteriostatic and bactericidal antibiotics. Yet, the only definitive takeaway is that distinct molecules such as antibiotics can induce multiple pathways that exert differential effects on CRISPR-Cas regulation.

Growth rate: One variable to unite them all

When interpreting the effects of various sensors on the regulation of CRISPR-Cas immunity, it can be useful to consider the evolutionary competition between bacteria and the viruses that invade them. The dynamics between phages and their hosts can be described as an arms-race where each

has been shown to influence the expression of *cas* genes and the overall strength of the immune response. In conditions of iron deprivation or in the presence of suboptimal carbon sources—which decreases bacterial proliferation—there is a heightened expression and activity of the CRISPR-Cas immunity^{21,25}.

There have been mixed results regarding the activity of the CRISPR-Cas machinery during the different phases of growth. Some groups report high activity of bacterial immunity during the exponential growth phase where bacteria replicate at a fast pace, and repression of the system during the stationary phase where bacteria replicate quite slowly¹⁸. Other groups have reported that the highest frequency of adaptation occurs during the late-exponential growth phase where bacterial growth rate declines²⁶.

Using growth rate as the primary determinant for CRISPR-Cas regulation is not an empirically true framework. As previously described, the alginate biosynthetic marker *amrZ* decreases *Csy1* expression upon-surface association but has no effect during planktonic growth¹⁸. This contradicts the growth-rate theory as alginate is produced during biofilm formation where slow-growing surface-associated bacteria are expected to exhibit high CRISPR-Cas activity. Applying growth rate analysis to predict the expression of the CRISPR-Cas system might not accurately describe the effects of all sensors in all conditions, but it might still be useful to explain the interaction of multiple sensors.

Conclusion

There is a seemingly endless array of signaling pathways that can be examined to identify the sensors of CRISPR-Cas regulation. In this review paper, data was gathered about components from the quorum-sensing system, biofilm formation, bacterial alginate synthesis, antibiotic treatments, and the Rcs stress response (Table 1). These networks are of particular interest given their relevance in clinical settings and therapeutic approaches such as genome editing and phage therapies.

Despite the contradictory nature of the data, it has been demonstrated that regulation is both species-specific and strain-specific, small alterations in external conditions can alter the relative influence of different regulatory pathways, and regulation varies with bacterial community organization, external stressors, and growth conditions.

Overall, the regulation of the CRISPR-Cas system is multi-dimensional and lies at the crossroads of numerous intracellular pathways. Within a single organism, different types of CRISPR-Cas systems can be regulated differently²². Considering that these different systems can share components such as conserved Cas proteins, it can become increasingly difficult to understand the effects of various regulators and sensors.

Our understanding of CRISPR-Cas regulation remains far from complete. From the data gathered in this review, we propose a few future avenues of research to fill the gaps. Firstly, the use of clinically isolated strains for molecular studies may be advantageous as these bacteria can behave very differently from the model organisms predominantly utilized thus far.

Secondly, studying bacteria encoding a single type of CRISPR system, concurrently with bacteria encoding multiple types of CRISPR systems would provide critical information about the nuances in regulation. As mentioned, different types of CRISPR systems encode conserved proteins with similar functions which renders data interpretation more convoluted. Adding single-system controls would enable a better understanding of system types co-regulation. Thirdly, when assessing the expression level of *cas* genes under various conditions, it is necessary to test more than a single subject protein, especially if Cas genes are induced by distinct promoters. Finally, future studies should consider the effect of various regulators and sensors through a growth-rate lens, as this might provide a unifying insight into the dynamics controlling CRISPR-Cas.

Regulator	System type	Mechanism	Step regulated
LasI: LasR RhII: RhIR	I-F	Signaling through quorum sensing signals at high cell densities	Adaptation Biogenesis Interference
SmaI: SmaR	I-E, I-F, III-A	Repressing quorum sensing signals at low cell densities	Adaptation Biogenesis Interference
Temperature	Range undefined	Controls growth rate, stabilizes complexes and binding	Adaptation
AlgR, AlgU	I-F	Transcriptional regulation during planktonic growth	Biogenesis
AmrZ	I-F	Transcriptional regulation during surface-association	Biogenesis
KinB	I-F	Prevents the accumulation of alginate-producing factors in acute virulence; promotes the latter in chronic virulence	Biogenesis
Bacteriostatic antibiotics	I-F	Slow bacterial growth rate	Adaptation
RcsA, RcsB	I-E, I-F, III-A	Signaling through the Rcs stress response pathway upon antimicrobial encounter or membrane alterations	Adaptation Biogenesis Interference
IgaA	I-E, I-F, III-A	Represses the Rcs stress response under normal conditions	Adaptation Biogenesis Interference

Table 1. A summary of regulators involved in CRISPR control.

opponent aims to damage the other. Bacteria must coordinate cell division with spacer acquisition, whereas phages must exploit the host machinery while avoiding bacterial adaptive immunity. Naturally, the growth rate has been suggested as an important factor in controlling the CRISPR-Cas machinery. It is hypothesized that slow bacterial growth rate might enable the bacteria to acquire spacers from the invading phage and integrate the genetic sequence to the spacer array before the phage can exit and lyse the cell¹³.

This framework can be used to explain some of the results described here: low temperature, biofilm growth, and bacteriostatic antibiotic treatment all induce conditions where bacterial growth rate is limited, and CRISPR-Cas adaptation is favored. Similarly, the availability of certain nutrients

Acknowledgements

Infinite gratitude to Dr. Jasmin Chahal who periodically guided and encouraged this writing process.

References

1. Mojica, F. J., Díez-Villaseñor, C., García-Martínez, J. & Soria, E. Intervening sequences of regularly spaced prokaryotic repeats derive from foreign genetic elements. *J. Mol. Evol.* **60**, 174-182 (2005). <https://doi.org/10.1007/s00239-004-0046-3>
2. Ishino, Y., Shinagawa, H., Makino, K., Amemura, M. & Nakata, A. Nucleotide sequence of the *iap* gene, responsible for alkaline phosphatase isozyme conversion in *Escherichia coli*, and identification of the gene product. *J. Bacteriol.* **169**, 5429-5433 (1987). <https://doi.org/10.1128/jb.169.12.5429-5433.1987>
3. Hille, F. et al. The Biology of CRISPR-Cas: Backward and Forward. *Cell.* **172**, 1239-1259 (2018). <https://doi.org/10.1016/j.cell.2017.11.032>
4. Makarova, K. S. et al. An updated evolutionary classification of CRISPR-Cas systems. *Nat. Rev. Microbiol.* **13**, 722-736 (2015). <https://doi.org/10.1038/nrmicro3569>
5. Westra, E. R., van Houte, S., Gandon, S. & Whitaker, R. The ecology and evolution of microbial CRISPR-Cas adaptive immune systems. *Philos. Trans. R. Soc. Lond. B. Biol. Sci.* **374**, 20190101 (2019). <https://doi.org/10.1098/rstb.2019.0101>
6. Makarova, K. S. et al. Evolutionary classification of CRISPR-Cas systems: a burst of class 2 and derived variants. *Nat. Rev. Microbiol.* **18**, 67-83 (2020). <https://doi.org/10.1038/s41579-019-0299-x>
7. Watson, B. N., Steens, J. A., Staals, R. H., Westra, E. R. & van Houte, S. Coevolution between bacterial CRISPR-Cas systems and their bacteriophages. *Cell Host Microbe.* **29**, 715-725 (2021). <https://doi.org/10.1016/j.chom.2021.03.018>
8. Weissman, J. L., Stoltzfus, A., Westra, E. R. & Johnson, P. L. Avoidance of self during CRISPR immunization. *Trends in microbiology.* **28**, 543-553 (2020). <https://doi.org/10.1016/j.tim.2020.02.005>
9. Shivram, H., Cress, B. F., Knott, G. J. & Doudna, J. A. Controlling and enhancing CRISPR systems. *Nat. Chem. Biol.* **17**, 10-19 (2021). <https://doi.org/10.1038/s41589-020-00700-7>
10. Preda, V. G. & Sandulescu, O. Communication is the key: biofilms, quorum sensing, formation and prevention. *Discoveries (Craiova)* **7**, e100 (2019). <https://doi.org/10.15190/d.2019.13>
11. Wu, L. & Luo, Y. Bacterial Quorum-Sensing Systems and Their Role in Intestinal Bacteria-Host Crosstalk. *Front. Microbiol.* **12**, (2021). <https://doi.org/10.3389/fmicb.2021.611413>
12. Mion, S., Plener, L., Rémy, B., Daudé, D. & Chabrière, É. Lactonase SsoPox modulates CRISPR-Cas expression in gram-negative proteobacteria using AHL-based quorum sensing systems. *Res. Microbiol.* **170**, 296-299 (2019). <https://doi.org/10.1016/j.resmic.2019.06.004>
13. Høyland-Kroghsbo, N. M., Muñoz, K. A. & Bassler, B. L. Temperature, by controlling growth rate, regulates CRISPR-Cas activity in *Pseudomonas aeruginosa*. *mBio.* **9**, e02184-18 (2018). <https://doi.org/10.1128/mBio.02184-18>
14. Broniewski, J. M., Chisnall, M. A. W., Høyland-Kroghsbo, N. M., Buckling, A. & Westra, E. R. The effect of Quorum sensing inhibitors on the evolution of CRISPR-based phage immunity in *Pseudomonas aeruginosa*. *I.S.M.E. J.* **15**, 2465-2473 (2021). <https://doi.org/10.1038/s41396-021-00946-6>
15. Chand, N. S., Clatworthy, A. E. & Hung, D. T. The two-component sensor KinB acts as a phosphatase to regulate *Pseudomonas aeruginosa* Virulence. *J. Bacteriol.* **194**, 6537-6547 (2012). <https://doi.org/10.1128/jb.01168-12>
16. David, S. R., Maheshwaram, S. K., Shet, D., Lakshminarayana, M. B. & Soni, G. V. Temperature dependent in vitro binding and release of target DNA by Cas9 enzyme. *Sci. Rep.* **12**, 15243 (2022). <https://doi.org/10.1038/s41598-022-19485-x>
17. Wozniak, D. J. et al. Alginate is not a significant component of the extracellular polysaccharide matrix of PA14 and PAO1 *Pseudomonas aeruginosa* biofilms. *Proc. Natl. Acad. Sci. U.S.A.* **100**, 7907-7912 (2003). <https://doi.org/10.1073/pnas.1231792100>
18. Borges, A. L. et al. Bacterial alginate regulators and phage homologs repress CRISPR-Cas immunity. *Nat. Microbiol.* **5**, 679-687 (2020). <https://doi.org/10.1038/s41564-020-0691-3>
19. Patterson, A. G., Yevstigneyeva, M. S. & Fineran, P. C. Regulation of CRISPR-Cas adaptive immune systems. *Curr. Opin. Microbiol.* **37**, 1-7 (2017). <https://doi.org/10.1016/j.mib.2017.02.004>
20. Cui, L. et al. CRISPR-cas3 of *Salmonella* Upregulates Bacterial Biofilm Formation and Virulence to Host Cells by Targeting Quorum-Sensing Systems. *Pathogens.* **9**, 53 (2020). <https://doi.org/10.3390/pathogens9010053>
21. Dimitriu, T. et al. Bacteriostatic antibiotics promote CRISPR-Cas adaptive immunity by enabling increased spacer acquisition. *Cell Host Microbe.* **30**, 31-40. e35 (2022). <https://doi.org/10.1016/j.chom.2021.11.014>
22. Smith, L. M. et al. The Rcs stress response inversely controls surface and CRISPR-Cas adaptive immunity to discriminate plasmids and phages. *Nat. Microbiol.* **6**, 162-172 (2021). <https://doi.org/10.1038/s41564-020-00822-7>
23. Wang, D. et al. Genome-wide identification of genes regulated by the Rcs phosphorelay system in *Erwinia amylovora*. *Mol. Plant Microbe Interact.* **25**, 6-17 (2012). <https://doi.org/10.1094/mpmi-08-11-0207>
24. Perez-Rodriguez, R. et al. Envelope stress is a trigger of CRISPR RNA-mediated DNA silencing in *Escherichia coli*. *Mol. Microbiol.* **79**, 584-599 (2011). <https://doi.org/10.1111/j.1365-2958.2010.07482.x>
25. Ahator, S. D., Jianhe, W. & Zhang, L.-H. The ECF sigma factor PvdS regulates the type I-F CRISPR-Cas system in *Pseudomonas aeruginosa*. *bioRxiv.* 2020.2001.2031.929752 (2020). <https://doi.org/10.1101/2020.01.31.929752>
26. Amlinger, L., Hoekzema, M., Wagner, E. G. H., Koskiniemi, S. & Lundgren, M. Fluorescent CRISPR Adaptation Reporter for rapid quantification of spacer acquisition. *Sci. Rep.* **7**, 10392 (2017). <https://doi.org/10.1038/s41598-017-10876-z>

The Role of Iron in Epidermal Healing and Infection

Abstract

In recent years, the field of iron studies has expanded into sub-domains that investigate the regulation of this metal in various tissues including the heart, mucosal surfaces, tumors, and the skin. Iron homeostasis in the skin and the role of other non-hepatic cells in the regulation of iron are currently incompletely understood. This paper summarizes the role of iron in wound healing, highlights the importance of maintaining iron concentrations within an intermediate range to avoid toxicity or defects; and integrates the antimicrobial role, interactions, and regulation of various cell types. Notably, the autoregulation of hepcidin secretion by keratinocytes and recruited myeloid cells is described. Additionally, the potential therapeutic role of iron chelators in infection control and their mechanisms of action are explored. This paper aims to elucidate the relevance of local iron control in epidermal infections. Although some of the molecular details underlying this condition remain unclear, published data suggest that iron-regulating therapies are a promising treatment for the eradication of skin infections due to their wound-healing and immune-modulating potential.

Keywords

Iron, wound healing, hepcidin, skin infection, chelators

Email Correspondence

idia.boncheva@mail.mcgill.ca

<https://doi.org/10.26443/msurj.v18i1.188>

© The Authors. This article is published under a CC-BY license: <https://creativecommons.org/licenses/by/4.0/>

Introduction

Iron plays a central role in the housekeeping processes in our cells and organs, making it one of the most essential components of our diet. Its functions are so vital that our bodies have evolved distinct ways to recycle iron rather than excrete it, as they have for other nutrients¹. A healthy individual ingests approximately 10-20 mg of iron daily¹. However, only 10% is absorbed into the circulation, while the rest is lost as waste². Additionally, around 1-2 mg of iron is shed daily in bodily fluids and through skin desquamation¹. The absorption of iron from our dietary intake is accomplished in the upper part of the digestive tract via various import proteins such as divalent metal transporter-1 (DMT-1) and heme carrier protein 1 (HCP1) on the surface of enterocytes². The details of this step vary with the ionic form and the protein-association state of iron².

Subsequently, iron is transported in the blood via plasma transferrin². Transferrin is an iron-binding protein which delivers the vital metal to the liver and the spleen for storage, and to all other cells in our body for their survival². Iron is vital because it is located within internal structures such as the iron-sulfur clusters of complexes within the electron-transport chain (ETC) in the mitochondrial membrane³. These iron-containing structures are required for the proteins to generate an electrochemical gradient which can subsequently be used to produce ATP—the predominant energy source in cellular metabolism³. Unbound iron is found in the body only at very low levels, as most of it is associated with ferritin and hemosiderin which are intracellular iron-storage proteins¹. Transferrin will also deliver iron to the bone marrow for erythropoiesis¹. Around 20 mg of iron is used up every day in the bone marrow for the formation of red blood cells¹. Such an investment is made because iron is an essential component of hemoglobin, the protein that binds, transports, and delivers oxygen through the blood to the entire body². Once red blood cells die, the iron that is held within them is processed by macrophages and brought back to the bone marrow to resume the cycle (Figure 1)^{1,2,4}.

Despite its abundance in nature, iron has low bioavailability as it is predominantly found in its insoluble ferric form (Fe^{3+})⁵. This has made it a highly coveted metal by all life forms, including microorganisms. In fact, bacteria have developed specialized iron uptake mechanisms to acquire this metal from the environment⁴. For example, siderophores are small organic molecules that diffuse out of bacteria, tightly bind extracellular iron, and deliver the metal to microbes through the reabsorption of iron-siderophore complexes⁵. Different bacterial species have evolved other enzymatic or receptor-mediated iron-uptake

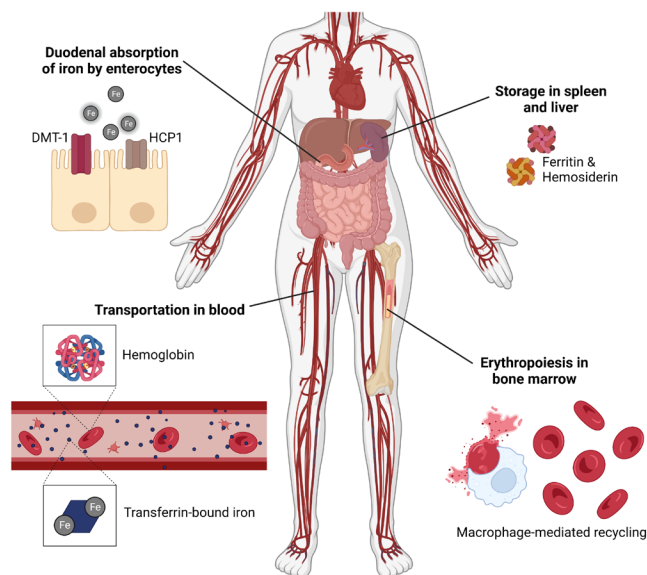


Figure 1. Simplified schematic of iron cycling in the body 1,2.

systems to optimize nutritional scavenging in their particular niches⁵. In the context of infection, these microbes will try to acquire iron from our cells. In response, our body will set off an immune defense mechanism that will sequester iron from the environment and stunt the proliferation of the invaders⁵. In a phenomenon called hypoferrremia of inflammation, individuals who develop an infection see their plasma iron levels decrease within hours⁵. This is one of the many mechanisms our bodies use to fight against microbes.

With predictions of increasing antibiotic resistance, there is an increased need for alternative antimicrobial protocols to treat infections. This review paper summarizes selected topics relating to the role of iron in wound healing and pathogen control in local skin infections. Additionally, it evaluates the potential therapeutic use of iron chelators on topical wounds. This review aims to gather and integrate the current knowledge and evidence in this emerging field to facilitate the modulation of iron homeostasis in the treatment of infections.

The Role of Iron in Skin Wound Healing

Even in the absence of infection, iron has a complex influence on our skin's health and healing. Upon tissue damage, the skin must undergo a series of temporally coordinated, dynamic, and locally controlled repair mechanisms¹. For instance, blood clotting, inflammation, immediate vascular responses, re-epithelialization, glandular tissue formation, and angiogenesis are a few of the vital steps involved in cutaneous wound healing¹. Many cells, such as keratinocytes, which are the primary cell type composing our skin, fibroblasts, and innate immune cells such as macrophages, are involved in this phenomenon⁶. This becomes even further convoluted when we consider chronically disturbed wound healing where the role of iron is heterogeneous⁶.

In healthy individuals, the concentration of iron in the skin, as measured by X-ray fluorescence, is around 10.22.5 µg per gram of dry weight, but this can greatly vary amongst the sites measured⁷. For instance, neutron activation analysis (NAA) of the abdomen epidermis records iron concentrations of 90.245.2 µg g⁻¹ in groups of healthy individuals⁷. There is also a wide variation in skin iron concentrations for different skin disease conditions and between individuals with the same disease⁷. Regardless of these differences, analysis of iron functions suggests that extreme concentrations can be damaging; high iron levels can cause cell death, whereas low levels impair wound healing.

At one end of this spectrum, iron can be toxic to cells due to reactive oxygen species (ROS) generated via the Fenton reaction¹. In this reaction, ferrous iron (Fe²⁺) reacts with hydrogen peroxide to generate ferric iron (Fe³⁺), hydroxide, and a hydroxyl radical⁸. Subsequently, ferrous iron can be regenerated via the superoxide-driven Fenton reaction⁸. Thus, low amounts of iron can power the Fenton reaction via this redox cycling (Figure 2)^{8,9}. The combination of high iron and abundant ROS can drive ferroptosis, a non-apoptotic programmed cell death that triggers the release of inflammatory immunogenic intracellular molecules and induces necroinflammation¹⁰. Mitochondria are a major source of ROS, as altered mitochondrial DNA upon cell damage increases the production of these small molecules¹¹. In fact, it was found that mitochondrial alterations within wound fibroblasts can impede the healing process by affecting nuclear transcription events, motility, and growth¹¹. Although ROS can be beneficial in combatting invading microbes, they are detrimental to the host at high concentrations upon prolonged periods as this perpetuates a non-healing state¹¹. Thus, local iron regulation is vital for homeostasis. To avoid the buildup of this waste product, labile iron can be released from keratinocytes¹⁰. The iron released into the extracellular environment minimizes intracellular oxidative damage¹. Additionally, intracellular iron storage proteins such as ferritin, and iron-regulatory proteins (IRPs), which are transcriptional regulators of iron-associated proteins, can regulate labile iron availability independently of systemic iron control such as to avoid toxicity¹².

At the other end of the spectrum, there is evidence suggesting that low iron levels can also be detrimental to skin regeneration¹. For example, in a comparative study, Sprague-Dawley rats were made anemic by weekly bleeding for 6 weeks and were fed a low-iron diet¹³. These rats were wounded by laparotomy incisions and the wound tensile strength was assessed 7 days later by the Howes method, which measures the force required to pull apart a segment of wound^{13,14}. It was found that the healing rate in iron-supplemented rats was on average twice as strong than in the low-iron group, as measured by wound tensile strength¹³. Additionally, there is evidence suggesting that increased local iron levels can be beneficial in wound healing¹⁵. For instance, lactoferrin is a glycoprotein that binds iron when it is released by glandular epithelial cells into various body fluids such as maternal milk, saliva, tears, and mucosal secretions¹⁵. When lactoferrin is present in infected tissues and pus, it locally concentrates iron which raises the initial levels of inflammation after injury, increases cell proliferation and recruitment, and enhances fibroblast-mediated collagen contraction¹⁵. Similarly, it was also found that iron concentrations were enhanced in animal wound-healing models compared to baseline¹⁶. Lewis rats were subjected to dorsal biopsy punctures, and the levels of iron were measured at various time points after injury via inductively coupled plasma mass spectrometry (ICP-MS) to assess the levels of iron at different healing stages¹⁶. The levels of iron recorded peaked during the proliferation phase which involves keratinocyte migration to the surface of the wound, granulation by fibroblasts, and neovascularization¹⁶. Thus, in some cases, iron can be an essential element for healing.

The studies described in this section indicate that neither iron-overload nor iron-deficiency is beneficial to our skin. The evidence summarized in this section is somewhat contradictory as elevated iron levels can potentially be toxic to cells due to ROS, but normal wound healing in rodents depends on iron abundance. This suggests an optimal level of iron must be maintained in the body under normal conditions and upon injury to promote healing.

Hepcidin Control of Myeloid Cells in Infection

To better understand how the iron levels in the body are balanced, outlining its regulators is vital. Hepcidin is the iron-regulating hormone. This peptide is encoded by the *HAMP* gene, and it is mainly secreted by hepatocytes². Hepcidin engages different interference mechanisms to promote the accumulation of iron inside cells and reduce iron export. It can either downregulate the expression of ferroportin—the only known iron-exporting membrane protein—and stimulate its degradation, or at higher plasma concentrations, hepcidin can directly block the efflux of iron through ferroportin^{5,17}. These functions have established hepcidin as an integrative regulator of iron in the body. For instance, upon microbial exposure, the cytokine-rich environment resulting from infection will promote systemic hepatocyte-derived hepcidin production⁵. Under high hepcidin concentrations, iron will be sequestered inside the cells and its availability to invading pathogens in extracellular fluids will be reduced⁴.

Hepcidin is also starting to be understood as an important molecule on a local scale, particularly in the skin. For instance, keratinocytes have been established as local modulators of hepcidin and as immunomodulatory cells during skin infections¹⁸. Indeed, histological staining of cross-sectional human skin biopsies has shown that keratinocyte production of hepcidin is increased in patients with cutaneous Group A *Streptococcus* (GAS) infection, compared to healthy patients¹⁸. Infections with GAS are the most common cause of necrotizing fasciitis (NF), which has a 35% mortality rate, so investigating the effect of iron on immune responses is of particular interest for this condition¹⁸. In a pioneer study done by Malerba et al. (2020), GAS NF was used as a model of skin infection to investigate the control of iron upon microbial attack¹⁸. Mutant mouse models with a keratinocyte-specific knockout in the *HAMP* gene were engineered. The mutant mice showed unchanged systemic iron parameters compared to normal mice, indicating that keratinocyte-derived hepcidin does not play a role in systemic iron control, which is mainly controlled by hepcidin-derived hepatocytes. However, the mutant mice did not secrete hepcidin in the infected tissue, whereas wild-type mice did. This result demonstrates that hepcidin stains in skin tissue of patients infected with GAS are a prod

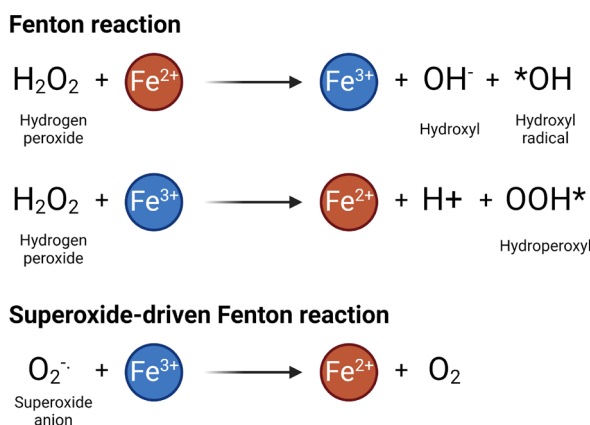


Figure 2. Generation of ROS via the Fenton reaction and the related superoxide-anion driven Fenton chemistry 3,4.

uct of keratinocyte secretion rather than systemic production by hepatocytes. Additionally, local hepcidin injection in the infected mice prevented the progression of a systemic disease, further emphasizing this peptide's antimicrobial role. Thus, hepcidin may be a marker for NF as it is upregulated in patients with this condition, and this iron-regulation hormone may also have protective roles against pathogens in skin infections as its presence is associated with a lower disease burden¹⁸.

Interestingly, the therapeutic effects of hepcidin are lost in mice with knockouts in the CXCL1 gene, the functional homologue of human IL-8¹⁸. This is because hepcidin prevents the dissemination of GAS infection via a chemokine-dependent pathway¹⁸. The IL-8/CXCL1 chemokines are known as chemotactic factors that recruit neutrophils and other granulocytes¹⁸. The pro-inflammatory cytokine CXCL1 is secreted by keratinocytes upon hepcidin binding to the corresponding surface receptor ferroportin¹⁸. Subsequently, this chemokine recruits and activates myeloid cells that play an essential role in the innate immune response upon infection or injury (Figure 3)¹⁸⁻²⁰. A defect in chemokine secretion by keratinocytes results in a failure to limit the spread of a microbe from a localized infection to a systemic one¹⁸. Additionally, both neutrophils and macrophages in subcutaneous compartments can secrete hepcidin upon recognition of microbial antigens in a TLR-4 dependent manner¹⁹. Indeed, mice mutants in this pattern recognition receptor cannot induce hepcidin production upon exposure to GAS 19. The details of this relationship have not yet been characterized, but it appears that keratinocytes and myeloid cells can protect our body from serious infections via a hepcidin-mediated regulatory feedback loop (Figure 3).

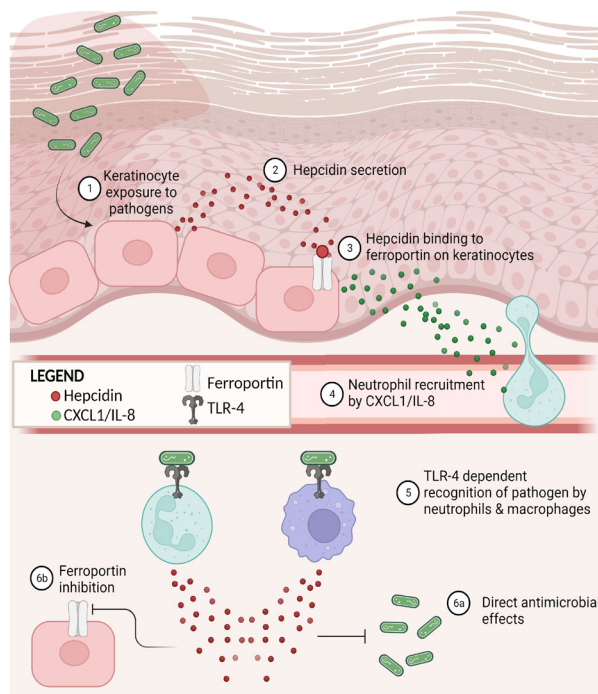


Figure 3. Regulatory feedback loop of hepcidin production and myeloid cell recruitment 5-7.

It is also possible that the relationship between iron and innate immune cells is more complex due to the presence of various iron-binding factors. For instance, the genetic deletion of ferroportin on macrophages will induce the retention of intracellular iron and affect various steps of skin homeostasis and repair such as stromal cell proliferation, angiogenesis, and fibrogenesis²¹. This is hypothesized to be a result of defective iron redistribution to neighboring cells, highlighting the importance of macrophages in skin regeneration²¹. Iron is also essential for the tissue repair functions of macrophages as the accumulation of this metal will induce the differentiation of macrophages into an M2 pro-healing phenotype that produces a

high level of wound-healing chemokines²². Additionally, neutrophils have been shown to depend on the iron-binding lactoferrin protein for their characteristic oxidative bursts²³. This functional response releases potent antimicrobial ROS into the environment, contributing to host defense²³.

Overall, hepcidin is an interesting candidate for the treatment of infections such as NF because it can provide protective effects against microorganisms by interacting with the surface receptors of immune cells and because hepcidin is able to camouflage itself from the invading microbes which lack a direct defense against hepcidin. It is also important to not overlook the importance of other iron-binding proteins and cell types, as these can greatly contribute to both innate immune modulation and tissue repair. Although more research must be done to characterize the self-regulatory mechanism of hepcidin in peripheral tissues, it can be hypothesized that the metabolism of iron in the skin is controlled by proximal cells, such as neutrophils, macrophages, and keratinocytes, and by locally secreted factors such as hepcidin, CXCL1/IL-8, and iron-associated factors.

Iron Chelators as Therapeutic Agents in Skin Infections

Iron chelators are synthetic or microbe-derived molecules that strongly bind iron via various chemical interactions⁴. There are multiple iron chelators that have long been approved for clinical use—Desferrioxamine (DFO), Deferiprone (DFP), and Deferasirox (DFX) are a few examples⁴. These diversely structured molecules will sequester the iron metal and enable its excretion through urine or feces²⁴. Iron-chelation therapy is primarily used to treat patients with iron-overload diseases which can be either genetic or acquired²⁴.

In clinical applications, the rationale for iron chelator therapy is analogous to how our bodies naturally mount a biological defense upon infection. Chelators will bind labile iron and reduce its accessibility to the invaders in the extra-cellular environment⁴. For example, DFX is a bidentate oral chelator with protective effects against *Candida albicans* infection⁴. Alternatively, the tridentate chelator DFP was shown to have beneficial effects in wound healing upon topical application in rodents, and in treating biofilms on surgical wounds of *in vitro* models of multi-drug resistant bacteria such as *Staphylococcus aureus* and *Pseudomonas aeruginosa*^{25,26}. A synthetic hydroxypyridinone-containing anti-microbial polymer called DIBI is another example of a promising iron chelator when tested *in vivo*. In fact, it was found to have a dose-dependent attenuation of *S. aureus* infection²⁷. This bacterium accounts for 84% of wound infections, half of which are methicillin-resistant staph aureus (MRSA)²⁷. When applied to the skin, DIBI reduced total bacterial titer and overall inflammation. This compound reduces the availability of iron to the pathogen and is particularly potent at fighting infections by enhancing the activity of the antibiotic it is combined with²⁷.

However, not all iron-chelators are good candidates: DFO—a hexadentate chelator—is not ideal for infection treatments, as it is derived from the *Streptomyces* bacterium, and it can be exploited by pathogens to favor their proliferation⁴. Furthermore, iron chelators are not yet used on a large scale for infection treatment because they are potentially toxic to cells and require high physiological concentrations to exert their therapeutic effects²⁷. Additionally, it is hypothesized that local iron chelation can have an impact on the immune capacity of tissues by impeding ROS production⁴. As previously established, reduced ROS can be either beneficial in tissue healing or disadvantageous in pathogen killing. There is great debate over the effect of chelators on the susceptibility to infections, especially after intravenous administration due to potential tissue toxicity²⁸. In general, topical application of any therapy reduces toxicity compared to systemic administration. Thus, local treatment of skin infection using iron chelators could present fewer risks, but the effects remain unclear.

Iron chelation therapy has great potential for its alternative application in infection control due to its indirect antimicrobial capacity and its anti-inflammatory potential. However, before it can be implemented as a standard treatment, we must first establish the adverse effects of the diverse chelators upon topical application and their chemical interactions with

different species of bacteria. Until then, it is recommended that the clinical use of iron chelators is done in a patient-specific and time-sensitive manner such as to minimize the dosage and avoid adverse effects²⁸.

Conclusion

The complex relationship between global iron homeostasis and local iron control is not entirely understood. Although the liver is responsible for the systemic control of iron levels in cells and fluids via hepcidin secretion, it does not account for local adaptive changes. The major research contributions described in this paper highlight the significance of local iron regulation in epidermal wound healing, the role of keratinocytes and myeloid cells in infection control via hepcidin and chemokine secretion, and the potential anti-microbial use of topical iron chelators. Analysis of these selected topics reveals that maintenance of iron levels within an intermediate range is essential for the homeostasis of tissue and organs, and that many innate immune cell functions are affected by iron and its associated factors. The vast role of iron in physiological functions renders it a critical subject of investigation with respect to skin conditions.

References

1. Wright, J. A., Richards, T. & Srai, S. K. The role of iron in the skin and cutaneous wound healing. *Front. Pharmacol.* **5**, 156 (2014). <https://doi.org/10.3389/fphar.2014.00156>
2. Waldvogel-Abramowski, S. et al. Physiology of iron metabolism. *Transfus. Med. Hemother.* **41**, 213-221 (2014). <https://doi.org/10.1159/000362888>
3. Merrill, J. F. et al. Iron deficiency causes a shift in AMP-activated protein kinase (AMPK) subunit composition in rat skeletal muscle. *Nutrition & Metabolism.* **9**, 104 (2012). <https://doi.org/10.1186/1743-7075-9-104>
4. Scott, C., Arora, G., Dickson, K. & Lehmann, C. Iron Chelation in Local Infection. *Molecules.* **26**, 189 (2021).
5. Ganz, T. Iron and infection. *Int. J. Hematol.* **107**, 7-15 (2018). <https://doi.org/10.1007/s12185-017-2366-2>
6. Eming, S. A., Martin, P. & Tomic-Canic, M. Wound repair and regeneration: mechanisms, signaling, and translation. *Sci. Transl. Med.* **6**, 265sr266 (2014). <https://doi.org/10.1126/scitranslmed.3009337>
7. Bagshaw, A. P. & Farquharson, M. J. Simultaneous determination of iron, copper and zinc concentrations in skin phantoms using XRF spectrometry. *X-Ray Spectrometry.* **31**, 47-52 (2002). <https://doi.org/https://doi.org/10.1002/xrs.535>
8. Messner, D. J., Murray, K. F. & Kowdley, K. V. in *Physiology of the Gastrointestinal Tract (Fifth Edition)* (eds Leonard R. Johnson et al.) 1507-1527 (Academic Press, 2012).
9. Meng, X. et al. Fenton reaction-based nanomedicine in cancer chemodynamic and synergistic therapy. *Appl. Mater. Today.* **21**, 100864 (2020). <https://doi.org/https://doi.org/10.1016/j.apmt.2020.100864>
10. Vats, K. et al. Keratinocyte death by ferroptosis initiates skin inflammation after UVB exposure. *Redox Biol.* **47**, 102143 (2021). <https://doi.org/10.1016/j.redox.2021.102143>
11. Janda, J., Nfonsum, V., Calienes, F., Sligh, J. E. & Jandova, J. Modulation of ROS levels in fibroblasts by altering mitochondria regulates the process of wound healing. *Archives of Dermatological Research.* **308**, 239-248 (2016). <https://doi.org/10.1007/s00403-016-1628-9>
12. Sandnes, M., Ulvik, R. J., Vorland, M. & Reikvam, H. Hyperferritinemia-A Clinical Overview. *J. Clin. Med.* **10** (2021). <https://doi.org/10.3390/jcm10092008>

[org/10.3390/jcm10092008](https://doi.org/10.3390/jcm10092008)

13. Bains, J. W., Crawford, D. T. & Ketcham, A. S. Effect of chronic anemia on wound tensile strength: correlation with blood volume, total red blood cell volume and proteins. *Ann. Surg.* **164**, 243-246 (1966). <https://doi.org/10.1097/00000658-196608000-00009>
14. Crawford, D. T., Bains, J. W. & Ketcham, A. S. A standard model for tensiometric studies. *J. of Surg. Res.* **5**, 265-269 (1965). [https://doi.org/10.1016/S0022-4804\(65\)80016-6](https://doi.org/10.1016/S0022-4804(65)80016-6)
15. Takayama, Y. & Aoki, R. Roles of lactoferrin on skin wound healing. *Biochem. Cell Biol.* **90**, 497-503 (2012). <https://doi.org/10.1139/o11-054>
16. Coger, V. et al. Tissue Concentrations of Zinc, Iron, Copper, and Magnesium During the Phases of Full Thickness Wound Healing in a Rodent Model. *Biol. Trace Elem. Res.* **191**, 167-176 (2019). <https://doi.org/10.1007/s12011-018-1600-y>
17. Nemeth, E. et al. Hepcidin Regulates Cellular Iron Efflux by Binding to Ferroportin and Inducing Its Internalization. *Science.* **306**, 2090-2093 (2004). <https://doi.org/10.1126/science.1104742>
18. Malerba, M. et al. Epidermal hepcidin is required for neutrophil response to bacterial infection. *J. Clin. Invest.* **130**, 329-334 (2020). <https://doi.org/10.1172/jci126645>
19. Peyssonnaud, C. et al. TLR4-dependent hepcidin expression by myeloid cells in response to bacterial pathogens. *Blood.* **107**, 3727-3732 (2006). <https://doi.org/10.1182/blood-2005-06-2259>
20. Barthe, C., Hocquelllet, A. & Garbay, B. Bacteriostatic activity of the proregion of human hepcidin. *Protein Pept. Lett.* **18**, 36-40 (2011). <https://doi.org/10.2174/092986611794328627>
21. Recalcati, S. et al. Macrophage ferroportin is essential for stromal cell proliferation in wound healing. *Haematologica.* **104**, 47-58 (2019). <https://doi.org/10.3324/haematol.2018.197517>
22. Wilkinson, H. N. et al. Tissue Iron Promotes Wound Repair via M2 Macrophage Polarization and the Chemokine (C-C Motif) Ligands 17 and 22. *Am. J. Path.* **189**, 2196-2208 (2019). <https://doi.org/10.1016/j.ajpath.2019.07.015>
23. Ward, P. P., Mendoza-Meneses, M., Park, P. W. & Conneely, O. M. Stimulus-Dependent Impairment of the Neutrophil Oxidative Burst Response in Lactoferrin-Deficient Mice. *Am. J. Path.* **172**, 1019-1029 (2008). <https://doi.org/10.2353/ajpath.2008.061145>
24. Mobarra, N. et al. A Review on Iron Chelators in Treatment of Iron Overload Syndromes. *Int. J. Hematol. Oncol. Stem Cell Res.* **10**, 239-247 (2016).
25. Richter, K. et al. A Topical Hydrogel with Deferiprone and Gallium-Protoporphyrin Targets Bacterial Iron Metabolism and Has Antibiofilm Activity. *Antimicrob. Agents Chemother.* **61**, e00481-00417 (2017). <https://doi.org/10.1128/AAC.00481-17>
26. Mohammadpour, M., Behjati, M., Sadeghi, A. & Fassihi, A. Wound healing by topical application of antioxidant iron chelators: kojic acid and deferiprone. *Int. Wound. J.* **10**, 260-264 (2013). <https://doi.org/10.1111/j.1742-481X.2012.00971.x>
27. Parquet, M. d. C., Savage, K. A., Allan, D. S., Davidson, R. J. & Holbein, B. E. Novel Iron-Chelator DIBI Inhibits Staphylococcus aureus Growth, Suppresses Experimental MRSA Infection in Mice and Enhances the Activities of Diverse Antibiotics in vitro. *Front. Microbiol.* **9** (2018). <https://doi.org/10.3389/fmicb.2018.01811>
28. Rund, D. Intravenous iron: do we adequately understand the short- and long-term risks in clinical practice? *Br. J. Haematol.* **193**, 466-480 (2021). <https://doi.org/10.1111/bjh.17202>

¹Department of Microbiology and Immunology, McGill University, Montreal, QC, Canada

Keywords

Myeloid-derived suppressor cells, Tuberculosis, Immunity

Email Correspondence

angela.nelson@mail.mcgill.ca

<https://doi.org/10.26443/msurj.v18i1.189>

© The Author. This article is published under a CC-BY license: <https://creativecommons.org/licenses/by/4.0/>

Angela Nelson¹

At Once Friends and Foes: Myeloid-Derived Suppressor Cells in Human Tuberculosis

Abstract

Mycobacterium tuberculosis (*Mtb*) is the causative agent of human tuberculosis (TB) disease. In chronic infections such as TB, consistent pro-inflammatory signalling promotes the generation of myeloid-derived suppressor cells (MDSCs). MDSCs are innate immune cells that are further divided into polymorphonuclear (PMN-MDSC) and monocytic (M-MDSC) subtypes on the basis of their morphology. These cells exert immunosuppressive effects on other immune cell types, thereby protecting the integrity of the lung tissue from damage caused by dysregulated *Mtb*. However, this comes at the expense of containing the *Mtb* infection. MDSCs' unique double-edged role makes them an attractive target for host-directed TB therapeutics. This review aims to summarize current knowledge on the role of MDSCs in TB.

Introduction

Before the COVID-19 pandemic, *Mycobacterium tuberculosis* (*Mtb*) was the deadliest single infectious agent worldwide. In 2021, 1.6 million people died from tuberculosis (TB)^{1,2}. *Mtb* is transmitted from person to person through aerosolized droplets that travel through the respiratory tract to the alveoli of the lungs, where it begins to replicate³. If the host's immune system can contain the infection without eliminating it, this is considered a latent TB infection (LTBI); *Mtb* will not cause symptoms nor spread to others⁴. There are two types of active TB disease: primary TB and TB reactivation. In the former, the host will produce an inadequate immune response to control bacterial replication. They will then become symptomatic and may spread *Mtb*^{5,6}. In the latter, immunosuppression will allow a previously contained infection (LTBI) to spread. This could be due to physical damage to the lung tissue, taking immunosuppressant drugs, or HIV co-infection^{7,8}. Standard treatment for TB disease is a combination of antibiotics and usually lasts 4-9 months⁹. First-line treatment has an 85% success rate with strict adherence to the regimen⁹. As patients initiate second- and even third-line therapy, the risk of their infection becoming drug-resistant increases⁹. Drug-resistant cases of TB are difficult to treat, and the financially and physically taxing treatment regimen can engender compliance issues among patients, leading to worse health outcomes¹⁰.

With antimicrobial resistance on the rise and precious few antibiotics in development, new strategies to combat TB are necessary. A better understanding of the immune response to *Mtb* could lead to the development of host-directed therapeutics such as vaccines. An emergent immune cell type in TB disease is the myeloid-derived suppressor cell (MDSC)¹¹. Originally studied in cancer, these cells have potent immunosuppressive activity¹². This review aims to describe an updated understanding of MDSCs' role in TB as both a protective and pathogenic cell type, at once limiting tissue damage and preventing *Mtb* clearance.

Methods

This review was conducted on PubMed and Google Scholar with the search terms, ("Tuberculosis" OR "*Mtb*") AND ("myeloid-derived sup-

pressor cell" OR "MDSC"). The most recent review in the field of MDSCs in TB was published in April 2019 by Magcwebeba et al.¹¹. Thus, the search period was adjusted to include papers published since 2019. Primary research articles were vetted for relevance to the topic, and additional background information on immunology and/or *Mtb* was located in primary research articles' citations, reputable reviews, or public health/government organizations' websites.

Myeloid-derived suppressor cells

MDSCs are a heterogeneous collection of immature neutrophils and monocytes¹³. As implied by their name, MDSCs originate in the bone marrow (myeloid) and have potent immunosuppressive activity¹³. Myeloid cells are a part of the innate immune response, which is typically activated in response to danger-associated molecular patterns (DAMPs) and pathogen-associated molecular patterns (PAMPs) through a series of pattern-recognition receptors (PRRs), of which the most prominent are toll-like receptors (TLRs)¹⁴.

Innate immune cells are recruited to the site of immunological threats by the release of attractant cytokines by damaged cells. Myeloid cells will then help clear pathogens through degranulation or phagocytosis¹⁵.

Macrophages, dendritic cells (DCs), and monocytes are all phagocytes; they will ingest target particles into the phagosome, a specialized vacuole, which will then mature to become the phagolysosome¹⁶. This organelle contains digestive enzymes to degrade the ingested particles¹⁶.

Neutrophils are the most abundant type of granulocytes, but they are also capable of phagocytosis¹⁷. In addition, they may release a neutrophil extracellular trap (NET), composed of the DNA contents of the neutrophil coated in cytoplasmic and granular proteins, with the goal of containing pathogens¹⁷.

MDSCs develop in prolonged states of inflammation, such as in cancer, persistent infections (e.g., active TB), sepsis, and autoimmunity¹³. In these

conditions, bone marrow precursors are consistently exposed to myeloid growth factors and inflammatory signals, such as granulocyte-macrophage colony-stimulating factor (GM-CSF), macrophage colony-stimulating factor (M-CSF), IL-1 β , IL-6, and cellular stress signalling¹⁸. MDSCs are mainly classified into two subtypes: granulocytic/polymorphonuclear MDSC (PMN-MDSC) and monocytic MDSC (M-MDSC), which have granulocytic and monocytic myeloid precursors, respectively¹⁸. PMN-MDSCs share cell surface markers with neutrophils (CD11b+CD14-CD15+/CD66b+) but PMN-MDSCs have lower density than neutrophils and distinct functionality¹⁹. M-MDSCs are CD14+CD15-HLA-DRlo/-, and they are distinguished from monocytes by low major histocompatibility complex class II (MHC-II) expression¹⁸. These methods of differentiating MDSCs from their brethren cell types are not infallible, however, and more accurate ways of characterizing MDSCs is an active area of research.

In patients with TB, MDSC subtype frequency has been found to be associated with disease severity; MDSCs generally are found more frequently in peripheral blood of patients with active TB versus LTBI²⁰. Within the group of patients with active TB, however, those with lower disease severity score had increased proportions of PMN-MDSCs compared to those with high disease severity score²⁰. These findings imply that MDSCs are not strictly pathogenic, and the PMN-MDSC subtype in particular may have a protective role in active TB^{20,21}.

Insults in the lung will induce the activation of an inflammatory state termed the inflammasome²². In its acute form, this state aids in the clearance of insults and preservation of lung function²³. In a prolonged *Mtb* infection, immune activation can be pathogenic. The inflammasome is first induced by PRR sensing of PAMPs or DAMPs, then leading to the cleavage of pro-Interleukin-1 β (pro-IL-1 β) to its active form, Interleukin-1 (IL-1 β)²². IL-1 β is highly inflammatory and drives fibrosis in the lung; excessive fibrotic tissue will impair respiration²⁴. As well, *Mtb*-infected macrophages release inflammatory cytokines tumour necrosis factor (TNF) and Interleukin-6 (IL-6), as well as attractant chemokines which recruit other inflammatory cell types, including monocytes, neutrophils, natural killer cells, and T cells²⁵. All of these cell types have been shown to produce matrix metalloproteinases (MMPs)²⁶. Excessive production of MMPs will degrade the extracellular matrix (ECM) to the point of outpacing tissue regeneration and lead to the formation of cavities in the lung (cavitation)²⁶. The induction of MDSCs, particularly PMN-MDSCs, is likely a homeostatic mechanism to limit inflammation and preserve lung function. Conversely, the dampened immune response might compromise the containment of *Mtb* and result in TB reactivation.

Human immunity against *Mtb*

In the typical response to *Mtb*, DCs encounter and phagocytose *Mtb* at the site of infection, then migrate to the lymph node to present *Mtb* antigens to naïve CD4+ T cells with T cell receptors (TCRs) specific to the *Mtb* antigen. Once activated by this interaction, *Mtb*-specific CD4+ T cells expand and mature and begin to produce pro-inflammatory cytokines; IFN- γ is of particular importance in anti-*Mtb* immunity, as it is responsible for activating macrophages²⁷. Alveolar macrophages (AMs) reside in the lung and are one of the first points of immune contact for *Mtb*. However, they are less effective in clearing *Mtb* via phagocytosis than interstitial macrophages (IM), which are recruited later in the response to infection²⁸.

CD8+ T cells, or cytotoxic T cells, may also directly kill *Mtb* by producing the cytolytic protein granulysin²⁹. CD4+ and CD8+ T cells are both typically activating cell types. T regulatory cells (Tregs) are key players in negative immune regulation³⁰. In short, Tregs release anti-inflammatory cytokines and bind other immune cells' receptors to diminish or completely shut down their function³¹.

When the immune system cannot clear *Mtb* infection, the next best thing is to limit bacterial spread by walling it off. Innate and adaptive immune cells will aggregate into a structure called the granuloma³². The granuloma is duplicitous as it prevents *Mtb* from spreading further, but also provides a niche which cannot be accessed by incoming immune cells, thus allowing *Mtb* to replicate within³². This structure is common in LTBI³³; the patient

may continue without symptoms indefinitely, provided a lapse in immunity does not occur, in which case *Mtb* may be reactivated⁷.

MDSCs' suppression of T helper function

In persistent *Mtb* infection, the frequency of MDSCs in peripheral blood correlates negatively with T cell responsiveness to *Mtb* antigens³⁴. An emerging body of evidence favours a causal relationship, as MDSCs produce factors that impede T cell functionality.

M-MDSCs, like macrophages, can produce nitric oxide (NO). However, where macrophages' NO production acidifies the phagolysosome and promotes *Mtb* lysis, MDSCs' NO production also mediates T helper cell suppression, and thus can promote *Mtb* survival³⁵. In patients with active TB, MDSCs highly express inducible nitric oxide synthase (NOS2), an enzyme that synthesizes NO^{36,37}. High levels of NO will nitrosylate the TCR and promote the degradation of its zeta-chain. Without a complete TCR, T cells have impaired antigen recognition and, because of this, will not effectively respond to immunological threats³⁸. PMN-MDSCs express reactive oxygen species (ROS) to a similar effect^{37,39}. However, in chronic infection, PMN-MDSCs' anti-immune function may be beneficial to curb tissue damage inflicted by the prolonged immune response²⁰.

MDSCs from active TB patients also express arginase-1 (ARG1), an enzyme that depletes L-arginine^{37,40}. The amino acid L-arginine is essential to T cell fitness and survival—without it, T cells have diminished cytokine production, proliferation, and expression of the TCR^{41,42}.

TB patients' MDSCs have also been shown to increase CD62L expression in T helper cells, although the mechanism is unclear⁴³. CD62L is a cell surface marker that promotes T cell trafficking to the lymph nodes⁴⁴. This marker is usually found on naïve T cells, and shedding CD62L is a critical step in their maturation, i.e., activation⁴⁴. This finding could either imply that MDSCs are preventing T cell maturation or that they are inducing mature T cells to begin expressing CD62L once again, impeding their ability to localize to the lung.

In a nonhuman primate study of TB, researchers found that MDSCs from macaques with active TB expressed interleukin-10 (IL-10) and programmed death-ligand 1 (PD-L1) at significantly higher levels than MDSCs from healthy controls and macaques with LTBI⁴⁵. IL-10 is an anti-inflammatory cytokine that can act on many cell types⁴⁶. It can first prevent dendritic cells from trafficking to the lymph node, which is a crucial step to T cell activation⁴⁶. Further, IL-10 can directly impact CD4+ T cells by inhibiting proliferation and inflammatory cytokine production, one of which is IFN- γ —as a downstream effect of MDSCs' IL-10 production, macrophage activation will be hindered⁴⁶. IL-10 will also act more immediately on macrophages by inhibiting a bactericidal phenotype and antigen presentation capabilities⁴⁶. The same effect of IL-10 is seen in monocytes⁴⁶. Upon TCR stimulation, T helper cells express programmed cell death protein 1 (PD-1), which binds PD-L1⁴⁷. The PD-L1/PD-1 interaction inhibits the activation, proliferation, and survival of all T helper cells. In the CD8+ subset, this interaction inhibits cytotoxic secretion⁴⁸. In a healthy individual, this mechanism serves to prevent pathological immune activation, where T cells continue to respond to and generate inflammatory signals to an immunological threat that no longer exists and thereby cause damage to the host. Additionally, MDSCs' PD-L1 expression could be directed at maintaining the hypoxic environment of the granuloma; when peripheral blood mononuclear cells (PBMCs) were infected with *Mtb* and then treated with anti-PD1 immunotherapy, TNF- α was secreted in excess, and this increased *Mtb* growth⁴⁹.

MDSCs would require close proximity to T cells to inhibit them through the PD-L1/PD-1 interaction, as well as through production of NO, NOS, ARG1, and IL-10⁵⁰. A non-human primate model of TB showed that T cells surround the granuloma, and a similar model placed MDSCs at the same location^{45,51}. This localization both supports MDSCs' ability to exert immunosuppressive functions on T cells, as well as their support of the hypoxic granuloma.

On the basis of similar findings in cancer, MDSCs have also been proposed to induce Tregs in TB¹². Tregs are present in significantly higher frequencies in the blood of patients with active TB and LTBI than in healthy controls, but MDSCs have yet to be proven to be implicated in this phenomenon⁵².

Phagocytosis and metabolic changes

Mtb may evade immune detection by persisting intracellularly in the phagosomes of macrophages, particularly in the granuloma⁵³. Once infected with *Mtb*, macrophages in the granuloma switch from glycolysis to lipid metabolism—this shift promotes the accumulation of intracellular lipid droplets (LD), which then favours further differentiation into “foamy” macrophages. *Mtb* can then use the fatty acids (FAs) and cholesterol contained in foamy macrophages’ LDs as an energy source⁵⁴. Whether this metabolic shift is a protective mechanism to curb *Mtb* growth or is somehow induced by *Mtb* to provide itself with an energy source is contentious, as the molecular mechanism of this change during TB is unknown⁵⁵.

As M-MDSCs share phagocytic abilities and a myeloid ancestor with macrophages, it has been hypothesized that they may also harbour *Mtb* and undergo similar metabolic changes. A recent study with M-MDSCs from TB patients showed that this cell subset had increased expressions of soluble proteins and cell surface markers involved in phagocytosis and that these proteins and markers significantly decreased after disease treatment, suggesting that M-MDSCs have increased phagocytic abilities in *Mtb* infection⁵⁶.

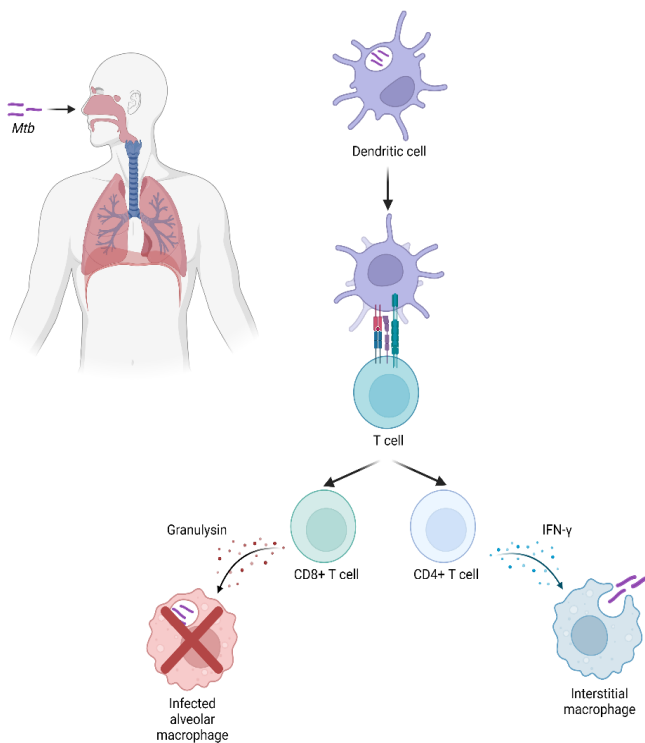


Figure 1. Summary of successful response to *Mtb* threat. *Mtb* enters the host’s respiratory tract and travels to the lungs. DCs will phagocytose the bacteria, and present antigens to T cells in the lymph node. Once activated, CD8+ T cells can kill infected macrophages by releasing granulysin, and CD4+ T cells can activate uninfected macrophages to properly lyse bacteria by releasing IFN- γ . Created with Biorender.com.

Moreover, proteins in the signalling pathway regulating the metabolic switch and LD formation are also upregulated in TB, and research in cancer found that immunosuppressive MDSCs rely primarily on lipid metabolism for their energetic demands³⁹. This evidence suggests a metabolic dimension of MDSCs’ pathogenicity, but no study has shown either *Mtb*’s inhabitation of M-MDSCs or MDSCs’ switch to lipid metabolism in TB.

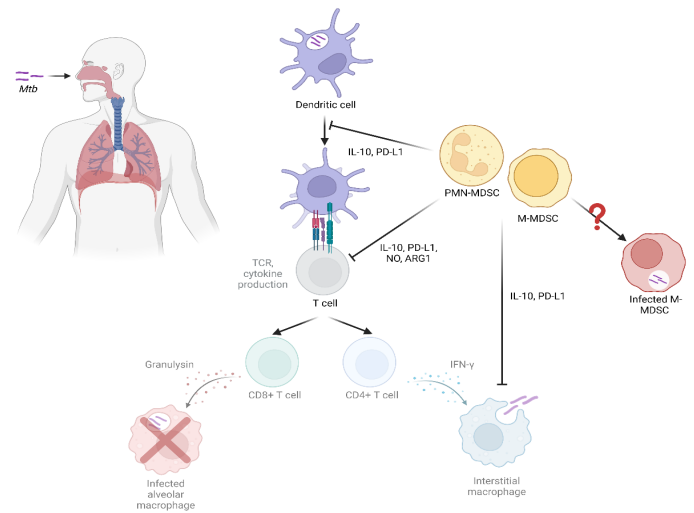


Figure 2. Summary of proposed mechanisms of MDSC intervention in chronic *Mtb* infection. MDSCs are proposed to interfere in the immune response at many levels. Expression of IL-10 and PD-L1 may inhibit DC antigen presentation as well as macrophage activation. In addition, NO and ARG1 production can inhibit T cells’ cytokine production as well as TCR stability. M-MDSCs are also suspected reservoirs for *Mtb*. Created with Biorender.com.

Conclusion

The interplay between *Mtb* and the immune system is multifaceted and complex. Myeloid-derived suppressor cells have surfaced as important players in this interaction in recent years, after their discovery in cancer. These cells of myeloid origin are induced in response to chronic inflammation and dampen T helper cell function through the sequestration of L-arginine and the release of NO, ROS, and soluble factors. This homeostatic balance is delicate, and if the infection is not resolved, long-term immunosuppression enables *Mtb* growth. Although intended to preserve lung function, MDSC induction can be ultimately detrimental to the host. To add another shade of nuance to this picture, MDSC subtypes, PMN-MDSCs and M-MDSCs, seem to have differing pathogenicity; PMN-MDSCs have been implicated in a more protective role, while M-MDSCs are hypothesized to alter their metabolism to provide nutrients for intracellular *Mtb* bacteria, promoting their growth and sheltering them from immune detection.

The picture, however, is not complete. On the basis of findings in cancer, additional immunosuppressive mechanisms of MDSCs have been proposed, such as killing DCs and inducing Tregs, but they have not been validated in TB³⁹. As well, no research has probed MDSCs’ interactions with other TB-relevant members of the innate immune compartment, that is, macrophages, natural killer cells, DCs, and neutrophils⁵⁷. Finally, the hypothesized intracellular infection with *Mtb* and altered metabolism of M-MDSCs, although well-supported, remains a hypothesis. More research is required before M-MDSCs can be seriously considered as a target for therapeutic intervention to limit niche availability for *Mtb*, be that through inhibition of phagocytosis or of their hypothesized metabolic reorganization. PMN-MDSCs would be less immediately effective in *Mtb* clearance, but their immunoregulatory abilities could be harnessed to improve outcomes of chronic infections.

References

1. World Health Organization. Tuberculosis (2022); <https://www.who.int/news-room/fact-sheets/detail/tuberculosis>
2. X., Hong, W., Pan, X., Lu, G. & Wei, X. SARS-CoV-2 Omicron variant: Characteristics and prevention. *MedComm*. 2, 838-845 (2021). <https://doi.org/10.1002/mco2.110>

3. Shiloh, M. U. Mechanisms of mycobacterial transmission: how does *Mycobacterium tuberculosis* enter and escape from the human host. *Future Microbiol.* **11**, 1503-1506 (2016). <https://doi.org/10.2217/fmb-2016-0185>
4. Kiazzyk, S. & Ball, T. B. Latent tuberculosis infection: An overview. *Can. Commun. Dis. Rep.* **43**, 62-66 (2017). <https://doi.org/10.14745/ccdr.v43i34a01>
5. Lyon, S. M. & Rossman, M. D. Pulmonary Tuberculosis. *Microbiol. Spectr.* **5**, 5.1.24 (2017). <https://doi.org/doi:10.1128/microbiolspec.TNMI7-0032-2016>
6. Latent TB Infection and TB Disease, <https://www.cdc.gov/tb/topic/basics/tbinfectiondisease.htm> (2020).
7. Jacobs, R. E. A., Gu, P. & Chachoua, A. Reactivation of pulmonary tuberculosis during cancer treatment. *Int. J. of Mycobacteriol.* **4**, 337-340 (2015). <https://doi.org/10.1016/j.ijmyco.2015.05.015>
8. Gupta, A., Kaul, A., Tsolaki, A. G., Kishore, U. & Bhakta, S. Mycobacterium tuberculosis: Immune evasion, latency and reactivation. *Immunobiology* **217**, 363-374 (2012). <https://doi.org/10.1016/j.imbio.2011.07.008>
9. Centers for Disease Control and Prevention. Treatment for TB Disease(2022); <https://www.cdc.gov/tb/topic/treatment/tbdisease.htm>
10. Zürcher, K. et al. Mortality from drug-resistant tuberculosis in high-burden countries comparing routine drug susceptibility testing with whole-genome sequencing: a multicentre cohort study. *Lancet Microbe* **2**, e320 (2021). [https://doi.org/10.1016/S2666-5247\(21\)00044-6](https://doi.org/10.1016/S2666-5247(21)00044-6)
11. Magcwebeba, T., Dorhoi, A. & du Plessis, N. The Emerging Role of Myeloid-Derived Suppressor Cells in Tuberculosis. *Front. Immunol.* **10**, 917 (2019). <https://doi.org/10.3389/fimmu.2019.00917>
12. Albeituni, S. H., Ding, C. & Yan, J. Hampering immune suppressors: therapeutic targeting of myeloid-derived suppressor cells in cancer. *Cancer J.* **19**, 490-501 (2013). <https://doi.org/10.1097/ppo.0000000000000006>
13. Talmadge, J. E. & Gabrilovich, D. I. History of myeloid-derived suppressor cells. *Nat. Rev. Cancer* **13**, 739-752 (2013). <https://doi.org/10.1038/nrc3581>
14. Kawai, T. & Akira, S. The role of pattern-recognition receptors in innate immunity: update on Toll-like receptors. *Nat. Immunology* **11**, 373-384 (2010). <https://doi.org/10.1038/ni.1863>
15. Bassler, K., Schulte-Schrepping, J., Warnat-Herresthal, S., Aschenbrenner, A. C. & Schultze, J. L. The Myeloid Cell Compartment—Cell by Cell. *Annu. Rev. Immunol.* **37**, 269-293 (2019). <https://doi.org/10.1146/annurev-immunol-042718-041728>
16. Uribe-Querol, E. & Rosales, C. Phagocytosis: Our Current Understanding of a Universal Biological Process. *Front. Immunol.* **11** (2020). <https://doi.org/10.3389/fimmu.2020.01066>
17. Kroon, E. E. et al. Neutrophils: Innate Effectors of TB Resistance? *Front. Immunol.* **9** (2018). <https://doi.org/10.3389/fimmu.2018.02637>
18. Veglia, F., Sanseviero, E. & Gabrilovich, D. I. Myeloid-derived suppressor cells in the era of increasing myeloid cell diversity. *Nat. Rev. Immunol.* **21**, 485-498 (2021). <https://doi.org/10.1038/s41577-020-00490-y>
19. Gabrilovich, D. I. Myeloid-Derived Suppressor Cells. *Can. Immunol. Res.* **5**, 3-8 (2017). <https://doi.org/10.1158/2326-6066.Cir-16-0297>
20. Grassi, G. et al. PMN-MDSC Frequency Discriminates Active Versus Latent Tuberculosis and Could Play a Role in Counteracting the Immune-Mediated Lung Damage in Active Disease. *Front. Immunol.* **12** (2021). <https://doi.org/10.3389/fimmu.2021.594376>
21. Grassi, G. et al. PMN-MDSC Frequency Discriminates Active Versus Latent Tuberculosis and Could Play a Role in Counteracting the Immune-Mediated Lung Damage in Active Disease. *Front. Immunol.* **12**, 594376 (2021). <https://doi.org/10.3389/fimmu.2021.594376>
22. Pinkerton, J. W. et al. Inflammasomes in the lung. *Molec. Immunol.* **86**, 44-55 (2017). <https://doi.org/10.1016/j.molimm.2017.01.014>
23. Moldoveanu, B. et al. Inflammatory mechanisms in the lung. *J. Inflamm. Res.* **2**, 1-11 (2009).
24. Borthwick, L. A. The IL-1 cytokine family and its role in inflammation and fibrosis in the lung. *Semin. Immunopathol.* **38**, 517-534 (2016). <https://doi.org/10.1007/s00281-016-0559-z>
25. Tiwari, D. & Martineau, A. R. Inflammation-mediated tissue damage in pulmonary tuberculosis and host-directed therapeutic strategies. *Sem. Immunol.* **65**, 101672 (2023). <https://doi.org/10.1016/j.smim.2022.101672>
26. Squeglia, F., Ruggiero, A. & Berisio, R. Collagen degradation in tuberculosis pathogenesis: the biochemical consequences of hosting an undesired guest. *Biochem. J.* **475**, 3123-3140 (2018). <https://doi.org/10.1042/bcj20180482>
27. Cavalcanti, Y. V. N., Brelaz, M. C. A., Neves, J. K. d. A. L., Ferraz, J. C. & Pereira, V. R. A. Role of TNF-Alpha, IFN-Gamma, and IL-10 in the Development of Pulmonary Tuberculosis. *Pulm. Med.* **2012**, 745483 (2012). <https://doi.org/10.1155/2012/745483>
28. Huang, L., Nazarova, E. V., Tan, S., Liu, Y. & Russell, D. G. Growth of *Mycobacterium tuberculosis* in vivo segregates with host macrophage metabolism and ontogeny. *J. Exp. Med.* **215**, 1135-1152 (2018). <https://doi.org/10.1084/jem.20172020>
29. Lin, P. L. & Flynn, J. L. CD8 T cells and *Mycobacterium tuberculosis* infection. *Semin. Immunopathol.* **37**, 239-249 (2015). <https://doi.org/10.1007/s00281-015-0490-8>
30. Kondělková, K. et al. Regulatory T cells (TREG) and their roles in immune system with respect to immunopathological disorders. *Acta Medica (Hradec Kralove)* **53**, 73-77 (2010). <https://doi.org/10.14712/18059694.2016.63>
31. Pentcheva-Hoang, T., Corse, E. & Allison, J. P. Negative regulators of T-cell activation: potential targets for therapeutic intervention in cancer, autoimmune disease, and persistent infections. *Immunologic. Rev.* **229**, 67-87 (2009). <https://doi.org/10.1111/j.1600-065X.2009.00763.x>
32. Sholeye, A. R. et al. Tuberculous Granuloma: Emerging Insights From Proteomics and Metabolomics. *Front. Neurol.* **13** (2022). <https://doi.org/10.3389/fneur.2022.804838>
33. Rubin, E. J. The Granuloma in Tuberculosis — Friend or Foe? *N. Engl. J. Med.* **360**, 2471-2473 (2009). <https://doi.org/10.1056/NEJMcibr0902539>
34. Amiano, N. O. et al. Circulating Monocyte-Like Myeloid Derived Suppressor Cells and CD16 Positive Monocytes Correlate With Immunological Responsiveness of Tuberculosis Patients. *Front. Cell. Infect. Microbiol.* **12** (2022). <https://doi.org/10.3389/fcimb.2022.841741>
35. Jamaati, H. et al. Nitric Oxide in the Pathogenesis and Treatment of Tuberculosis. *Front. Microbiol.* **8**, 2008 (2017). <https://doi.org/10.3389/fmicb.2017.02008>
36. Yang, B., Wang, X., Jiang, J., Zhai, F. & Cheng, X. Identification of CD244-expressing myeloid-derived suppressor cells in patients with active tuberculosis. *Immunol. Lett.* **158**, 66-72 (2014). <https://doi.org/10.1016/j.imlet.2013.12.003>

37. Leukes, V., Walzl, G. & du Plessis, N. Myeloid-Derived Suppressor Cells as Target of Phosphodiesterase-5 Inhibitors in Host-Directed Therapeutics for Tuberculosis. *Front. Immunol.* **11** (2020). <https://doi.org/10.3389/fimmu.2020.00451>
38. García-Ortiz, A. & Serrador, J. M. Nitric Oxide Signaling in T Cell-Mediated Immunity. *Trends Mol. Med.* **24**, 412-427 (2018). <https://doi.org/10.1016/j.molmed.2018.02.002>
39. Kotzé, L. A. et al. Mycobacterium tuberculosis and myeloid-derived suppressor cells: Insights into caveolin rich lipid rafts. *E Bio Medicine* **53**, 102670 (2020). <https://doi.org/10.1016/j.ebiom.2020.102670>
40. Obregón-Henao, A., Henao-Tamayo, M., Orme, I. M. & Ordway, D. J. Gr1(int)CD11b+ myeloid-derived suppressor cells in Mycobacterium tuberculosis infection. *PLoS One* **8**, e80669 (2013). <https://doi.org/10.1371/journal.pone.0080669>
41. Rodriguez, P. C., Quiceno, D. G. & Ochoa, A. C. L-arginine availability regulates T-lymphocyte cell-cycle progression. *Blood* **109**, 1568-1573 (2007). <https://doi.org/10.1182/blood-2006-06-031856>
42. Geiger, R. et al. L-Arginine Modulates T Cell Metabolism and Enhances Survival and Anti-tumor Activity. *Cell* **167**, 829-842.e813 (2016). <https://doi.org/10.1016/j.cell.2016.09.031>
43. du Plessis, N. et al. Increased frequency of myeloid-derived suppressor cells during active tuberculosis and after recent mycobacterium tuberculosis infection suppresses T-cell function. *Am. J. resp. crit. care med.* **188**, 724-732 (2013). <https://doi.org/10.1164/rccm.201302-0249OC>
44. Yang, S., Liu, F., Wang, Q. J., Rosenberg, S. A. & Morgan, R. A. The shedding of CD62L (L-selectin) regulates the acquisition of lytic activity in human tumor reactive T lymphocytes. *PLoS One* **6**, e22560 (2011). <https://doi.org/10.1371/journal.pone.0022560>
45. Singh, B. et al. Myeloid-Derived Suppressor Cells Mediate T Cell Dysfunction in Nonhuman Primate TB Granulomas. *mBio* **12**, e03189-03121 (2021). <https://doi.org/10.1128/mbio.03189-21>
46. Couper, K. N., Blount, D. G. & Riley, E. M. IL-10: The Master Regulator of Immunity to Infection. *J. Immunol.* **180**, 5771-5777 (2008). <https://doi.org/10.4049/jimmunol.180.9.5771>
47. Simon, S. & Labarriere, N. PD-1 expression on tumor-specific T cells: Friend or foe for immunotherapy? *Oncoimmunology* **7**, e1364828 (2017). <https://doi.org/10.1080/2162402x.2017.1364828>
48. Han, Y., Liu, D. & Li, L. PD-1/PD-L1 pathway: current researches in cancer. *Am. J. Cancer Res.* **10**, 727-742 (2020).
49. Tezera, L. B. et al. Anti-PD-1 immunotherapy leads to tuberculosis reactivation via dysregulation of TNF- α . *eLife* **9**, e52668 (2020). <https://doi.org/10.7554/eLife.52668>
50. Leukes, V. N. et al. Targeting of myeloid-derived suppressor cells by all-trans retinoic acid as host-directed therapy for human tuberculosis. *Cell. Immunol.* **364**, 104359 (2021). <https://doi.org/10.1016/j.cellimm.2021.104359>
51. Gideon, H. P. et al. Variability in tuberculosis granuloma T cell responses exists, but a balance of pro- and anti-inflammatory cytokines is associated with sterilization. *PLoS Pathog.* **11**, e1004603 (2015). <https://doi.org/10.1371/journal.ppat.1004603>
52. Stringari, L. L. et al. Increase of CD4+CD25highFoxP3+ cells impairs in vitro human microbicidal activity against Mycobacterium tuberculosis during latent and acute pulmonary tuberculosis. *PLOS Negl. Trop. Dis.* **15**, e0009605 (2021). <https://doi.org/10.1371/journal.pntd.0009605>
53. Maphasa, R. E., Meyer, M. & Dube, A. The Macrophage Response to Mycobacterium tuberculosis and Opportunities for Autophagy Inducing Nanomedicines for Tuberculosis Therapy. *Frontiers in Cell. Infect. Microbiol.* **10** (2021). <https://doi.org/10.3389/fcimb.2020.618414>
54. Howard, N. C. & Khader, S. A. Immunometabolism during Mycobacterium tuberculosis Infection. *Trends Microbiol.* **28**, 832-850 (2020). <https://doi.org/10.1016/j.tim.2020.04.010>
55. Laval, T., Chaumont, L. & Demangel, C. Not too fat to fight: The emerging role of macrophage fatty acid metabolism in immunity to Mycobacterium tuberculosis. *Immunol. Rev.* **301**, 84-97 (2021). <https://doi.org/10.1111/imr.12952>
56. Kotze, L. A. et al. Evaluation of autophagy mediators in myeloid-derived suppressor cells during human tuberculosis. *Cell. Immunol.* **369**, 104426 (2021). <https://doi.org/10.1016/j.cellimm.2021.104426>
57. Liu, C. H., Liu, H. & Ge, B. Innate immunity in tuberculosis: host defense vs pathogen evasion. *Cell. Mol. Immunol.* **14**, 963-975 (2017). <https://doi.org/10.1038/cmi.2017.88>

Bacterial Interactions Affecting Chemotherapy Effectiveness

Review Article

¹ School of Human Sciences,
University of Derby, Derby,
United Kingdom

Abstract

Chemotherapy resistance is a recurring challenge in cancer treatment, with specific bacteria impairing the effectiveness of certain chemotherapies. This study reviews three bacteria and their impact on chemotherapy drugs: *Mycoplasma* and gemcitabine, *Fusobacterium nucleatum* and oxaliplatin, bacterial β -glucuronase and irinotecan. Bacteria can have wide-ranging effects on cancer treatment; for instance, they may affect drug metabolism, alter toxin conversion, and encourage cancer growth. Whilst the presence of these bacteria was found to have a detrimental effect on the efficacy of chemotherapy treatment, we also consider wider interactions and interdependencies of the microbiota with drug treatments. Some cancer therapies depend on the delicate balance of the microbiome whilst simultaneously disrupting it by their very nature, particularly when antibiotics are introduced. Further research into the complex relationship between bacteria and the tumour micro-environment is needed. Treatments that focus on the immune-oncology microbiome axis or that explore genetic predisposition through the use of biomarkers could also support a more personalised approach.

Keywords

Chemotherapy resistance,
microbiotic interactions, bacteria,
gemcitabine, oxaliplatin,
irinotecan

Email Correspondence

j.chambers21@unimail.derby.ac.uk
t.illingworth@derby.ac.uk

<https://doi.org/10.26443/msurj.v18i1.190>

©The Authors. This article is
published under a CC-BY license:
<https://creativecommons.org/licenses/by/4.0/>

Introduction

Cancer presents an ongoing health burden globally, with an estimated 19.3 million new cases and 10 million deaths in 2020¹; it is estimated to be the first or second leading cause of death in 112 countries². Ageing populations contribute to this incidence rising by 47% by 2040¹, with early diagnosis and treatment considered key to improving prognosis and survival.

Chemotherapy has become a well-established cancer treatment since its initial use in the treatment of non-Hodgkin's lymphoma in the 1940s. It is frequently employed alongside other interventions including surgery, radiotherapy, and more recently immunotherapy³. Chemotherapy is usually administered intravenously or orally⁴, and uses cytotoxic or cytostatic drugs that can interfere with the cell cycle, preventing cell division and proliferation. These can include mitotic inhibitors, topoisomerase inhibitors, alkylating agents, cytotoxic antibiotics, and antimetabolites⁵. Chemotherapy targets non-specifically, so the maximum tolerated dose (MTD) needs to be high enough to be toxic to the cancerous cells without being excessively detrimental to a patient's quality of life⁶. Chemotherapy drug mechanisms depend on various factors such as the nature and location of the tumour. For example, nucleoside analogues such as gemcitabine are taken up through the cell membrane, and they disrupt DNA/RNA synthesis, and either halt the cell division cycle and prevent further cell proliferation (cytostatic), or cause lethal damage leading to apoptosis (cytotoxic)⁷.

However, chemotherapy resistance represents an ongoing challenge^{8,9} and frequently results in recurrence of the disease and reduced survival rates¹⁰. Bacterial interactions with chemotherapy drugs have been identified as a potential factor that may reduce the effectiveness of existing treatments^{9,11}.

Gemcitabine and *Mycoplasma*

Gemcitabine is a commonly prescribed nucleoside analogue antimetabolite chemotherapy prodrug primarily used to treat solid tumours in pancreatic, lung breast, blood, ovarian, bladder and non-small-cell lung cancers¹². As a hydrophilic drug, it is transported across the cell membrane by nucleoside transporters, phosphorylated by deoxycytidine into its active form as gemcitabine triphosphate, and finally incorporated into DNA and RNA¹². It cross-primers CD8+ T cells whilst suppressing myeloid-derived suppressor cells (MDSCs), which can otherwise act to downregulate adaptive immune T cell responses¹³. It enhances antigen presentation, downregulating checkpoint molecules and inducing tumour cell apoptosis through various pathways¹⁴. Although chemotherapy is generally associated with immune suppression, gemcitabine has also been shown to support an adaptive immune response^{14,15}.

Gemcitabine has been found to be metabolised into an inactive form at solid tumour sites by a long form cytidine deaminase enzyme produced by *Mycoplasma*, a gammaproteobacteria, which renders the treatment less effective or ineffective^{5,9,16,17}. Higher *Mycoplasma* infection rates in late-stage cancerous tumour samples compared to benign tissue infections were found in 76% of cancerous pancreatic cells compared to 15% of healthy pancreatic tissue samples⁹; 100% of surgically removed lung tissue was also found to be infected¹⁶. A higher ratio of *Mycoplasma* infection was found in stage 3-4 gastric cancer samples compared to stage 1-2 gastric cancer samples⁷. This higher occurrence of *Mycoplasma* in tumorous tissue is not yet fully understood⁵. The preferential colonisation of bacteria observed in these studies could arise from the nutrient-rich microenvironment of the tumour due to necrosis⁷ or hypoxic anaerobic conditions¹⁸. Although mycoplasmas usually prefer an aerobic environment, they can also function in the anaerobic environment found in dead or dying tissue. This environmental transition, which is often observed in necrosing tumour tissue, can cause increased production of bacterial toxins and provoke an immune response; the ensuing inflammation may also contribute to chemotherapy resistance¹⁹.

It is also thought that *Mycoplasma* has carcinogenic properties and may contribute to malignant transformations and metastasis²⁰ through the induction of chromosomal instability, oncogene overexpression, growth factor production, and apoptosis prevention⁷. This raises questions about cause and effect, and whether the bacteria is attracted to the environment of an existing tumour as an opportunistic resident, or if it is a causative agent for the tumour²¹.

The bacterial-mediated tumour resistance of gemcitabine is not limited to *Mycoplasma*; thirteen of the twenty-seven types of gammaproteobacteria were found to eradicate the effects of the drug⁹. *Escherichia coli* and γ -*amastigotes* are also associated with gemcitabine resistance^{11,17,18}. As *Mycoplasma* is far from being an isolated case, the broader range of bacteria interacting with cancer treatments may have far reaching implications as a subject for further research.

The administration of gemcitabine with antibiotics such as levofloxacin hydrate, cefdinir, ciprofloxacin, and meropenem hydrate has proven useful in improving treatment efficacy by eradicating bacteria^{17,22,23}.

Oxaliplatin and *Fusobacterium nucleatum*

Oxaliplatin is a platinum analogue of diaminocyclohexane¹¹, commonly used to treat cancer of the intestines, stomach, pancreas, and oesophagus. It is often administered in combination with other chemotherapy drugs such as cisplatin. Oxaliplatin's anti-tumour activity relies on the production of reactive oxygen species (ROS) in myeloid cells, which is stimulated by the gut microbiota. Gut microbes can prime tumour-infiltrating myeloid cells via the MYD88-dependent pathway for ROS production in response to chemotherapeutic drugs^{5,11}.

Increased ROS levels are indicative of oxidative stress. This leads to oxaliplatin genotoxicity, inhibiting the synthesis of RNA and DNA. Immunologic reactions are also triggered, with the release of tumour antigens and the translocation of calreticulin phagocytic markers to the cell surface. These promote danger-associated molecule pattern (DAMP) secretions, such as HMGB1 and ATP, which bind to receptors that promote the maturation of death cells and tumour-specific CD8+ T-cells^{5,11,14}.

Commensal bacteria and microbial metabolites also support oxaliplatin effectiveness by bolstering the immune system. Immunogenic bacteria such as *Bacteroides fragilis* and *Erysipelotrichaceae* work synergistically with antigenicity from epithelial cell apoptosis induced by oxaliplatin to stimulate B cell activation. Butyrate, a microbial metabolite, can enhance oxaliplatin efficacy by activating B cells and cytotoxic CD8+ T cells⁵.

Given that an intact microbiome is essential to the functioning of platinum drugs such as oxaliplatin⁷, gut microbiota disruption can contribute to chemotherapy resistance or failure. The use of antibiotics can interfere with the microbiome, reducing immune cell mediation of tumour suppressors and pro-inflammatory responses^{11,18}. Therefore, care should be taken when prescribing antibiotics and other additional medications alongside oxaliplatin to avoid reducing bacterial diversity, removing beneficial microbes, and having a potential detrimental impact on treatment responses^{5,24}.

Although the microbiome plays an important role in oxaliplatin efficacy, other types of bacteria can also have a detrimental effect on chemotherapy patients. *Fusobacterium nucleatum* is found to be more prevalent in colorectal cancer patients and is associated with worse prog-

nosis¹⁵ and greater colorectal tumourigenesis. This is due to FadA adhesin and E-cadherin interactions; it induces oxaliplatin chemoresistance by activating toll receptors and switching cell pathways from apoptosis to autophagy, resulting in tumour cell survival^{18,25,26}. *F. nucleatum* also contributes to mechanical hyperalgesia, causing sensitivity and pain response in the patient as a dose-limiting complication²⁶. These factors all contribute to the limited effectiveness or failure of oxaliplatin as a chemotherapy cancer treatment, and antibiotics are not always a suitable combination treatment due to the impact they can have on microbiome balance²².

Irinotecan and β -glucuronase

Irinotecan is an antineoplastic semisynthetic water-soluble analogue drug. It is S-phase specific, and inhibits DNA topoisomerase to interfere with DNA replication, transcription, and repair. This causes fatal double-stranded DNA breakage, leading to cell cycle arrest and apoptosis. It is a broad-spectrum chemotherapeutic used mostly in solid tumours, including in brain, gastric, colorectal, pancreatic, lung and ovarian cancers²⁷.

Although considered an effective chemotherapy drug, irinotecan use is problematic as it often comes with severe side effects²⁸. These include delayed diarrhoea (occurring more than 24 hours after administration, generally 5 days), neutropenia (low white blood cell count and impaired immunity), and sometimes an acute cholinergic reaction, resulting from inhibition of acetyl-cholinesterase activity by irinotecan within the first 24 hours of treatment^{27,28}.

These side effects are attributed to bacterial activity in the gastrointestinal tract. The active form of irinotecan, CPT-11, is administered intravenously and converted by carboxylesterase 2 into the active product SN-38, which subsequently activates anti-neoplastic activity and neutropenia²⁷. SN-38 is then detoxified in the liver by UGT1A1 through hepatic glucuronidation to produce SN-38G²⁹; however, upon excretion into the gut, bacterial β -glucuronase converts the drug back into the toxic SN-38 metabolite due the deconjugation and reactivation actions of β -glucuronidase³⁰. This causes gastric toxicity and intestinal mucosal damage, which in some patients can be severe to life-threatening^{5,27,31}. This means drug dosage is often lowered or treatment ceased before the end of treatment, rendering it less effective.

β -glucuronase inhibitors have proven useful alongside irinotecan to limit bacterial β -glucuronidase activity and epithelial damage, as seen in uronic isofagomine derivatives³². However, some studies have found that suppressing this activity could produce a secondary SN-38 peak due to enterohepatic recirculation, and the effect on CPT-11 anti-tumour effectiveness is not clear²⁹. Ciprofloxacin and other antibiotics have been found to reduce this recycling effect³³.

The microbiota-host-irinotecan axis has identified several supplementary treatments to alleviate the side effects of irinotecan³³. Benefits of probiotics such as *Bifidobacterium longum*^{28,34} and *Lactobacillus rhamnosus*³⁵ help to regulate the gut microbiota, and faecal microbiota transplantation has also been found effective²⁸. Berberine, a plant-based supplement, has been found to strengthen the gut lining, reduce inflammation, and increase production of goblet cells³⁶.

The ability to metabolise and clear irinotecan can vary ten-fold between patients, which has been partly attributed to polymorphisms in the gene encoding UGT1A1²⁷. Genotyping for these mutations may help to detect patients at high risk of irinotecan-induced gastric toxicity as a useful

biomarker for a more personalised treatment³⁷.

Discussion

Bacteria act as both a friend and a foe in chemotherapy treatment. While balanced bacterial interactions are necessary for immune system drug interactions⁷, some microbial interactions may also undermine chemotherapy treatment and thus contribute to chemotherapy resistance or failure. Examples include metabolising drugs before they can be effective, as seen in *Mycoplasma* with gemcitabine^{5,9,16}; acting as carcinogens as with *Fusobacterium nucleatum* and oxaliplatin^{18,20,25,26}; and producing toxins with side effects so severe that they are intolerable for the patient such as with β -glucuronase with irinotecan^{27,28,30,31}. Effects vary even between strains of the same species of bacteria. Notably, the non-enterotoxigenic strain of *Bacteroides fragilis* can enhance efficacy of oxaliplatin while the enterotoxigenic strain of this bacteria promotes colorectal cancer⁵.

Higher rates of bacterial infections in cancerous tumours^{7,9,16} suggest either a causal relationship as a carcinogen^{20,21}, an increased attraction of bacteria to the tumour micro-environment^{6,11,16,18}, or both; there is no consensus as of yet⁵.

Much emphasis is placed on the immune-oncology microbiome axis⁵ and the bi-directional actions of chemotherapy and the immune system¹¹. Effective chemotherapy treatment often relies on aspects of the immune system functioning properly; this is in turn reliant on a balanced microbiome. Chemotherapy treatment can disrupt this balance, contributing to chemotherapy resistance and failure³⁰. This is seen for example in the microbiota-host-irinotecan axis³⁶.

Although antibiotics are useful for treating some cases of bacterial-mediated resistance such as with gemcitabine²³, these drugs are notorious for causing gut dysbiosis and biome imbalance^{25,34}, so caution must be taken when prescribing these to immunocompromised chemotherapy patients. An emphasis on complementary treatments such as probiotics and faecal microbiota transplants can be a supplementary way to support the immune system as well as the natural balance of the gut, particularly where platinum drugs such as oxaliplatin and irinotecan are being used^{28,34,35,36,38}.

Understanding an individual's predisposition to bacterial chemotherapy resistance with the use of biomarkers and genotyping for bacterial activity can help medical professionals select the most appropriate drug and dosage for that patient, avoiding unnecessary treatment that is likely to be ineffective or even harmful^{131,37}. For example, polymorphisms in gene expression of UGT1A1 may indicate a more severe reaction to irinotecan²⁷, suggesting that a lower dosage or alternative medication is needed.

In wider research, the importance of bacteria and its role in the immune system is a key part of emerging immunotherapy research as an alternative or complementary form of cancer treatment to chemotherapy^{14,27}. Although it has some limitations, such as being more costly as a form of personalised medicine, research outcomes in this area could provide valuable insight into any synergies or crossovers³⁰.

Conclusion

Bacteria play a significant role in chemotherapy resistance through mechanisms such as tumour growth (*Fusobacterium nucleatum* and *Mycoplasma*), drug metabolism (*Mycoplasma*), and toxin conversion (bacterial β -glucuronase)^{19,25,26}. Elucidating the link between bacteria and chemotherapy resistance can help us refine personalised medicine approaches¹⁰. These include maximizing the effectiveness of chemotherapy treatments by employing biomarkers to measure bacterial activity or by genotyping to identify genetic predisposition³⁰.

Since bacteria play an essential role in the immune system⁵, and with several types of chemotherapy reliant on a healthy balanced microbiome to work effectively¹¹, there should be an emphasis for future research with some potential synergies with immunotherapy research. Care should be taken with use of antibiotics, as although these may destroy some types of bacteria instrumental in treatment resistance²³, they may destroy other types such as commensal bacterial essential to a healthy microbiota^{24,38}, so more emphasis on alternatives such as probiotics and faecal microbiota transplants would be of benefit^{28,38,34,35,36}.

Although there are several factors that may encourage chemotherapy resistance, the role of bacteria is a significant one. Further research is needed to better understand the interplay between the tumour micro-environment and preferential bacterial colonisation, carcinogenic bacterial properties, and the balance between the microbiome and the immune system.

References

1. Sung, H. *et al.* Global Cancer Statistics 2020: GLOBOCAN Estimates of Incidence and Mortality Worldwide for 36 Cancers in 185 Countries. *CA: Cancer J. Clin.* **71**, 209–249 (2021). <https://acsjournals.onlinelibrary.wiley.com/doi/10.3322/caac.21660>.
2. WHO. *Global Health Estimates 2020: Deaths by Cause, Age, Sex, by Country and by Region* [\(2000–2019\)](https://www.who.int/data/gho/data/themes/mortality-and-global-health-estimates/ghe-leading-causes-of-death).
3. Bae, J., Park, K. & Kim, Y.-M. Commensal Microbiota and Cancer Immunotherapy: Harnessing Commensal Bacteria for Cancer Therapy. *Immune Netw.* **22** (2022). <https://immunetwork.org/DOIx.php?id=10.4110/in.2022.22.e3>.
4. King, R. J. B. & Robins, M. W. *Cancer Biology* (Pearson Education Limited, 2006).
5. Ting, N. L.-N., Lau, H. C.-H. & Yu, J. Cancer pharmacomicrobiomics: targeting microbiota to optimise cancer therapy outcomes. *Gut* **71** (2022). <http://dx.doi.org/10.1136/gutjnl-2021-326264>.
6. McKinnell, R. G. *et al.* *The Biological Basis of Cancer* (Cambridge University Press, 2006).
7. Voorde, J. V., Balzarini, J. & Liekens, S. Mycoplasmas and cancer: focus on nucleoside metabolism. *EXCLI J.* **13**, 300–322 (2014).
8. Binenbaum, Y., Na'ara, S. & Gil, Z. Gemcitabine resistance in pancreatic ductal adenocarcinoma. *Drug Resist. Updat.* **23**, 55–68 (2015). <http://doi.org/10.1016/j.drup.2015.10.002>.
9. Geller, L. T. *et al.* Potential role of intratumor bacteria in mediating tumor resistance to the chemotherapeutic drug gemcitabine. *N. Y. Sci. J.* **357**, 1156–1160 (2017). <https://doi.org/10.1126/science.aah5043>.

10. Joyce, J. A. & Klemm, F. Microenvironmental regulation of therapeutic response in cancer. *Trends Cell Biol.* **25**, 198–213 (2015). <https://doi.org/10.1126/science.aah5043>.
11. Yin, B. *et al.* Research progress on the effect of gut and tumor microbiota on antitumor efficacy and adverse effects of chemotherapy drugs. *Front. Microbiol.* **13**, 55–68 (2022). <https://doi.org/10.3389/fmicb.2022.899111>.
12. Ciccolini, J., Serdjebi, C., Peters, G. J. & Giovannetti, E. Pharmacokinetics and pharmacogenetics of Gemcitabine as a mainstay in adult and pediatric oncology: an EORTC-PAMM perspective. *Cancer Chemother. Pharmacol.* **78**, 1–12 (2016). <https://doi.org/10.1007/s00280-016-3003-0>.
13. Gimeno, R. & Barquinero, J. Myeloid-derived suppressor cells (MDSC): Another player in the orchestra. *Immunology* **30**, 45–53 (2011). [https://doi.org/10.1016/S0213-9626\(11\)70015-4](https://doi.org/10.1016/S0213-9626(11)70015-4).
14. Emens, L. A. & Middleton, G. The interplay of immunotherapy and chemotherapy: harnessing potential synergies. *Cancer Immunol. Res.* **3**, 436–443 (2015). <https://doi.org/10.1158/2326-6066.CIR-15-0064>.
15. Chen, S. *et al.* Fusobacterium nucleatum promotes colorectal cancer metastasis by modulating KRT7-AS/KRT7. *Gut Microbes* **11**, 511–525 (2020). <https://doi.org/10.1080/19490976.2019.1695494>.
16. Zerdan, M. B. *et al.* The Lung Microbiota and Lung Cancer: A Growing Relationship. *Cancers* **14**, 4813 (2022). <https://doi.org/10.3390/cancers14194813>.
17. Choy, A. T. F. *et al.* The microbiome of pancreatic cancer: from molecular diagnostics to new therapeutic approaches to overcome chemoresistance caused by metabolic inactivation of gemcitabine. *Expert Rev. Mol. Diagn.* **18** (2018). <https://doi.org/10.1080/14737159.2018.1544495>.
18. Wilkinson, E. M., Ilhan, Z. E. & Herbst-Kralovetz, M. M. Microbiota-drug interactions: Impact on metabolism and efficacy of therapeutics. *Maturitas* **112**, 53–63 (2019). <https://doi.org/10.1016/j.maturitas.2018.03.012>.
19. Benedetti, F. *et al.* Proteome analysis of Mycoplasma fermentans cultured under aerobic and anaerobic conditions. *Transl. Med. Commun.* **4** (2019). <https://doi.org/10.1186/s41231-019-0047-2>.
20. Kim, M. K. *et al.* Mycoplasma infection promotes tumor progression via interaction of the mycoplasmal protein p37 and epithelial cell adhesion molecule in hepatocellular carcinoma. *Cancer Lett.* **454**, 44–52 (2019). <https://doi.org/10.1016/j.canlet.2019.04.007>.
21. Cummins, J. & Tangney, M. Bacteria and tumours: causative agents or opportunistic inhabitants? *Infect. Agents Cancer* **8** (2013). <https://doi.org/10.1186/1750-9378-8-11>.
22. Imai, H. *et al.* Antibiotic therapy augments the efficacy of gemcitabine-containing regimens for advanced cancer: a retrospective study. *Cancer Biol. Ther.* **11**, 7953–7965 (2019). <http://doi.org/10.2147/CMAR.S215697>.
23. Nakano, S. *et al.* Association between the use of antibiotics and efficacy of gemcitabine plus nab-paclitaxel in advanced pancreatic cancer. *Medicine* **99** (2020). <https://doi.org/10.1097/MD.00000000000022250>.
24. Li, B. *et al.* Mining the Gut Microbiota for Microbial-Based Therapeutic Strategies in Cancer Immunotherapy. *Front. Oncol.* **11** (2021). <https://doi.org/10.3389/fonc.2021.721249>.
25. Ma, C. T. *et al.* Fusobacterium nucleatum promotes the progression of colorectal cancer by interacting with E-cadherin. *Oncol. Lett.* **16**, 2602–2612 (2018). <https://doi.org/10.3892/ol.2018.8947>.
26. Rubinstein, M. R. *et al.* Fusobacterium nucleatum Promotes Colorectal Carcinogenesis by Modulating E-Cadherin/ β -Catenin Signaling via its FadA Adhesin. *Cell Host Microbe* **14**, 195–206 (2013). <http://dx.doi.org/10.1016/j.chom.2013.07.012>.
27. Chamseddine, A. N. *et al.* Intestinal bacterial β -glucuronidase as a possible predictive biomarker of irinotecan-induced diarrhea severity. *Pharmacol. Ther.* **119**, 1–5 (2019). <https://doi.org/10.1016/j.pharmthera.2019.03.002>.
28. Ren, Z. *et al.* Effect of Bifidobacterium animalis subsp. lactis SF on enhancing the tumor suppression of irinotecan by regulating the intestinal flora. *Pharmacol. Res.* **184** (2022). <https://doi.org/10.1016/j.phrs.2022.106406>.
29. Cheng, K. W. *et al.* Pharmacological inhibition of bacterial β -glucuronidase prevents irinotecan-induced diarrhea without impairing its antitumor efficacy in vivo. *Pharmacol. Res.* **139**, 41–49 (2019). <https://doi.org/10.1016/j.phrs.2018.10.029>.
30. Heshiki, Y. *et al.* Predictable modulation of cancer treatment outcomes by the gut microbiota. *Microbiome* **8** (2020). <https://doi.org/10.1186/s40168-020-00811-2>.
31. Paulik, A. *et al.* Irinotecan toxicity during treatment of metastatic colorectal cancer: focus on pharmacogenomics and personalized medicine. *Tumori J.* **106**, 87–94 (2020). <https://doi.org/10.1177/0300891618811283>.
32. Lin, H. Y. *et al.* Entropy-driven binding of gut bacterial β -glucuronidase inhibitors ameliorates irinotecan-induced toxicity. *Commun. Biol.* **4** (2021). <https://doi.org/10.1038/s42003-021-01815-w>.
33. Kodawara, T. *et al.* The Inhibitory Effect of Ciprofloxacin on the β -Glucuronidase-mediated Deconjugation of the Irinotecan Metabolite SN-38-G. *Basic Clin. Pharmacol. Toxicol.* **118** (2016). <https://doi.org/10.1111/bcpt.12511>.
34. Quintanilha, M. F. *et al.* Bifidobacterium longum subsp. longum 51A attenuates intestinal injury against irinotecan-induced mucositis in mice. *Life Sci.* **289** (2022). <https://doi.org/10.1016/j.lfs.2021.120243>.
35. Hu, W. *et al.* A cellular chip-MS system for investigation of Lactobacillus rhamnosus GG and irinotecan synergistic effects on colorectal cancer. *Chin. Chem. Lett.* **33**, 2096–2100 (2022). <https://doi.org/10.1016/j.ccllet.2021.08.041>.
36. Yue, B. *et al.* Berberine Improves Irinotecan-Induced Intestinal Mucositis Without Impairing the Anti-colorectal Cancer Efficacy of Irinotecan by Inhibiting Bacterial β -glucuronidase. *Chin. Chem. Lett.* **12** (2021). <https://doi.org/10.3389/fphar.2021.774560>.
37. Velez-Velez, L. M., Hughes, C. L. & Kasi, P. M. Clinical Value of Pharmacogenomic Testing in a Patient Receiving FOLFIRINOX for Pancreatic Adenocarcinoma. *J. Clin. Oncol.* **36**, 814 (2018). <https://doi.org/10.3389/fphar.2018.01309>.
38. Yue, B. *et al.* Microbiota-Host-Irinotecan Axis: A New Insight Toward Irinotecan Chemotherapy. *Life Sci.* **289** (2022). <https://doi.org/10.3389/fcimb.2021.710945>.

¹Department of Earth and Planetary Sciences, McGill University, Montreal, QC, Canada

Keywords

Pumice Rafting, Submarine Volcanism, Remote Sensing, Coastal Environments, Pumice Saturation

Email Correspondence

nathalie.redick@mail.mcgill.ca

<https://doi.org/10.26443/msurj.v18i1.187>

©The Author. This article is published under a CC-BY license: <https://creativecommons.org/licenses/by/4.0/>

Nathalie R. Redick¹

A Review of Pumice Raft Formation Environments, Saturation, and Dispersal Mechanisms

Abstract

Pumice rafting events are a common result of volcanic eruptions occurring near or beneath bodies of water. Such events are frequently associated with hazards such as tsunamis, and drift pumice is known to cause local economic disruptions, damage ships, impede naval traffic, devastate marine populations, and distribute potentially invasive species over long distances. However, our current understanding of the mechanisms that drive the formation and dispersal of drift pumice are extremely limited. This article reviews historical and characteristic pumice raft-forming eruptions, how interactions with water factor into macro- and micro- scale controls on pumice clast formation and dispersal, and current methods for detection and analysis to better track and mitigate hazards associated with explosive volcanic eruptions and pumice rafts.

Introduction

Understanding the formation and dispersal of pumice rafts can provide important insights into the mechanisms of subaqueous eruptions; the risk they pose to coastal environments, marine life, and naval travel and transport; and their dispersal of flora and fauna populations¹. Pumice rafts can form in a wide array of volcanic settings, but are particularly prevalent in subaqueous volcanism. Despite making up approximately 85% of the world's volcanic eruptions, our understanding of submarine volcanism is extremely limited because eruptions and deposits are hard to observe, detect, and access²⁻⁴. This review aims to provide an overview of our contemporary understanding of how pumice rafts form and are subsequently deposited by bridging current research in geology, materials science, and remote sensing.

To do so, I will explore characteristic eruptions that formed pumice rafts for each of three volcanic settings, characterized as (1) subaerial volcanism, (2) sublacustral volcanism, and (3) submarine volcanism. To illustrate subaerial volcanism, I selected the 1883 eruption of Krakatau and the more recent 1985 eruption of the Niuafōʻou Island caldera; Krakatau provides an example of a volcanic island producing a pumice raft that is dispersed via the ocean, whereas Niuafōʻou demonstrates a caldera lake dispersal setting. I use the 13300±500 BP Surtseyan eruption of the Black Point basaltic cone in Mono Basin, California to exemplify a sublacustral eruption environment. Finally, I discuss the 2012 eruption of the Havre seamount, north of New Zealand, and the Hunga Tonga-Hunga Haʻapai submarine volcanoes to elucidate the mechanisms of deep and shallow submarine eruptions, respectively.

In order to better understand the part water plays in the formation of pumice, I provide a broad overview of macro- and micro- scale controls on pumice formation. In particular, I will discuss how hydrostatic pressure, eruption depth, and thermochemical interactions with water affect the texture and vesicularity of pumice formed in different volcanic settings with new supporting evidence from field observations made at Mono Lake,

California (see Figure 1). These ideas will be extended to pumice raft dispersal to examine the factors controlling how and when a pumice clast will become saturated with water and sink.

Finally, to understand how pumice rafts are currently studied and possible avenues for further research, I discuss current analytical methods for identifying subaqueous eruptions and pumice rafts. This review focuses on analytical methods for recent or ongoing eruptions and rafting events, rather than identifying historical pumice raft deposits in the geologic record.

Background

Pumice is a relatively common product of explosive volcanic eruptions. Its most impressive characteristic is, arguably, that it has a range of densities lower than 1.0 g cm⁻³, allowing it to float on water⁵. While it is typically felsic to intermediate in composition, samples of basaltic pumices and other variable compositions have also been found. Pumice is a highly microvesicular volcanic glass that forms when magma is rapidly ejected during an eruption. As a result of a rapid decrease in temperature and pressure, volatiles in the magma begin to exsolve; the resulting bubbles are preserved because the rock is cooled quickly^{6,7}. Experiments demonstrating vacuum impregnation of resin in pumice indicate that the vesicles form an interconnected network⁸. This has important consequences for the fate of pumices deposited in water.

Pumice rafts, also referred to as drift pumice, are mobile accumulations of pumice floating on the water's surface^{7,8}. They have been known to span tens of thousands of square kilometres of the ocean surface and are capable of travelling thousands of kilometres^{2,9}. Pumice rafts have the potential to form from explosive volcanic eruptions in a number of volcanic settings; however, they are most commonly associated with shallow subaqueous eruptions^{8,10}. These eruptions are often referred to as Surtseyan eruptions, named for the shallow submarine eruption off the coast of Iceland in 1963 that resulted in the emergence of a new island, Surtsey¹¹.



Figure 1. Silicic Rafted Pumice. A partially buried silicic pumice clast on the modern western shore of Mono Lake in California. At this time, it is unclear which Mono dome or island produced the clast pictured; the Negit Island domes or the Paoha Island dome are both likely candidates given that Black Point is basaltic¹². Mono Basin has been a site of frequent volcanism for the past 60,000 years, and the lavas erupted between 500 and 150 years ago from the northwestern quadrant of Paoha Island are the youngest in the region¹². Photo by author, taken at 37.97818N, 119.13274W in October 2022.

As a result, pumice rafts can have significant effects on coastal and marine environments and human activities. Additionally, they can be used to map drift trajectories and better understand ocean currents and wind fields. The vesicular nature of pumice and the extensive rafts formed facilitate floral and faunal dispersion. For example, beached pumice on Fiji was populated with organisms such as algae, goose barnacles, serpulid worms, calcareous algae, bryozoans, coral, oysters, and more. The size of some corals on the rafted pumice indicated it had been carried by the raft for at least 12 months, indicating that the pumice is a significant dispersal mechanism^{1,13,14}. Consequently, pumice rafts deposited on coastlines may be sources of marine pests and invasive species that pose both short- and long-term threats to coastal ecosystems^{15,16}. Similarly, pumice rafts may have played an important part in global speciation and biodiversity; recent research suggests that pumice rafts are a favourable environment for the initial origins of life on Earth^{1,17}. Pumice rafting can also have important consequences for marine populations, for instance, Akiyama et al. observed a mass mortality of cultured fish after they ingested pumice stones from a rafting event¹⁸. Pumice rafts also block sunlight and inhibit the air-water heat and gas exchange in the upper ocean, damaging ecosystems beneath the raft¹⁹.

The impressive extent of pumice rafts can also impose major disruptions to human activities such as fishing, shipping, and tourism. Rafts can block harbours for many months at a time, as well as make beaches inaccessible or unattractive for tourism. Pumice rafts can rapidly alter local ecosystems for weeks to months, forcing fish populations to move or causing (local) population extinctions which can have devastating effects on fishing. Additionally, the rough nature of pumice often results in damage to boat hulls. The effects on fishing, shipping, and tourism can significantly disrupt local economies¹⁹.

Volcanic Settings

Subaerial Volcanism

Subaerial volcanic events in near-shore and crater lake environments have been known to produce pumice rafts. In a subaerial eruption, pumice is produced when the magma is ejected from the vent and rapidly cools in the atmosphere. The pumice is then deposited into a lake or ocean, where it floats on the surface and accumulates as a raft. Crater lakes commonly form after an explosive eruption; the emptying of the magma chamber induces a caldera collapse^{20,21}. Groundwater, precipitation, and snow melt fill the resulting crater to form a lake²¹.

Krakatau (1883)

In 1883, the volcanic island of Krakatau erupted in the Sunda Strait between the Indonesian islands of Sumatra and Java²². Preceding the 1883 eruption, the Krakatau Group consisted only of the Danan, Perbuatan, and Rakata islands which were parts of an ancient caldera^{23,24}. Krakatau is aligned with the Sunda trench, a subduction zone where the Indo-Australian plate is subducting beneath the Eurasian plate²⁴. The unrest spanned August 26th and 27th, 1883, starting with small eruptions that transitioned into Plinian-style activity, followed by ignimbrite-forming activity on the 27th²⁴. This activity is expected along subduction zones, in which water and other volatiles that are subducted result in explosive eruptions. The eruption produced abundant pumiceous material that was deposited in the Sunda Strait, accumulating as rafts. The tsunami waves, thought to have been generated by the displacement of water by pyroclastic flows, stranded floating pumice fragments in low-lying shoreline regions after receding^{22,23}.

Niuafou Island Caldera (1985)

The 1985 eruption of the Niuafou Island caldera, Tonga also reportedly produced pumice rafts. The island is approximately 8 km wide with an impressively spherical caldera lake that spans 4.6 km in diameter²¹. It is located at the northern end of the Lau-Basin, an actively spreading back-arc basin west of the Tonga subduction trench^{21,25}. A study published by Regelous et al. in indicates that Niuafou likely formed via intraplate magmatism resulting from decompression melting beneath a microplate²⁶. The Niuafou caldera is known to erupt both effusively and explosively, but the characteristics of the 1985 eruption are not well documented²⁵. Unlike the 1883 Krakatau event, pumice accumulated in the lake formed by the steep-sided caldera rather than the surrounding ocean^{22,25}.

Sublacustral Volcanism

Similar to the pumice rafting event on Niuafou's crater lake, pumice rafts have been observed in sublacustrine environments. The major difference between a sublacustral and subaerial eruption at a volcanic lake is that pumice formed during a sublacustral event is quenched by water rather than air. Sublacustral eruptions occur when magma erupts under the surface of a lake.

Black Point (13300±500)

The 13300 ± 500 BP Surtseyan eruption of the Black Point basaltic cone in Mono Basin, California is a prime example of a sublacustral event that produced a pumice raft. The cone formed alongside what is now Mono Lake, a volcanogenic lake in the Mono Basin-Long Valley region of California^{27,28}. The eruption initially occurred approximately 105 m below the surface of the water before transitioning to an emergent Surtseyan eruption as the deposits built up the volcanic cone^{29,30}. Motion along the San Andreas and Walker Lane fault complexes on either side of the Sierra Nevada mountains

account for the transtension deformation in the Mono Basin-Long Valley area. Volcanism is induced by the range front faulting allowed by regional transtension^{28,31}. Subaerial volcanic islands in Mono Lake have also been known to produce silicic rafted pumice, such as the white cone illustrated to the southeast of Black Point in Figure 2.



Figure 2. Paoha Island and Black Point. Satellite image of Mono Lake on Sept. 2nd, 2022, sourced from NASA/USGS Landsat-8 and centered at approximately 38.02192N, -119.02042E. Black Point is marked by a red triangle, the Negit Islands are marked by a blue triangle, and Paoha Island is marked by a green triangle. Black Point is a basaltic Surtseyan emergent volcano that formed at approximately 13300 ± 500 BP in Lake Russell, the Pleistocene predecessor of Mono Lake (present). Image courtesy of the U.S. Geological Survey.

Pyroclast textures from the eruption are consistent with water modification, indicating that the eruption occurred beneath the lake's surface²⁹. The modern shore of Mono Lake is primarily composed of white to grey drift pumice which is visible via satellite (see Figure 2), rafted there by the waves and currents of the lake³².

Submarine Volcanism

Submarine volcanoes are found in intraplate settings as well as along all types of plate boundaries, but predominantly at spreading centers, the Pacific Ring of Fire, and over mantle hotspots². As with sublacustral volcanism, products of submarine eruptions are quenched by water rather than air. Submarine eruptions differ from sublacustrine activity primarily in the depth at which they occur².

Havre Seamount (2012)

On July 7th, 2012, the Havre seamount along the Kermadec arc erupted 800 km north of Auckland, New Zealand³³. The caldera is 4 km long and 3 km wide (elongate northwest-southeast). Havre erupted effusively at around 900 m depth³⁴. This eruption was the largest recorded submarine eruption since A.D. 1650—likely twice the size of the 1980 subaerial eruption of Mount St. Helens—the bulk volume of erupted rhyolitic pumice reached 1.2 km^3 ^{33,35}. Significantly, the Havre eruption was the first to unambiguously establish that deep silicic submarine eruptions can generate pumice rafts, where "deep" is defined as greater than 700 m below sea level (MBSL)⁷. An approximately $22,000 \text{ km}^3$ raft of floating pumice and a 0.1 km^3 field of giant (>1 m) pumice clasts up to 10 m in diameter were observed down-current from the vent^{34,36}.

Hunga Tonga-Hunga Ha'apai (2009, 2014–2015, 2021–2022)

West of the main inhabited islands of the Kingdom of Tonga lies the Hunga Tonga-Hunga Ha'apai volcano, a submarine volcano that includes small islands, islets, and shallow submarine reefs along the caldera rim of a much larger submarine structure. It exists at approximately 150 m depth along

the Tofua arc, a segment of the Tonga-Kermadec volcanic arc that formed as a result of subduction of the Pacific Plate beneath the Indo-Australian Plate³⁷. On March 17th, 2009 material erupted effusively from two vents, located northwest and south of Hunga Ha'apai, a pre-existing, uninhabited volcanic island near Tonga³⁸. The Hunga Tonga-Hunga Ha'apai volcanic group erupted again from September 2014 through January 2015, during which a tephra cone coalesced the two existing islands³⁹. It erupted yet again from December 2021–January 2022, obliterating the tephra cone from the 2014–2015 eruption and triggering a giant atmospheric shock wave and a tsunami⁴⁰.

In 2009, satellite imagery was used to measure the distribution of pumice rafts and determine the volume of erupted material. A minimum bound on the volume of pumice raft in 2009 was estimated to be approximately 0.0158 km^3 , with a total erupted volume of at least 0.0176 km^3 ³⁸. Large pumice rafts, each spanning up to 4 km in its widest dimension, were visible in satellite imagery in early January 2022 and found drifting nearly 100 km away from the volcano⁴¹.

Interactions with Water

The relative temperature difference between a magma and water is greater than that between a magma and air³⁹. The rapid heat transfer from the magma to the water leads to rapid volume expansion of vaporized seawater which is likely related to the explosive eruptive style of Surtseyan and deep submarine eruptions^{2,42}.

Surtseyan eruptions that transition to sustained emergence above the water's surface are typically observed to shift their eruptive style to weak fire-fountaining or effusive lava flow activity. For this reason, Surtseyan eruptions are generally considered to be Strombolian or Hawaiian eruptions that have been modified by water²⁹. This transition exemplifies the importance of the effects water has on eruption dynamics and the quenching of eruptive products. Furthermore, water drives the dispersal patterns of pumice rafts.

Microtextural Controls on Pumice Formation

Eruptions that occur in water are subjected to a higher confining pressure from the overlying water column than subaerial eruptions. Hydrostatic pressure suppresses volatile exsolution, expansion of erupting magma, bubble coalescence, and permeability development^{42,43}. Prefragmentation vesiculation may be hindered by hydrostatic pressure at depth and postfragmentation vesiculation of erupted products may be interrupted by rapid quenching³⁹. Specifically in deep submarine pumice, [43] noted that samples had homogeneous textures with low-vesicularity clasts and contained sub-round or ellipsoidal bubbles with thick vesicle walls. Deep submarine pumices have been shown to have similar colour, density, and macrotexture to subaerial and Surtseyan pumices⁴³. However, the deep submarine pumices present with fewer small vesicles and have narrower vesicle size distributions when compared to subaerially erupted pumices⁴³. A recent study of pumice from the 2012 Havre eruption by Mitchell et al. in also concurs that interactions with water have microtextural controls on pumice formation⁴⁴. Their analysis of microtextural characteristics revealed that rafted pumice clasts have lower pore space connectivity and higher vesicle density than sunken clasts⁴⁴. Field observations of rafted pumices at Mono Lake, California display centimeter-scale surface jointing that is similar to the columnar jointing that is commonly observed in rapidly cooled basaltic flows, as seen in Figure 3.



Figure 3. Micro-jointing on the Surface of Rafted Pumice. This image is a closer look at the drift pumice pictured in Figure 1. Micro-jointing on the surface of a rafted pumice clast on the contemporary western shore of Mono Lake, California. The joints can be seen at a variety of different length scales. Photo by author, taken at 37.97818N, 119.13274W in October 2022.

Buoyancy and Saturation

The initial buoyancy of pumice is determined by its size, shape, vesicularity, permeability and temperature when it comes into contact with water^{7,34,45}. Its buoyancy changes over time as the clast becomes saturated with water, ultimately reaching a critical buoyancy at which point the clast will sink, given that it is not washed ashore first. Once a clast is sufficiently saturated, it will drop out and sink in a fashion that is hydrodynamically-similar to normal clastic material. Saturation of a pumice clast is intrinsically related to pore space connectivity and overall vesicularity⁵.

Observations of reverse-graded bedding (saturation bedding) composed of sunken pumice clasts in subaqueous environments indicates that the flotation residence time of pumice is inversely proportional to its size⁴⁶. Using an analogue behavioural model based on Darcy's law for the flow of fluids in porous material, Manville et al. modelled pumice saturation to determine residence times for pumice saturation⁵. Their work shows that there is a first-order proportional relationship between time and the square radius of a clast⁵. Experimental observations confirm that smaller clasts tend to saturate faster, however, their experiments were only conducted with clast sizes up to 16 mm in diameter. Pumice vesicularity varies depending on where and how it was formed, which I elaborated on in the previous section on "Microtextural Controls on Pumice Formation." In regards to buoyancy, studies suggest that rafted pumices typically have a higher vesicle density than their sunken counterparts⁴⁴. In general, pumice has a high pore connectivity which would suggest a rapid sinking rate⁴⁷. However, laboratory experiments by Whitham & Sparks show that some pumice clasts can remain afloat in a laboratory environment for over a year and a half⁸. To reconcile observations of long-floating pumice and the expectation of rapid sinking, Fauria et al. propose that the diffusion of trapped gas ultimately determines pumice flotation residence time⁴⁵. Their proposal is supported by experimental measurements on pumice flotation, finding a flotation residence time (τ) that can be described by equation 0.1, where L is the characteristic length of pumice, D is the gas-water diffusion coefficient, and θ is pumice water saturation⁴⁵.

$$\tau \propto \frac{L^2}{D\theta^2} \quad (0.1)$$

The temperature of pumice at the time it comes into contact with water is largely determined by the environment in which it formed; pumices that formed in subaerial eruptions and become rafted due to fallout, shore erosion, and fluvial transport⁷ may have cooled before rafting began. Experiments by Whitham & Sparks suggest that a critical temperature of pumice exists at which point a clast will sink, regardless of its other physical properties⁸. Rapid saturation of pumices during subaqueous eruptions occurs as a result of quenching when the water phase change from steam to liquid creates strong negative pore pressure within pumice vesicles and hydrodynamic instabilities due to steam generation^{46,48,49}.

Dispersal and Deposition Mechanisms

Pumice rafts have been known to travel thousands of kilometers from their source, capable of drifting several kilometers a day^{38,50}. The dispersal of pumice rafts is largely controlled by prevailing ocean currents, waves, and wind^{38,50}. Some subaqueous eruptions cause tsunamis, which also contribute to the dispersal patterns of pumice rafts^{22,51}. Jutzeler et al. observed a pumice raft produced by an unnamed submarine volcano in the Tonga Islands in the Pacific Ocean in August 2019 that progressively split into several hundred smaller rafts. Areal dispersion, pumice abrasion, saturation, overloading of clast by biota, and stranding decreased the volume of the rafts⁵⁰. They also noted the formation of patchy, elongate raft "ribbons" forming alongside or behind the main raft. Fauria & Manga provide useful equations (17,18 in their work) for estimating average saturation and cooling rates for drift pumice based on clast porosity, size, and initial temperature that can inform models of raft dispersal⁵².

After pumice rafting events, mass swaths of pumice clasts are often observed to wash up on shorelines. However, not all pumice clasts are floated during a raft-forming event; a large volume of pumice clasts are also deposited on the subaqueous flanks of the vent^{6,42}. These observations suggest float pumice is typically deposited in three ways: stranding, critical saturation, and saturated-clast redeposition in which clasts are re-entrained and deposited by standard sedimentary processes⁴⁶.

Current Analytical Methods

Studying pumice rafts is difficult due to the large scale of dispersal, the unpredictability of volcanism, and the inaccessibility of the subaqueous source vents and historical deposits. Traditional methods for understanding the distribution of pumice rafts primarily focus on clasts deposited on shores, which presents an issue with survivorship bias regarding the size and vesicularity of pumice clasts. Other studies also look at uplifted subaqueous volcanic successions, but this presents problems when determining the source of the pumice rafts and erosion reduces our ability to constrain the initial erupted volume of a pumice raft^{8,42,51,53}. Recent advances in remote sensing and modelling have allowed for the study of pumice rafts in a variety of ways. It should be noted that new pumice rafts are often reported first by ocean traffic, which poses issues in terms of studying the initiation and full evolution of pumice rafting events since they may not be discovered immediately, especially in the case of deep submarine raft-forming eruptions.

Remote sensing is a powerful tool for studying pumice rafts. Satellite imagery can be used to track the dispersal of pumice rafts over large areas of the ocean surface³⁸. For example, high-temporal resolution Moderate Resolution Imaging Spectroradiometer (MODIS) was used to estimate the magnitude, location, start time, and eruption duration of the 2009 Hunga Ha'apai eruption. More recently, MODIS, Visible Infrared Imag-

ing Radiometer Suite (VIIRS), Sentinel-3 Ocean and Land Color Instrument (OCLI), and Sentinel-3 Sea and Land Surface Temperature Radiometer (SLSTR) satellite images were used for automatic detection and monitoring pumice raft dispersion from a submarine eruption near the Vava'u island group of Tonga⁵⁴. Jutzeler et al. was able to track the evolution and dispersal of the August 7th, 2019 pumice raft that originated from the Tonga Arc in real-time using satellite imagery. They coupled remote sensing observations with oceanographic Lagrangian simulations to conduct near-real time forecasting of the event⁵⁰.

Remote sensing methods can only be used to study pumice clasts once they reach the surface. To address this issue, Mittal & Delbridge propose the use of existing Argo floats in concert with hydrophone and seismic arrays for the detection of subaqueous volcanism which could be paired with remote sensing techniques to better constrain eruption time and distinguish pumice rafting events. Their model indicates that the spatial sampling resolution of Argo floats is sufficient to detect anomalies generated by submarine eruptions⁵⁵.

Murch et al. used a remotely operated vehicle (ROV) to analyze submarine deposits of ash with lapilli that drapes the Havre caldera⁴². ROVs have also been used to directly observe two small submarine eruptions at the NW Rota-1 volcano located on the Marianas arc and the West Mata volcano located in the Lau Basin^{2,3}. Numerical modelling and simulations have also been shown to accurately forecast the dispersal of pumice rafts^{19,56}.

Conclusion

Pumice rafts have important impacts on the environment, the economy, and can provide important insights about subaqueous eruptions. Understanding which regions are susceptible to pumice raft-forming subaerial, sublacustral, and submarine eruptions will help improve how we detect and mitigate the effects of rafting events and other risks associated with explosive eruptions, such as tsunamis. Existing technologies, such as satellite sensors, remotely operated vehicles, hydrophones, and submarine seismic arrays can be co-opted to improve the way we detect and track rafting events, without requiring costly installations of new equipment. When combined with our understanding of historical pumice drift events such as Krakatau (1883) or the Havre seamount eruption (2012), we can better understand the mechanisms of submarine eruptions and the extent of hazards posed by such eruptions.

Acknowledgements

The author acknowledges funding provided by the McGill Department of Earth and Planetary Sciences which made field observations of the Mono Lake drift pumices possible. In particular, the author would like to thank Dr. John Stix for organizing the trip and inspiring this review.

References

1. Elser, J. J. *et al.* Community Structure and Biogeochemical Impacts of Microbial Life on Floating Pumice. *Appl. Environ. Microbiol.* **81**, 1542–1549 (2015). <https://doi.org/10.1128/AEM.03160-14>.
2. White, J. D. L., Schipper, C. I. & Kano, K. in *The Encyclopedia of Volcanoes (Second Edition)* (ed Sigurdsson, H.) 553–569 (Academic Press, 2015). <https://doi.org/10.1016/B978-0-12-385938-9.00031-6>.
3. Chadwick Jr, W. W. *et al.* Direct Video and Hydrophone Observations of Submarine Explosive Eruptions at NW Rota-1 Volcano, Mariana Arc. *J. Geophys. Res. Solid Earth* **113**, (2008). <https://doi.org/10.1029/2007JB005215>.
4. Resing, J. A. *et al.* Active Submarine Eruption of Boninite in the Northeastern Lau Basin. *Nat. Geosci.* **4**, 799–806 (2011). <https://doi.org/10.1038/ngeo1275>.
5. Manville, V., White, J., Houghton, B. & Wilson, C. The Saturation Behaviour of Pumice and Some Sedimentological Implications. *Sediment. Geol.* **119**, 5–16 (1998). [https://doi.org/10.1016/S0037-0738\(98\)00057-8](https://doi.org/10.1016/S0037-0738(98)00057-8).
6. Rotella, M. D., Wilson, C. J. N., Barker, S. J. & Wright, I. C. Highly Vesicular Pumice Generated by Buoyant Detachment of Magma in Subaqueous Volcanism. *Nat. Geosci.* **6**, 129–132 (2013). <https://doi.org/10.1038/ngeo1709>.
7. Jutzeler, M. *et al.* On the Fate of Pumice Rafts Formed during the 2012 Havre Submarine Eruption. *Nat. Commun.* **5**, 3660 (2014). <https://doi.org/10.1038/ncomms4660>.
8. Whitham, A. G. & Sparks, R. S. J. Pumice. *Bull. Volcanol.* **48**, 209–223 (1986). <https://doi.org/10.1007/BF01087675>.
9. Wunderman, R. Report on Havre Seamount (New Zealand) — September 2012 (2012); <https://doi.org/10.5479/si.GVP.BGVN201209-242005>.
10. Allen, S. R., Fiske, R. S. & Tamura, Y. Effects of Water Depth on Pumice Formation in Submarine Domes at Sumisu, Izu-Bonin Arc, Western Pacific. *Geology* **38**, 391–394 (2010). <https://doi.org/10.1130/G30500.1>.
11. Moore, J. G. Structure and Eruptive Mechanisms at Surtsey Volcano, Iceland. *Geol. Mag.* **122**, 649–661 (1985). <https://doi.org/10.1017/S0016756800032052>.
12. Bray, B., Stix, J. & Cousens, B. Mafic Replenishment of Multiple Felsic Reservoirs at the Mono Domes and Mono Lake Islands, California. *Bull. Volcanol.* **79**, 54 (2017). <https://doi.org/10.1007/s00445-017-1123-y>.
13. Bryan, S. *et al.* Pumice Rafting and Faunal Dispersion during 2001–2002 in the Southwest Pacific: Record of a Dacitic Submarine Explosive Eruption from Tonga. *Earth Planet. Sci. Lett.* **227**, 135–154 (2004). <https://doi.org/10.1016/j.epsl.2004.08.009>.
14. Velasquez, E. *et al.* Age and Area Predict Patterns of Species Richness in Pumice Rafts Contingent on Oceanic Climatic Zone Encountered. *Ecol. Evol.* **8**, 5034–5046 (2018). <https://doi.org/10.1002/ece3.3980>.
15. Bryan, S. E. *et al.* Rapid, Long-Distance Dispersal by Pumice Rafting. *PLoS One* **7**, e40583 (2012). <https://doi.org/10.1371/journal.pone.0040583>.
16. Ohno, Y., Iguchi, A., Ijima, M., Yasumoto, K. & Suzuki, A. Coastal Ecological Impacts from Pumice Rafts. *Sci. Rep.* **12**, 11187 (2022). <https://doi.org/10.1038/s41598-022-14614-y>.
17. Brasier, M., Matthewman, R., McMahon, S. & Wacey, D. Pumice as a Remarkable Substrate for the Origin of Life. *Astrobiology* **11**, 725–35 (2011). <https://doi.org/10.1089/ast.2010.0546>.
18. Akiyama, Y., Okada, T. & Yuhara, T. Observations of Mobile Macro-Epifauna on Pumice Rafts Generated by Fukutoku-Oka-no-Ba Volcano in Oku Port, Okinawa Prefecture. *Aquat. Anim.* **2022**, AA2022–13 (2022). https://doi.org/10.34394/aquaticanimals.2022.0_AA2022-13.
19. Jutzeler, M. *et al.* Ongoing Dispersal of the 7 August 2019 Pumice Raft From the Tonga Arc in the Southwestern Pacific Ocean. *Geophys. Res. Lett.* **47**, e1701121 (2020). <https://doi.org/10.1029/2019GL086768>.

20. Bailey, R. A., Dalrymple, G. B. & Lanphere, M. A. Volcanism, Structure, and Geochronology of Long Valley Caldera, Mono County, California. *J. Geophys. Res.* **81**, 725–744 (1976). <https://doi.org/10.1029/JB081i005p00725>.
21. Kempe, S. & Kazmierczak, J. in *Life on Earth and Other Planetary Bodies* (eds Hanslmeier, A., Kempe, S. & Seckbach, J.) 195–234 (Springer Netherlands, 2012). https://doi.org/10.1007/978-94-007-4966-5_13.
22. Carey, S., Morelli, D., Sigurdsson, H. & Bronto, S. Tsunami Deposits from Major Explosive Eruptions: An Example from the 1883 Eruption of Krakatau. *Geology* **29**, 347–350 (2001). [https://doi.org/10.1130/0091-7613\(2001\)029%3C0347:TDFMEE%3E2.0.CO;2](https://doi.org/10.1130/0091-7613(2001)029%3C0347:TDFMEE%3E2.0.CO;2).
23. Self, S. Krakatau Revisited: The Course of Events and Interpretation of the 1883 Eruption. *GeoJournal* **28**, 109–121 (1992). <https://doi.org/10.1007/BF00177223>.
24. Schaller, N., Griesser, T., Fischer, A., Stickler, A. & Brönnimann, S. Climate Effects of the 1883 Krakatoa Eruption: Historical and Present Perspectives. *Vierteljahrsschr. Nat. Ges. Zuerich* **154**, 31–40 (2009).
25. Taylor, P. W. *The Geology and Petrology of Niuafoʻou Island, Tonga: Subaerial Volcanism in an Active Back-Arc Basin* (Macquarie University, 2022). <http://oatd.org/oatd/record?record=handle%5C%5C%5C%3A10.25949%5C%5C%5C%2F19440851.v1>.
26. Regelous, M. *et al.* Mantle Dynamics and Mantle Melting beneath Niuafoʻou Island and the Northern Lau Back-Arc Basin. *Contrib. Mineral. Petrol.* **156**, 103–118 (2008).
27. Hildreth, W. Volcanological Perspectives on Long Valley, Mammoth Mountain, and Mono Craters: Several Contiguous but Discrete Systems. *J. Volcanol. Geotherm. Res.* **136**, 169–198 (2004). <https://doi.org/10.1016/j.jvolgeores.2004.05.019>.
28. Bursik, M. & Sieh, K. Range Front Faulting and Volcanism in the Mono Basin, Eastern California. *J. Geophys. Res. Solid Earth* **94**, 15587–15609 (1989). <https://doi.org/10.1029/JB094iB11p15587>.
29. Murtagh, R. M. & White, J. D. L. Pyroclast Characteristics of a Subaqueous to Emergent Surtseyan Eruption, Black Point Volcano, California. *J. Volcanol. Geotherm. Res.* **267**, 75–91 (2013). <https://doi.org/10.1016/j.jvolgeores.2013.08.015>.
30. Verolino, A., White, J. D. & Dürig, T. Black Point: A Peculiar Surtseyan Emergent Basaltic Volcano in the Mono Basin in *Geophysical Research Abstracts* **21** (European Geosciences Union, 2019).
31. Wesnousky, S. G. The San Andreas and Walker Lane Fault Systems, Western North America: Transpression, Transtension, Cumulative Slip and the Structural Evolution of a Major Transform Plate Boundary. *J. Struct. Geol.* **27**, 1505–1512 (2005). <https://doi.org/10.1016/j.jsg.2005.01.015>.
32. Russell, I. C. *Quaternary History of Mono Valley, California* (U.S. Government Printing Office, 1889). <https://books.google.ca/books?id=AE7nAAAAMAAJ>.
33. Carey, R. J., Wysoczanski, R., Wunderman, R. & Jutzeler, M. Discovery of the Largest Historic Silicic Submarine Eruption. *Eos* **95**, 157–159 (2014). <https://doi.org/10.1002/2014EO190001>.
34. Manga, M. *et al.* The Pumice Raft-Forming 2012 Havre Submarine Eruption Was Effusive. *Earth Planet. Sci. Letters* **489**, 49–58 (2018). <https://doi.org/10.1016/j.epsl.2018.02.025>.
35. Manga, M., Mitchell, S. J., Degruyter, W. & Carey, R. J. Transition of Eruptive Style: Pumice Raft to Dome-Forming Eruption at the Havre Submarine Volcano, Southwest Pacific Ocean. *Geology* **46**, 1075–1078 (2018). <https://doi.org/10.1130/G45436.1>.
36. Mitchell, S. J. *et al.* Submarine Giant Pumice: A Window into the Shallow Conduit Dynamics of a Recent Silicic Eruption. *Bull. Volcanol.* **81**, 42 (2019). <https://doi.org/10.1007/s00445-019-1298-5>.
37. Venzke, E. Report on Hunga Tonga-Hunga Haʻapai (Tonga) (2022); <https://volcano.si.edu/ShowReport.cfm?doi=10.5479/si.GVP.BGVN202202-243040>.
38. Vaughan, R. G. & Webley, P. W. Satellite Observations of a Surtseyan Eruption: Hunga Haʻapai, Tonga. *J. Volcanol. Geotherm. Res.* **198**, 177–186 (2010). <https://doi.org/10.1016/j.jvolgeores.2010.08.017>.
39. Colombier, M. *et al.* Vesiculation and Quenching During Surtseyan Eruptions at Hunga Tonga-Hunga Haʻapai Volcano, Tonga. *J. Geophys. Res. Solid Earth* **123**, 3762–3779 (2018). <https://doi.org/10.1029/2017JB015357>.
40. Astafyeva, E. *et al.* The 15 January 2022 Hunga Tonga Eruption History as Inferred From Ionospheric Observations. *Geophys. Res. Lett.* **49**, e2022GL098827 (2022). <https://doi.org/10.1029/2022GL098827>.
41. Voiland, A. Dramatic Changes at Hunga Tonga-Hunga Haʻapai (2022); <https://earthobservatory.nasa.gov/images/149367/dramatic-changes-at-hunga-tonga-hunga-haapai>.
42. Murch, A. P., White, J. D. L. & Carey, R. J. Characteristics and Deposit Stratigraphy of Submarine-Erupted Silicic Ash, Havre Volcano, Kermadec Arc, New Zealand. *Front. Earth Sci.* **7**, (2019). <https://doi.org/10.3389/feart.2019.00001>.
43. Rotella, M. D. *et al.* Dynamics of Deep Submarine Silicic Explosive Eruptions in the Kermadec Arc, as Reflected in Pumice Vesicularity Textures. *J. Volcanol. Geotherm. Res.* **301**, 314–332 (2015). <https://doi.org/10.1016/j.jvolgeores.2015.05.021>.
44. Mitchell, S. J., Fauria, K. E., Houghton, B. F. & Carey, R. J. Sink or Float: Microtextural Controls on the Fate of Pumice Deposition during the 2012 Submarine Havre Eruption. *Bull. Volcanol.* **83**, 80 (2021). <https://doi.org/10.1007/s00445-021-01497-6>.
45. Fauria, K. E., Manga, M. & Wei, Z. Trapped Bubbles Keep Pumice Afloat and Gas Diffusion Makes Pumice Sink. *Earth Planet. Sci. Lett.* **460**, 50–59 (2017). <https://doi.org/10.1016/j.epsl.2016.11.055>.
46. White, J. D. L. *et al.* in *Volcaniclastic Sedimentation in Lacustrine Settings* 141–150 (John Wiley & Sons, 2001). <https://doi.org/10.1002/9781444304251.ch7>.
47. Vella, D. & Huppert, H. E. The Waterlogging of Floating Objects. *J. Fluid Mech.* **585**, 245–254 (2007). <https://doi.org/10.1017/S002211200700715X>.
48. Allen, S. R., Fiske, R. S. & Cashman, K. Quenching of Steam-Charged Pumice: Implications for Submarine Pyroclastic Volcanism. *Earth Planet. Sci. Lett.* **274**, 40–49 (2008). <https://doi.org/10.1016/j.epsl.2008.06.050>.
49. Dufek, J., Manga, M. & Staedter, M. Littoral Blasts: Pumice-water Heat Transfer and the Conditions for Steam Explosions When Pyroclastic Flows Enter the Ocean. *J. Geophys. Res. Solid Earth* **112**, (2007). <https://doi.org/10.1029/2006JB004910>.
50. Jutzeler, M. *et al.* Ongoing Dispersal of the 7 August 2019 Pumice Raft From the Tonga Arc in the Southwestern Pacific Ocean. *Geophys. Res. Lett.* **47**, e1701121 (2020). <https://doi.org/10.1029/2019GL086768>.
51. Yu, N.-T., Yen, J.-Y., Yen, I.-C. & Chu, M.-F. An Extended, 2.4-Ka Long Record of Western Pacific Tsunamis and Pumice Rafts in Northern Taiwan: Tsunami Recurrence, Pumice Sources, and Drifting Routes. *Quat. Sci. Rev.* **281**, 107423 (2022). <https://doi.org/10.1016/j.quascirev.2022.107423>.
52. Fauria, K. E. & Manga, M. Pyroclast Cooling and Saturation in Water. *J. Volcanol. Geotherm. Res.* **362**, 17–31 (2018). <https://doi.org/10.1016/j.jvolgeores.2018.07.002>.
53. Kano, K., Yamamoto, T. & Ono, K. Subaqueous Eruption and Emplacement of the Shinjima Pumice, Shinjima (Moeshima) Island, Kagoshima Bay, SW Japan. *J. Volcanol. Geotherm. Res.* **71**, 187–206 (1996). [https://doi.org/10.1016/0377-0273\(95\)00077-1](https://doi.org/10.1016/0377-0273(95)00077-1).

54. Whiteside, A. *et al.* Automatic Detection of Optical Signatures within and around Floating Tonga-Fiji Pumice Rafts Using MODIS, VIIRS, and OLCI Satellite Sensors. *Remote Sens.* **13**, 501 (2021). <https://doi.org/10.3390/rs13030501>.
55. Mittal, T. & Delbridge, B. Detection of the 2012 Havre Submarine Eruption Plume Using Argo Floats and Its Implications for Ocean Dynamics. *Earth Planet. Sci. Lett.* **511**, 105–116 (2019). <https://doi.org/10.1016/j.epsl.2019.01.035>.
56. Nishikawa, H., Kuwatani, T., Tada, N. & Watanabe, H. K. Simulated Distributions of Pumice Rafts in Japan Following Eruptions at Volcanic Islands and Submarine Volcanoes, Preprint at <https://doi.org/10.21203/rs.3.rs-2177000/v1> (2022).

An Enduring Controversial Story in the Human Brain: Adult Hippocampal Neurogenesis in the Dentate Gyrus

¹Douglas Mental Health University Institute, Montreal, QC, Canada

²Department of Anatomy & Cell Biology, McGill University, Montreal, QC, Canada

³Faculty of Science, McGill University, Montreal, QC, Canada

Keywords

Adult hippocampal neurogenesis, major depressive disorder, Alzheimer's Disease

Email Correspondence

zhipeng.niu@mail.mcgill.ca
tanya.capolicchio@mail.mcgill.ca

<https://doi.org/10.26443/msurj.v18i1.194>

© The Author. This article is published under a CC-BY license: <https://creativecommons.org/licenses/by/4.0/>

Abstract

Adult hippocampal neurogenesis (AHN) is a well-studied phenomenon that involves the derivation of new neurons from neural progenitor cells in the dentate gyrus region of the hippocampus, an area responsible for cognitive functions such as learning and memory storage. Moreover, the hippocampus is known to be implicated in neurological conditions such as Alzheimer's disease. Although AHN has been extensively observed in animal models for twenty years, its existence and persistence in humans have been widely debated in academia, heavily based on post-mortem immunohistochemical markers. Using the search engines PubMed and Google Scholar for "Adult Human Neurogenesis," 143 articles that were most relevant to the history of AHN discovery, detection in rodents, immunohistochemical studies on post-mortem human sections, and therapeutic development targeting AHN were reviewed. This review article highlights the current understanding of AHN in rodents and humans, its implications in neurodegenerative diseases and therapeutics, and the inconsistencies and methodological variabilities encountered in studying AHN in humans. Furthermore, the correlation between AHN and diseases such as mood disorders and Alzheimer's disease is still not well established, with conflicting findings reported. Standardization of transcriptomic methodologies and increased availability of post-mortem human brain samples are crucial in advancing AHN research. This review article attempts to discover the fascinating and controversial world of adult human neurogenesis and its potential implications in treating neurological disorders. Apart from the discussion on AHN existence, tackling devastating diseases with this supplemental knowledge can lead to therapeutic advancements which greatly rely on understanding not only the presence of AHN but the mechanisms mediating its availability.

Introduction

In the 1960s, Joseph Altman was the first biologist who discovered a generation of new neurons within the hippocampal region of rodents, via autoradiographic investigation^{1,2}. The traditional view held by researchers was that neurogenesis did not occur in adult mammalian brains³⁻⁶. However, these findings were groundbreaking as they challenged this belief and demonstrated that newly born neurons could be incorporated into adult brains. Neuroscientists within academia did not entirely accept this development until the late 1990s³⁻⁶. Novel technologies such as bromodeoxyuridine (BrdU) labelling⁷ and immunohistochemistry targeting polysialylated neural cell adhesion molecule (PSA-NCAM), a plasma membrane glycoprotein expressed by neuronal progenitors⁸⁻¹⁰, allowed for the labelling of newly generated granule cells and neural progenitor cells. Utilizing this labeling technique, scientists observed AHN in the dentate gyrus (DG) of rodents' hippocampal region, which supported Altman's proposal of hippocampal neurogenesis within rodent brains.

In 1994, an immunohistochemistry study was performed on the hippocampi of children with extrahippocampal seizures, to expand the study of hippocampal neurogenesis into human subjects¹¹. In structurally non-atrophic brains of children under two years of age with epilepsy, PSA-NCAM-positive immature neurons were observed in the granule cell layer (GCL) and subgranular zone (SGZ) of their hippocampi¹¹. Furthermore, early studies by Eriksson and colleagues used the BrdU-labeling technique to mark newly formed neurons within post-mortem hippocampi from adult cancer patients that colocalized with the neuronal marker NeuN¹². This provided evidence for the presence of neurogenesis within the human hippocampus. Alternatively, through immunohistochemistry with stem cell markers and immature neuronal markers (INMs), different research groups demonstrated hippocampal neurogenesis in mammals^{13,14}.

After several years of research, the term "adult hippocampal neurogenesis (AHN)" was coined and refers to the constant generation of dentate granule cells from neural stem cells (NSCs) in the SGZ of the hippocampal dentate gyrus^{15,16}, a narrow band between the hilus and GCL with a highly distinct molecular profile containing doublecortin positive (DCX+) and

PSA-NCAM+ cells¹⁷. These newborn NSCs are described as type 1 radial glia-like cells (RGLs), which go through several consecutive stages of development¹⁸. Proliferating intermediate progenitor cells (IPCs, type 2 cells) can form from RGLs, further differentiating into neuroblasts (type 3)^{19,20}. Once they fully integrate into the GCL, they mature and become dentate granule neurons^{21,22}. Each developmental stage corresponds to different neuronal markers such as GFAP, Sox2, and Nestin for RGLs; Ki67, MCM2, and PAX6 for IPCs; DCX, PSA-NCAM, and NeuroD for neuroblasts; and NeuN/Calretinin for young immature neurons²²⁻²⁵. Currently, AHN has drawn much attention and is widely studied in the field of neuroscience due to its role in hippocampal neural circuits involved in learning and memory^{5,26}; regeneration of brain tissues^{27,28}; and various diseases such as epilepsy²⁹, ischemia^{30,31}, Alzheimer's disease^{32,33}, and several psychiatric conditions³⁴. Progress has also been made in terms of improving experimental techniques, such as using nuclear magnetic resonance spectroscopy to find neural progenitor cells and NSCs in the living human brain via their respective markers^{35,36}. Integration of research on AHN suggests that the topic should be studied at the transcriptomic level using single-cell RNA sequencing and other transcriptomic methods³⁷⁻⁴¹.

Controversial evidence has been brought forward by Sorrells and colleagues that has put into question the existence of human AHN⁴². According to Sorrells et al., a sharp decline in hippocampal neurogenesis is observed during the infancy period, suggesting that neurogenesis in the dentate gyrus does not continue in adult humans⁴². Soon after this study, Boldrini and colleagues showed stable immature neuron pools and proliferating progenitor cells within human hippocampi throughout aging, whereas only quiescent stem cells decrease in number in aged human hippocampal dentate gyri⁴³. Comparably, Moreno-Jiménez and colleagues applied improved immunohistochemical techniques to illustrate many DCX+ immature neurons in the human DG, which serves as evidence for the persistence of AHN across development in humans⁴⁴.

The exact reasons underlying the varying presence of AHN remains unclear since results can vary due to differences in techniques and specimens studied⁴⁴. The processing of post-mortem brains may vary from study to

studied⁴⁴. The processing of post-mortem brains may vary from study to study, as well as immunohistochemical aspects in terms of tissue preparation and procedure, and variations in antibody and probe utilization⁴⁵. In this review, we will examine the history of and recent progress in understanding AHN in different experimental models. Moreover, we will discuss how AHN is implicated in major depressive disorder and especially in Alzheimer's disease, and the therapies targeting AHN, concluding with future goals for this topic of research.

Methods and Search Criteria

To conduct a thorough research of rodent and post-mortem brain tissue studies, we entered "Adult Human Hippocampal Neurogenesis" in Pubmed and Google Scholar and narrowed down the results to only highly cited research articles that employed immunohistochemistry (IHC) procedure. To ensure comprehensiveness, it should be noted that the search criteria for both Pubmed and Google Scholar includes all articles found on those search engines, regardless of their publication year. We also used AND to connect adult hippocampal neurogenesis with terms such as "dentate gyrus", "subgranular zone", and "neural stem cells" in our keyword search. We do not include niches such as AHN signaling pathways or AHN included as a subsection for research focusing predominantly on other topics. We limit our focus to studies mainly dissecting the existence or absence of AHN in rodents and humans but not non-human primates with complementary approaches besides IHC. For later sections on disease-induced changes in AHN and therapeutics, we conducted a more specialized systematic search with targeted terms involving "neurodegeneration", "Alzheimer's disease", "major depressive disorder", "treatment", and "therapeutics" to further discuss AHN and summarize findings for different disciplinary perspectives that suggest the presence or absence of neurogenesis rather than conclusive proof on the topics.

Adult Neurogenesis in Rodents

Most of the scholarly understanding of AHN comes from mouse studies performed in the past three decades, specifically in mice^{22,38,46,47}. Besides the techniques using thymidine-H3 (2) and thymidine analogs¹⁰ to confirm division and differentiation of NSCs inside the SGZ of DG, at least one other study applied similar methods to find the subventricular zone (SVZ) of lateral ventricles to constitute a specialized source of neuronal progenitor cells with lifelong neurogenesis⁴⁸. Until now, many studies using a modern genetic manipulation technique with rodents consistently demonstrate that granule cell generation occurs within the SGZ of the adult DG in the hippocampus⁴⁶. The adult NSCs harboured in the SGZ express glial fibrillary acidic protein as an astrocyte marker and have the characteristics of astrocytes⁴⁹ while possessing a radial glial cell morphology⁵⁰. However, these markers do not distinguish NSCs from astrocytes and non-NSCs, which also express molecular markers like the glutamate-aspartate transporter⁵¹. Therefore, the field of AHN research continues to develop new techniques such as colocalized cellular markers to better distinguish NSCs from other cell lineages and to improve our appreciation of the mechanisms behind AHN.

Through the proliferation of intermediate progenitors or self-renewing progenitor cells, neurons are generated from NSCs; however, a majority of NSCs do not undergo active proliferation but remain in a quiescent state⁵². The activated NSCs divide into daughter cells which enter quiescence, self-renewal, or differentiation into neurons or glia over approximately 7 weeks in mice²⁵. There are four phases of neurogenesis: (1) precursor cell activation/proliferation, (2) early survival, (3) early postmitotic maturation, and (4) late maturation⁵³. At the precursor stage, activated, multipotent astrocyte-like quiescent NSCs divide asymmetrically to form both progenitor cells and NSCs⁵⁴.

Comparatively, *Ascl1* and *Prox1* expressions are reported in early proliferating intermediate progenitor cells whereas *PSA-NCAM*, *NeuroD*, and *DCX* expressions are observed in late proliferating intermediate progenitor cells^{51,55}.

The cell morphologies of neural progenitor cells differ from mature dentate granule cells: they remain as round or ovoid cells smaller than mature dentate granule neurons with short processes, and form clusters²⁴.

Progenitor cells with neuronal fate specification become newly formed neuroblasts which develop into immature dentate granule neurons via excitation by GABAergic input to promote neuronal differentiation⁵⁶. Many newly generated cells experience cell death following division, and these cells are eliminated by apoptosis with 50% of BrdU-labeled cells remaining, thereby reducing the quantity of newly generated granule cells/neurons⁵⁷. Two weeks later, the subpopulation of surviving newly generated immature neurons migrates horizontally in the SGZ to establish fusiform cells with horizontally oriented extensions⁵⁸. Finally, the neurons migrate to the GCL and are incorporated into the hippocampal network where they extend their apical dendrites and develop axons⁵⁹.

Newly formed neurons displaying INMs undergo axon elongation, branched dendritic spine formation, and synapse formation during the maturation process^{22,60,61}. The development of granular cells is first marked by strong expression of *PSA-NCAM* and *DCX* with limited syntactic contact with CA3 pyramidal cells⁶², axon terminals, radial glial processes, and nonpyramidal cells⁶³. A potent negative regulator of cell interactions is *PSA-NCAM*⁶⁴, which diminishes from half of the immature neurons to allow synaptic contacts during dendrite formation of mature dentate granule cells²⁴. The late maturational stage is also characterized by switching *calretinin* expression to *calbindin* expression⁶⁵, accounting for the decreased excitability in developed granule cells eight weeks after generation^{66,67}. This eight-week period is critical for new neurons to create glutamatergic synapses with a diminished propensity for long-term potentiation (LTP)⁶⁸, which mediates the synaptic plasticity necessary for hippocampal memory formation⁶⁹.

Promising evidence that AHN declines with age is consistently reported in mouse models^{9,70-72}. A small portion of proliferating cells (*Ki67+*), INM-cells, and BrdU-labelled cells persists across development as seen through experiments in aged rodents—implicating a decreasing rate of AHN in older rodents⁷¹⁻⁷³. Blockage or genetic ablation of new neuron formation interferes with cognitive abilities, such as conditioned learning, emotional processing, and memory, which involves hippocampal circuitry and neuronal generation from AHN^{74,75}. It is noted that environmental and behavioral cues such as exercise could enhance neurogenesis in rodents to improve cognitive performance⁷⁶; accordingly, AHN is negatively impacted in high-stress conditions, such as depression and neurodegeneration^{10,77,78}. AHN is a specialized process within the neurogenic niche, where interruptions of such a niche can result in cognitive impairment of learning and memory processes⁷⁹. Mechanistically, AHN is a simple process; however, due to its translational characteristic, it has an essential role in disease formation and maintenance, as well as researchers' understanding of cognitive processes. Rodent models of AHN have paved the way for future analysis and provoked translational studies aiming at humans, mainly through the use of post-mortem hippocampal tissues. It is worth mentioning that non-human primates greatly contribute to the discussion of AHN; however, for feasibility reasons, they will not be covered in this review.

Adult Neurogenesis in Humans

The first endorsement of AHN stemmed from an immunohistochemical investigation in 1994, when Mathern and colleagues conducted *PSA-NCAM* IHC staining on non-atrophic brains of children with extrahippocampal seizures¹¹. Neural storms manifest as massive surges in neural activity resulting in seizures and can cause seizure-induced neuronal damage or aberrant sprouting, which can impact the postnatal neurogenic development of the hippocampus^{11,80,81}. Decreased quantities of immature neurons were detected in hippocampi of children with frequent seizures¹¹. This further illustrated that severe epilepsy adversely affects processes involved with normal postnatal neurogenesis^{11,80}. Mikkonen and colleagues obtained post-mortem hippocampi and the entorhinal cortex of patients with temporal lobe epilepsy to further scrutinize the immunoreactivity of

PSA-NCAM in comparison to specimens from autopsy controls without neurological diseases⁸¹. Likewise, a considerable number of PSA-NCAM+ cells in the hippocampal SGZ was reported in adult controls and patients with mild neuronal loss⁸¹. However, in epileptic patients with severe neuronal loss, PSA-NCAM+ cells in the SGZ are drastically undermined⁸¹. In summary, the initial investigations on post-mortem epileptic patients have yielded comparable results to Altman's research on rodents regarding existence of AHN in humans. These studies have uncovered that severe epilepsy can have a negative impact on normal neurogenic development of the hippocampus. Early studies on AHN using post-mortem epileptic patient brains have provided important guidance for future studies on AHN in the context of human tissues. These early studies have highlighted the potential impact of neurological diseases on the AHN process and have pioneeringly illustrated the intertwined relationship between AHN and disease. While much of the understanding of AHN comes from rodent studies, these findings suggest that continued investigation of AHN in human tissues may yield important insights into the mechanisms of neurogenesis and its role in the pathophysiology of neurological diseases.

Furthermore, Gu and colleagues offered evidence for postnatal neurogenesis by studying the distribution of Nestin immunoreactivity in human brain tissues⁸². They demonstrated that there are elevated concentrations of Nestin in SGZ cells, which have astrocyte-like morphology but are not double-labeled with astrocytic GFAP, suggesting the presence of neural stem cells or progenitors⁸². A methodologically unique study by Eriksson and colleagues utilized BrdU incorporation on post-mortem brains from adult cancer patients to estimate proliferating cells in the adult human hippocampal region¹². Using immunofluorescent labeling for BrdU and colocalizing cells with neuronal markers including calbindin+ and NeuN+ cell bodies, new neurons in both the GCL of the DG and in the SVZ were illustrated¹². Early IHC studies have provided evidence for postnatal neurogenesis in the adult human hippocampus through the distribution of a neuronal marker immunoreactivity, suggesting the presence of NSCs or progenitors and new neurons in the SGZ. However, there exist some inconsistencies in studies from the 1990s. One study that collected human brain tissues ranging from 7 months to 82 years old found that the maximal cell number of PSA-NCAM+ immature granule cells in GCL and SGZ exists during the first 3 years of life⁸³. This level of PSA-NCAM+ immature granule cells is followed by a considerable decrease in PSA-NCAM+ cells from 3 years of age onwards, implying an age-dependent PSA-NCAM-mediated neuroplasticity with attenuation across the human lifespan⁸³. This incongruent finding was not systematically examined in-depth, but certain factors such as individual differences in patients, sample conditions, and immunohistochemical methods could be contributing factors⁸⁴. After a period of varying identification methods for neurogenesis in the SGZ, researchers investigating early adulthood agreed upon the existence of AHN in human hippocampi. Despite initial debates and inconsistencies, the consensus among early researchers was that AHN is present in the hippocampal SGZs, challenging long-held beliefs about the inability of the adult brains to generate new neurons.

As it became known that BrdU is toxic to humans, researchers turned to immunohistochemistry for more molecular markers. For example, an extensive IHC study from the Kempermann group mapped fourteen neurogenic markers associated with rodent AHN and evaluated DCX (a microtubule-associated protein found in differentiating neurons) co-expression in samples from the human hippocampus across the entire lifespan, ranging in age from 1 day to 100 years of age⁸⁵. Their efforts illustrated the existence of DCX immunoreactivity in the GCL and SGZ of every sample across this age range, but an exponential decline in DCX+ cell density due to aging⁸⁵. Furthermore, all fourteen neurogenesis-associated markers were detected in DCX+ cells and double-labeling confirmed the neuronal lineage of these cells, but colocalization with DCX decreased with age⁸⁵, consistent with other reports of qualitative and quantitative reductions in the DCX expression patterns due to aging in the SGZ⁸⁶⁻⁸⁸. Additional innovative measures were also applied for neurogenic marker detection, such as nuclear magnetic resonance spectroscopy^{35,36}. Scientists used this spectroscopy for non-invasive identification of augmented biomarkers in neural progenitor cells and NSCs from living human brains, with the potential of quantification at different neurogenic stages^{35,36}. One creative alternative approach was to use carbon-14 incorporation from nuclear bomb test-derived ¹⁴C in the genomic DNAs of human hippocampal neurons

for cell turnover dynamics⁸⁹. Using ¹⁴C incorporation data, they found occurrence of continuous AHN with an additional 700 newborn neurons to the hippocampus every day⁸⁹. Furthermore, a sizable subpopulation of newly generated hippocampal neurons is subject to annual turnover with a rate of 1.75% that persists across the lifespan⁸⁹. The total level of additional neurons formed in humans is debated, historically due to the difficulty in quantification and the controversy over the extent of postnatal neurogenesis. Nevertheless, modern research utilizing advanced techniques has provided compelling evidence to support the presence of AHN, which is heavily and negatively affected by aging in adults.

Although it is necessary to investigate a vast demographic range of post-mortem brains via different methodologies and from different perspectives, the proposal of persistent neurogenesis in the human SGZ was opposed by a study from Dennis and colleagues⁹⁰. This group used IHC and immunofluorescent biomarkers on post-mortem brain tissues from adults and juveniles that had been fixed for 2-3 weeks⁹⁰. They discovered a reduction in proliferating cells in neurogenic niches of early infancy—marked by a dramatic decline of Ki67+ proliferating cells in the DG or SGZ shortly after the first years of life⁹⁰. Dennis and colleagues also described a drastic decline in DCX+ clusters over the age of three, and localized a sparse amount of Ki67+/DCX+ cells in the SGZs of juvenile and adult individuals⁹⁰. They marked a low density of proliferating cells and neuroblasts in neurogenic niches⁹⁰, in conflict with earlier discoveries of continued neurogenesis in the human SGZ. Similarly, a study by Sorrells and colleagues, which collected intraoperative and post-mortem specimens of human hippocampi from fetal and postnatal subjects to adult patients with epilepsy, demonstrated a rich neurogenic niche in infants⁴². After a post-mortem interval of approximately 48 hours, hippocampal samples were fixed for less than 1 hour before they were sliced and stained using immunohistochemistry for twenty-two neurogenic markers and in-situ hybridization against a single marker, DCX⁴². They observed that the number of Ki67+/Sox1+ or Ki67+/Sox2+ dividing neural progenitors and DCX+/PSA-NCAM+ immature neurons in the DG intensely diminished in the first year of life with nearly undetectable levels of DCX+ PSA-NCAM+ newborn neurons for neurogenesis cells in the adult SGZ aged between 18 and 77 years old⁴². These results, especially ones by Sorrell et al. published in *Nature*, stirred considerable debate in the field of neuroscience since they provided evidence that disputed drastically against previous findings on the existence of AHN across ages^{47,91,92}. They demonstrated a lack of evidence for persistent neurogenesis in the adult hippocampus and called into question the validity of previous studies that reported long-lasting neurogenesis in the human SGZ, indicating the need for further investigation and scrutiny in the field.

Interestingly, a separate study performed in the same year of 2018 also characterized DCX+/PSA-NCAM+ cells but found contradicting results utilizing hippocampi collected during autopsy⁴³. Boldrini and colleagues set a narrow post-mortem interval of only 26 hours to prevent brain protein degradation, and conducted immunocytochemistry and immunofluorescence experiments targeting seven widely-used neurogenic biomarkers⁴³. They illustrated persistent and stable numbers of DCX+ PSA-NCAM+ proliferating neuronal progenitors and Ki67+/Nestin+ immature neurons in the SGZ of DG across the ages of 14-79, disregarding a smaller pool of quiescent stem cells in aged DG indicated by Sox2 and GFAP expression⁴³. The authors interpreted the results as firmly suggesting a reduction in the pool of dormant stem cells and an enduring population of intermediate neural progenitors driving AHN in the SGZ⁴³. Further immunohistochemical studies using improved tissue-processing methods supported the work by Boldrini and colleagues^{44,84}. Based on experiments testing the influence of fixation time on the detection of markers of AHN in humans, Llorens-Martin's group limited their post-mortem interval to a shorter delay ranging from 2.5 to 10 hours and restricted their fixation time to 24 hours before applying their adapted slicing procedure, which minimizes tissue damage^{44,84}. To ensure the specificity of the DCX+ signal, the authors assessed and selected the most specific antibody, a polyclonal goat anti-DCX antibody, and demonstrated the expression of several differentiated markers in a subset of DCX+ cells, including neuronal nuclei (NeuN), calretinin (CR), PSA-NCAM, calbindin (CB), and prospero homeobox 1 (Prox1)^{44,84}. Using a well-defined immunofluorescence and optimized autofluorescence/background elimination approach on eight neurogenic markers, the researchers provided convincing evidence of fre-

quent AHN in humans by detecting thousands of DCX+ immature neurons with unambiguous neuronal morphologies in the DG up to the ninth decade of human life^{44,84}. These findings reinforced the validity of their methodology, indicating the presence of mature and functional neurons originating from adult neurogenesis in the healthy human DG^{44,84}. After conducting neuropathological assessments and screening subjects for cognitive impairment and Alzheimer's disease at different stages, the presence of persistent neurogenesis in the SGZ was observed throughout the tenth decade of life, as evidenced by the presence of DCX+ neuroblasts, immature neurons, and Nestin+/Sox2+/Ki67+ neural progenitor cells, in both elderly individuals and patients with Alzheimer's disease^{44,93}. However, it was also noted that compared to healthy individuals, patients with Alzheimer's disease exhibited a progressive decline in the number and maturation of these neurons as the disease advanced^{44,93}. Although the quantity of cells detected greatly varied between patients, and the proliferative capacity of DCX+ cells was somewhat inconsistent in findings^{93,94}, these studies effectively refuted prior research and established the persistent occurrence of AHN in humans across the lifespan, regardless of health status or age. They employed advanced immunofluorescence analyses and improved methodologies to provide strong evidence of the presence of immature neurons and neural progenitor cells in the SGZ. However, this also highlights the necessity of a standardized protocol to avoid inconsistencies and increase reliability in future studies. These findings provide additional implications for understanding the role of neurogenesis in cognitive function and aging. The relationship between neurogenesis and AD will be discussed in a later section to further explore the implications of the findings.

Many factors may have played a role in the discrepancies of these findings; the incapacity to identify pronounced emergence of newborn neurons in postnatal humans could be attributable to inconsistencies in methodologies for tissue fixation and storage of samples in long-term conditions⁸⁴. By analyzing effects of post-mortem delay/interval; fixative use and its duration; antibodies used for immunohistochemistry; and other parameters, Llorens-Martin's group addressed the technical issue of fixation in which detection of immature neuron marker DCX will dramatically decrease if over-fixation of tissue occurs after a 24 hour fixation^{44,84}. Regarding immunohistochemistry, Dennis and colleagues analyzed samples with post-mortem delay up to 90 hours⁹⁰, and Sorrells and colleagues included tissues with post-mortem delay up to 48 hours⁴². On the other hand, Boldrini and colleagues limited their post-mortem interval up to 26 hours⁴³, and Moreno-Jiménez and colleagues applied an even shorter delay fewer than 10 hours⁴⁴. The change in delay could contribute to the absence of detection in the human DG considering degradation and undetectable DCX epitope after 24 hours post-mortem delay before fixation^{42,84,90}. The use of a narrow post-mortem interval, as employed by Boldrini et al. and Moreno-Jiménez et al., may provide a more accurate representation of the extent of adult neurogenesis in human brains, as it prevents protein degradation and other factors that may affect the detection of neurogenic markers. However, while the tissue processing procedures used in the studies above may provide more scientifically sound evidence for the persistence of AHN in adult humans, the topic remains heavily debated and underscores the need for an agreed upon protocol to minimize conflicting results in future research.

Aside from immunohistochemistry, the manner by which different studies recognize the region of interest —SGZ—may also contribute to contradictory findings^{42,45,85,90}. Based on DCX expression in the DG, Knoth and colleagues did not observe a sharp hilar border of the GCL as distinct as in rodents, and there was no apparent SGZ to be easily distinguished⁸⁵. Similarly, Sorrell and colleagues described a less defined SGZ in fetal or juvenile brains regarding their Ki67+ cells and a coalesced region with isolated cells marking an absence of continuous SGZ in the cohort of brains⁴². By contrast, SGZ was defined by Moreno-Jiménez and colleagues as the part of the GCL closer to the hilus and having a thickness of one to two cells⁴⁴. As not all literature clearly reported their quantitative or qualitative definition of the SGZ region, it would be difficult for researchers to remain on the same page and the opposite findings regarding the persistence of AHN may be attributed, in part, to the varying definitions of the SGZ locations. With the latest progress in single-cell genomic analysis, innovative technologies may riddle out the considerable debate on AHN presence and

pave the way for future studies³⁷⁻⁴¹. For instance, considering the heterogeneity of cell lineages within neurogenic niches³⁷⁻⁴⁰, single cell-RNA sequencing can help map cell heterogeneity and gene expression associated with stem cell functions that have been previously observed in mice. This method has been applied in both the developing and adult human cerebral cortex⁹⁵⁻⁹⁷, so researchers potentially can validate the optimal markers and antibodies for identifying cell subtypes in the SGZ of humans through single-cell RNA sequencing in the future. The extent to which AHN occurs in diseased versus healthy individuals can be further explored, while minimizing confounding variables and maximizing signal specificity for more congruous views^{47,53,92}.

Disease-induced changes in AHN & Therapeutics

Major Depressive Disorder & Antidepressants

Individuals with mood disorders, such as major depressive disorder (MDD) and bipolar disorder, exhibit altered hippocampal volume and circuitry⁹⁸⁻¹⁰⁰. With fluorescence-based immunohistochemistry, Walton and colleagues further characterized bipolar patients as having an "immature dentate gyrus," demarked by increased numbers of calretinin-positive immature neuronal progenitors compared to the mature DG marker calbindin¹⁰¹. While Walton's group found differences between the SGZ of bipolar patients and healthy controls, they were unable to detect any statistically significant immunohistochemical differences in calretinin, calbindin, or PCNA expression in MDD patients¹⁰¹. Comparatively, Reif and colleagues, using sections of the anterior hippocampus from bipolar and MDD patients for IHC, detected no change in Ki67+ cells between MDD patients and controls¹⁰². In both studies, the changes in proliferative capacity marked by Ki67 and PCNA expression in SGZ of bipolar patients and controls were considered non-significant^{101,102}. Additionally, Lucassen and colleagues recognized a significant reduction in Mcm2+ cells but not in PH3+ cells from post-mortem brains of MDD patients¹⁰³. They concluded that progenitors or putative stem cells decrease in number and proliferation is unchanged¹⁰³. One factor that can account for the differing data in bipolar disorder and MDD is the phasic nature of mood disorders, which contributes to the inability to examine whether patients suffered from the active symptoms of the mood disorders at the time of death if no further case details are provided^{104,105}. Based on the studies reviewed, it appears that there is no significant change in the proliferative capacity of NSCs within the SGZ in patients with MDD. These findings suggest that the reduced hippocampal volume observed in patients with MDD may be not due to a decrease in neurogenesis. However, it is important to note limitations including small sample sizes and differences in the methods used to measure neurogenesis. Further research is needed to fully understand the role of neurogenesis in the pathophysiology of MDD and its potential as a therapeutic target.

Another factor to take into account is the consumption of antidepressants and its effect on altering AHN in bipolar and MDD patients. Some studies found no correlation between the use of antidepressants and altered AHN^{102,103}. In contrast, Boldrini and colleagues collected autopsy post-mortem samples and compared medication-free MDD, medicated MDD, and nonpsychiatric control subjects, with the medicated group separated by tricyclic antidepressant (TCA) or selective serotonin reuptake inhibitor (SSRI) prescriptions^{106,107}. Through immunohistochemistry for Nestin and Ki67, they observed increased progenitor cells (Nestin-immunoreactive) and proliferation (Ki67+) in medicated MDD patients. Also, differential effects of SSRIs and TCAs were observed: MDD subjects treated with SSRI (MDDT-SSRI) exhibited greater DG volume and a greater number of Nestin+ neural progenitor cells than MDDT-TCA subjects; whereas, MDDT-TCA subjects demonstrated significantly more Ki67+ proliferative cells than MDD-SSRI subjects^{106,107}. One proposed mechanism is that these drugs enhance the expression of growth factors such as brain-derived neurotrophic factor (BDNF) which is known to promote neurogenesis^{108,109}. Although Boldrini and colleagues observed increased neurogenic proliferation in medicated MDD patients, with distinct effects of SSRIs and TCAs on progenitor cells, the conflicting results, again, can be attributed to various factors such as individual differences in neuro-

anatomy and sample size differences^{106,107}. For example, individuals with smaller hippocampal volumes may have a reduced capacity for neurogenesis, which could affect their response to antidepressant treatment¹¹⁰. Additionally, differences in the functional connectivity of the hippocampus with other brain regions, such as the prefrontal cortex, may also play a role in determining the effects of antidepressants on neurogenesis¹¹¹. Furthermore, the double labeling of Ki67/Nestin is not adequate to delineate neural versus non-neural lineages or to extrapolate conclusions on neurogenesis. Regardless, the studies on neurogenic progenitors and proliferation provide valuable insight into the complex interplay between neural stem cells, their microenvironment, and the effect of various factors, such as medication, on the pathophysiology of depression. Specifically, they shed light on the mechanisms of adult neurogenesis in the hippocampus and how it may be altered in individuals with MDD. As the hippocampus is implicated in mood disorders, a more in-depth understanding of neurogenesis is necessary to develop more effective therapies and treatment. While AHN may play a role in MDD, it is important to keep in mind that depression is a complex multifaceted disorder with many factors at play beyond specific biological brain regions. Therefore, we should view AHN as just one piece of the puzzle, rather than a definitive explanation for the development or treatment of MDD.

Alzheimer's Disease & Neurodegeneration

Alzheimer's disease (AD) is a debilitating, relentlessly progressive neurodegenerative disease characterized by memory and cognitive impairments, affecting millions of people worldwide¹¹². AD is often marked by early neuron loss and cell death in the hippocampus as a pathological feature, so SGZ neurogenesis may be impacted in AD progression and implicated for AD prevention¹¹³. However, early studies investigating AHN in AD have reported conflicting results. Some studies found increased neurogenesis in the SGZ of AD patients through heightened expression of AHN immunohistochemical markers. For example, Jin and colleagues observed elevated expression of NeuroD, PSA-NCAM, DCX, and TUC-4 (a protein expressed in early neuronal differentiation) in fourteen post-mortem AD brains based on double-label immunohistochemistry³². DCX, PSA-NCAM, and TUC4-positive cells also co-expressed cleaved caspase-8, suggesting that AHN is upregulated in AD brains to compensate for proliferating neuronal precursors that underwent caspase-dependent programmed cell death during degeneration³². Another study of progressive chronic neurodegeneration described an increased number of non-microglial Ki67+ cells and calretinin+ cells in ten AD SGZs, consistent with the previously proposed notion of increased neurogenesis during the progression of AD to counteract the effects of chronic neurodegeneration¹¹⁴. Contradiction arose in experiments by Lovell and colleagues that show lower viable Ki-67+/Musashi-1+ precursor cells isolated from three AD patient post-mortem tissue samples compared to NSCs isolated from healthy controls, and senescence was faster reached in AD cells compared with controls¹¹⁵. Later in 2006, a study using single IHC documented a reduction in the amount of progenitor cells in seven AD patients' SVZ regarding the decrease in Musashi-1 immunoreactivity, but an increase in GFAP-negative and Nestin+ astrocyte-like stem cells with progenitor characteristics¹¹⁶. It should be noted that earlier studies examining the relationship between AD and AHN are limited by sample availability and differences in methodologies due to the lack of advanced technology. Furthermore, differences in the stages of AD progression studied may also play a role in these conflicting findings. As the understanding of the complex interplay between AD and AHN continues to evolve, further research with standardized methodologies and larger sample sizes may provide more definitive insights.

Recent studies have consistently shown impaired SGZ neurogenesis in AD through a reduced number of cells positive for various neurogenic markers, such as GFAP, PH3, PSA-NCAM, Ki67, PCNA, DCX, Sox2, Nestin, Prox1, NeuN, β III-tubulin, and calbindin^{44,94}. Furthermore, Moreno-Jimenez and colleagues showed a persistence of SGZ neurogenesis until the tenth decade of life by evaluation of forty five patients with AD between 52 and 97 years of age⁴⁴. However, they observed a tendency for DCX+ cells to have impaired maturation and decreased density compared to healthy aged subjects as AD advances, based on their analysis of immunohistochemical colocalization of DCX and the lineage markers listed to demonstrate deterioration⁴⁴. A separate study assessed cognitive diagnosis to determine disease progression stages in AD patients and discerned a

decreased quantity of DCX+PCNA+ cells in patients with mild cognitive impairments—illustrating an association between neurogenesis and cognitive status⁹³. In addition, patients with AD exhibited lower counts of DCX+/PCNA+ neuroblasts with a significant drop in neurogenesis even at early stages of dementia development⁹³. Terreros-Roncal and colleagues studied post-mortem human tissues from patients with neurodegenerative diseases such as Huntington's disease, Parkinson's disease, amyotrophic lateral sclerosis (ALS), and frontotemporal dementia¹¹⁷. They highlighted aberrant morphologies of DCX+ immature dentate granule cells and variations in the immunoreactivity of DGC differentiation biomarkers in these neurodegenerative diseases, suggestive of altered homeostasis of DG neurogenic niche functions and vulnerability of the AHN to neurodegeneration in humans¹¹⁷. These studies collectively demonstrate the dynamic nature of both AD and neurogenesis, as they show how the processes of neurogenesis and disease progression are closely intertwined and how the impairment of SGZ neurogenesis contributes to the progression of neurodegenerative AD. Furthermore, the studies emphasize the complex and evolving nature of both AD and neurogenesis, highlighting the need for ongoing investigation into their interplay.

Targeting AHN in Alzheimer's Disease

Our analysis of surface albedo numbers in the literature revealed that the atIt was established that therapeutics targeted at alleviating the neurodegenerative process were not successful¹¹⁸. Taking into consideration the negative correlation between AD progression and neurogenesis, improving neurogenesis has drawn attention as a new therapeutic target for AD¹¹⁸. One proposed approach to upregulating neurogenesis in the hippocampus proposed preventing microglial activation during neuroinflammation, with the anti-inflammatory drug minocycline¹¹⁹⁻¹²¹. Wadhwa and colleagues demonstrated that impaired neurogenesis can be improved via minocycline administration at different developmental stages: proliferation (more Ki-67+/BrdU+ DG cells), phases of differentiation (increased DCX+ cells) and growth factor (restored level of BDNF proteins)¹¹⁹. Comparably, the usage of retinoic acid derived from vitamin A can be a potential therapeutic to induce unspecialized stem cell differentiation and reinstate neurogenesis in AD patients¹²². The proposed mechanism is that retinoic acid, through direct activation of retinoid X receptors (RXRs) and retinoic acid receptors (RARs), impedes the pathogenesis of AD in mice by suppressing the release of pro-inflammatory cytokines and chemokines in glia cells, including astrocytes and microglia¹²². As an antioxidant, retinoic acid also attenuates A β plaque accumulation in APP/PS1 mice, an animal model for AD, while restoring spatial learning and memory deficits in treated mice¹²³.

As it was well-documented that excessive oxidative stress could inhibit neurogenesis in the SGZ of the hippocampus¹²⁴⁻¹²⁶, researchers adopted the therapeutic potential of antioxidants to target reactive oxygen species (ROS) and alleviate pathogenesis of AD. Montiel and colleagues revealed that nerve-end lesioning and enhanced lipoperoxidation (LPO) elicited by A β administration in the hippocampus of rats was efficiently prevented with antioxidant α -tocopherol (vitamin E)¹²⁷. Since vitamin E is known for its protective antioxidant effects against free radicals¹²⁸, another epidemiological prospective cohort study concluded that participants with diets abundant in vitamin E may carry a modestly lower long-term risk of AD and dementia¹²⁹. Another vitamin with known antioxidant effects and feasibility to lower the risk of AD is vitamin C^{130,131}, which was also shown to attenuate A β oligomerization alongside lower cerebral oxidative damage and to restore behavioural deficits associated with AD progression in mouse models¹³². Another antioxidant implicated in AD therapeutics is curcumin: a curry spice found in turmeric with radical scavenging activity and anti-inflammatory activities^{133,134}. In a transgenic mouse model of AD, low-dose curcumin significantly suppressed interleukin-1 β (a proinflammatory cytokine), lowered oxidized proteins, and diminished soluble/insoluble amyloid accounting for the overall plaque burden, which suggests that curcumin contributes to AD prevention^{135,136}.

Exercise as an alternative and adjunct treatment has been illustrated to enhance cell proliferation and neurogenesis in DG of adult mice, where running doubled the quantity of surviving newborn cells¹³⁷. Van Praag and colleagues reported improved LTP and spatial learning in exercised mice with more BrdU+ cell numbers, which signify elevated AHN in the hipp-

ocampal DG¹³⁸. Other literature has connected the brain-derived neurotrophic factor (BDNF) to exercise-mediated neurogenesis^{139,140}. A study using AD mouse models demonstrated that exacerbation of DG neuron loss and cognitive impairment could be induced by blocking AHN¹⁴⁰. They noted that induction of neurogenesis alone showed no significant effect in improving cognition in AD mice¹⁴⁰. However, simultaneous induction of neurogenesis and increased levels of BDNF mimics the effect of exercise-mediated AHN and could alleviate cognitive deficits observed in AD mice¹⁴⁰.

Therapeutic interventions that enhance neurogenesis in neurodegenerative diseases such as AD are a fruitful area of investigation but face many ongoing challenges due to the multifaceted nature of these diseases¹⁴¹. The translational limitations of animal models to humans and conflicting findings on the pathology of neurological disorders involving AHN can be frustrating in the context of treatments and interventions. Through increased insight on the topic of disease-induced changes on AHN and interventions targeting AHN, future therapeutic approaches can be devised in order to improve cognitive abilities in aging populations if AHN as a target is further explored. For example, a deeper understanding of the mechanisms involved in AHN and how they relate to cognitive decline in conditions such as Alzheimer's disease could lead to the development of targeted therapies aimed at enhancing neurogenesis and improving cognitive function. In addition, continued research into the relationship between AHN and other factors such as environment, diet, and stress could provide valuable insights into how lifestyle interventions may help to support healthy neurogenesis and promote cognitive health in aging populations. Ultimately, by gaining a better understanding of the complex interplay between AHN and cognitive function, researchers may be able to devise more effective strategies for promoting healthy brain aging and mitigating the effects of age-related cognitive decline.

Future Directions

In the past, most of our understanding of AHN came from rodents, and researchers agreed on the presence of AHN, which involves the proliferation and differentiation of neural stem cells into neurons through distinct phases of neurogenesis. While AHN is a simple process mechanistically, it plays an essential role in disease formation and maintenance, as well as in scholars' views of cognitive processes. Early findings from rodent models of AHN paved the way for translational studies aimed at humans, but discrepancies arise when studying post-mortem tissues in a manner similar to exploring mice. More recent studies have utilized molecular markers, such as DCX, to confirm the existence of AHN throughout the entire lifespan, but with a decline due to aging. Although the lack of standardized methodologies has led to reports of both absence and persistence of AHN; overall, modern research utilizing advanced techniques has provided strong support for the presence of AHN in the adult human hippocampus, which is negatively impacted by aging. The implications of AHN have been investigated in other fields, including mood disorders such as MDD, neurodegeneration such as AD, and various therapeutics. However, without a clear understanding of its fundamental existence, further research on these topics would only create more confusion and contradiction.

Presently, there is a pressing need for consensus on the presence of AHN in humans and a more coherent comprehension of defective AHN implicated in aged and diseased brains. This neuropharmacological field has fallen short in part due to technological hindrance and the shortage of post-mortem human tissues, but the emergence of a unified understanding of AHN is plausible in the future. Our current knowledge about how AHN works and how it interacts with the rest of the human brain is still quite limited. Our knowledge about the role of AHN in aging, neurodegeneration or psychiatric disorders is also impacted by heterogenous manipulation procedures. Recent development in transcriptomic methodologies, such as RNAscope and single cell-RNA sequencing, allows for precise collection of cell profiles from both human tissue and genetically altered disease-specific mouse strains, allowing for increased insight into disease mechanisms/consequences¹⁴². The highly sensitive in-situ hybridization method known as RNAscope permits multiplex detection for up to four

target genes and ensures visualization of genes with low expression levels¹⁴³. This allows for a more precise colocalization profile, which in turn facilitates the accurate identification of the cell type and potential quantification of mRNA levels in each cell. The RNAscope approach is particularly useful in unraveling the heterogeneity of neurogenic lineages in the SGZ. Although funding can be restrictive depending on the scope of the project, new approaches combined with the latest findings would improve our understanding of AHN in humans. Ultimately, this knowledge would help produce potential treatments for devastating diseases such as AD, dementia, and psychiatric illnesses.

Acknowledgements

ZN wrote the manuscript and TC edited the body of work. I would like to thank Sophie Simard and Prof Naguib Mechawar for providing useful suggestions and supervision. The authors have no conflict of interest to declare.

References

1. Altman, J. & Das, G. D. Post-Natal Origin of Microneurons in the Rat Brain. *Nature* **207**, 953-956 (1965). <https://doi.org/10.1038/207953a0>
2. Altman, J. Autoradiographic investigation of cell proliferation in the brains of rats and cats. *Anat. Rec.* **145**, 573-591 (1963). <https://doi.org/10.1002/ar.1091450409>
3. Gross, C. G. Neurogenesis in the adult brain: death of a dogma. *Nat. Rev. Neurosci.* **1**, 67-73 (2000). <https://doi.org/10.1038/35036235>
4. Altman, J. in *Neurogenesis in the Adult Brain I: Neurobiology* (eds Seki, T., Sawamoto, K., Parent, J. M. & Alvarez-Buylla, A.) 3-46 (Springer Japan, 2011). https://doi.org/10.1007/978-4-431-53933-9_1
5. Kempermann, G. The pessimist's and optimist's views of adult neurogenesis. *Cell* **145**, 1009-1011 (2011). <https://doi.org/10.1016/j.cell.2011.06.011>
6. Seki, T. in *Neurogenesis in the Adult Brain I: Neurobiology* (eds Seki, T., Sawamoto, K., Parent, J. M. & Alvarez-Buylla, A.) 193-216 (Springer, 2011). https://doi.org/10.1007/978-4-431-53933-9_7
7. Seki, T. & Arai, Y. Highly polysialylated NCAM expression in the developing and adult rat spinal cord. *Dev. Brain Res.* **73**, 141-145 (1993). [https://doi.org/10.1016/0165-3806\(93\)90056-G](https://doi.org/10.1016/0165-3806(93)90056-G)
8. Seki, T. & Arai, Y. Highly polysialylated neural cell adhesion molecule (NCAM-H) is expressed by newly generated granule cells in the dentate gyrus of the adult rat. *J. Neurosci.* **13**, 2351-2358 (1993). <https://doi.org/10.1523/jneurosci.13-06-02351.1993>
9. Seki, T. & Arai, Y. Age-related production of new granule cells in the adult dentate gyrus. *Neuroreport* **6**, 2479-2482 (1995). <https://doi.org/10.1097/00001756-199512150-00010>
10. Kuhn, H. G., Dickinson-Anson, H. & Gage, F. H. Neurogenesis in the dentate gyrus of the adult rat: age-related decrease of neuronal progenitor proliferation. *J. Neurosci.* **16**, 2027-2033 (1996). <https://doi.org/10.1523/jneurosci.16-06-02027.1996>
11. Mathern, G. W. et al. Children with severe epilepsy: evidence of hippocampal neuron losses and aberrant mossy fiber sprouting during postnatal granule cell migration and differentiation. *Dev. Brain Res.* **78**, 70-80 (1994). [https://doi.org/10.1016/0165-3806\(94\)90011-6](https://doi.org/10.1016/0165-3806(94)90011-6)
12. Eriksson, P. S. et al. Neurogenesis in the adult human hippocampus. *Nat. Med.* **4**, 1313-1317 (1998). <https://doi.org/10.1038/33005>

13. Gould, E. How widespread is adult neurogenesis in mammals? *Nat. Rev. Neurosci.* **8**, 481-488 (2007). <https://doi.org/10.1038/nrn2147>
14. Yuan, T.-F., Li, J., Ding, F. & Arias-Carrion, O. Evidence of adult neurogenesis in non-human primates and human. *Cell Tissue Res.* **358**, 17-23 (2014). <https://doi.org/10.1007/s00441-014-1980-z>
15. Kempermann, G., Kuhn, H. G. & Gage, F. H. More hippocampal neurons in adult mice living in an enriched environment. *Nature* **386**, 493-495 (1997). <https://doi.org/10.1038/386493a0>
16. Palmer, T. D., Takahashi, J. & Gage, F. H. The adult rat hippocampus contains primordial neural stem cells. *Mol. Cell. Neurosci.* **8**, 389-404 (1997). <https://doi.org/10.1006/mcne.1996.0595>
17. Miller, J. A. et al. Conserved molecular signatures of neurogenesis in the hippocampal subgranular zone of rodents and primates. *Development* **140**, 4633-4644 (2013). <https://doi.org/10.1242/dev.097212>
18. Bond, A. M. et al. BMP signaling regulates the tempo of adult hippocampal progenitor maturation at multiple stages of the lineage. *Stem Cells* **32**, 2201-2214 (2014). <https://doi.org/10.1002/stem.1688>
19. Hodge, R. D. et al. Intermediate progenitors in adult hippocampal neurogenesis: Tbr2 expression and coordinate regulation of neuronal output. *J. Neurosci.* **28**, 3707-3717 (2008). <https://doi.org/10.1523/jneurosci.4280-07.2008>
20. Hodge, R. D. et al. Tbr2 is essential for hippocampal lineage progression from neural stem cells to intermediate progenitors and neurons. *J. Neurosci.* **32**, 6275-6287 (2012). <https://doi.org/10.1523/jneurosci.0532-12.2012>
21. Sultan, S. et al. Synaptic integration of adult-born hippocampal neurons is locally controlled by astrocytes. *Neuron* **88**, 957-972 (2015). <https://doi.org/10.1016/j.neuron.2015.10.037>
22. Gonçalves, J. T. et al. In vivo imaging of dendritic pruning in dentate granule cells. *Nat. Neurosci.* **19**, 788-791 (2016). <https://doi.org/10.1038/nn.4301>
23. Kumar, A. et al. Transcriptomic Analysis of the Neurogenesis Signature suggests Continued but Minimal Neurogenesis in the Adult Human Hippocampus. Preprint at <https://doi.org/10.1101/664995> (2019).
24. Seki, T., Namba, T., Mochizuki, H. & Onodera, M. Clustering, migration, and neurite formation of neural precursor cells in the adult rat hippocampus. *J. Comp. Neurol.* **502**, 275-290 (2007). <https://doi.org/10.1002/cne.21301>
25. Kempermann, G., Song, H. & Gage, F. H. Neurogenesis in the adult hippocampus. *Cold Spring Harb. Perspect. Biol.* **7**, a018812 (2015). <https://doi.org/10.1101/2Fchshperspect.a018812>
26. Treves, A., Tashiro, A., Witter, M. P. & Moser, E. I. What is the mammalian dentate gyrus good for? *Neuroscience* **154**, 1155-1172 (2008). <https://doi.org/10.1016/j.neuroscience.2008.04.073>
27. Sawada, M. & Sawamoto, K. Mechanisms of neurogenesis in the normal and injured adult brain. *Keio. J. Med.* **62**, 13-28 (2013). <https://doi.org/10.2302/kjm.2012-0005-re>
28. Jessberger, S. Neural repair in the adult brain. *F1000Res.* **5** (2016). <https://doi.org/10.12688/f1000research.7459.1>
29. Liu, Y. et al. Doublecortin expression in the normal and epileptic adult human brain. *Eur. J. Neurosci.* **28**, 2254-2265 (2008). <https://doi.org/10.1111/j.1460-9568.2008.06518.x>
30. Jin, K. et al. Evidence for stroke-induced neurogenesis in the human brain. *Proc. Natl. Acad. Sci. U. S. A.* **103**, 13198-13202 (2006). <https://doi.org/10.1073/pnas.0603512103>
31. Macas, J., Nern, C., Plate, K. H. & Momma, S. Increased generation of neuronal progenitors after ischemic injury in the aged adult human forebrain. *J. Neurosci.* **26**, 13114-13119 (2006). <https://doi.org/10.1523/JNEUROSCI.4667-06.2006>
32. Jin, K. et al. Increased hippocampal neurogenesis in Alzheimer's disease. *Proc. Natl. Acad. Sci. U. S. A.* **101**, 343-347 (2004). <https://doi.org/10.3389/fnins.2016.00178>
33. Liu, H. & Song, N. Molecular mechanism of adult neurogenesis and its association with human brain diseases. *J. Cent. Nerv. Syst. Dis.* **8**, JCNSD.S32204 (2016). <https://doi.org/10.4137/JCNSD.S32204>
34. Duque, A. & Spector, R. A balanced evaluation of the evidence for adult neurogenesis in humans: implication for neuropsychiatric disorders. *Brain Struct. Funct.* **224**, 2281-2295 (2019). <https://doi.org/10.1007/s00429-019-01917-6>
35. Manganas, L. N. et al. Magnetic resonance spectroscopy identifies neural progenitor cells in the live human brain. *Science* **318**, 980-985 (2007). <https://doi.org/10.1126/science.1147851>
36. Castiglione, F. et al. NMR Metabolomics for Stem Cell type discrimination. *Sci. Rep.* **7**, 1-12 (2017). <https://doi.org/10.1038/s41598-017-16043-8>
37. Habib, N. et al. Div-Seq: Single-nucleus RNA-Seq reveals dynamics of rare adult newborn neurons. *Science* **353**, 925-928 (2016). <https://doi.org/10.1126/science.aad7038>
38. Hochgerner, H., Zeisel, A., Lönnerberg, P. & Linnarsson, S. Conserved properties of dentate gyrus neurogenesis across postnatal development revealed by single-cell RNA sequencing. *Nat. Neurosci.* **21**, 290-299 (2018). <https://doi.org/10.1038/s41593-017-0056-2>
39. Dulken, B. W., Leeman, D. S., Boutet, S. C., Hebestreit, K. & Brunet, A. Single-cell transcriptomic analysis defines heterogeneity and transcriptional dynamics in the adult neural stem cell lineage. *Cell Rep.* **18**, 777-790 (2017). <https://doi.org/10.1016/j.celrep.2017.11.050>
40. Mizrak, D. et al. Single-cell analysis of regional differences in adult V-SVZ neural stem cell lineages. *Cell Rep.* **26**, 394-406.e5 (2019). <https://doi.org/10.1016/j.celrep.2018.12.044>
41. Shah, P. T. et al. Single-cell transcriptomics and fate mapping of ependymal cells reveals an absence of neural stem cell function. *Cell* **173**, 1045-1057.e9 (2018). <https://doi.org/10.1016/j.cell.2018.03.063>
42. Sorrells, S. F. et al. Human hippocampal neurogenesis drops sharply in children to undetectable levels in adults. *Nature* **555**, 377-381 (2018). <https://doi.org/10.1038/nature25975>
43. Boldrini, M. et al. Human hippocampal neurogenesis persists throughout aging. *Cell Stem Cell* **22**, 589-599.e5 (2018). <https://doi.org/10.1016/j.stem.2018.03.015>
44. Moreno-Jiménez, E. P. et al. Adult hippocampal neurogenesis is abundant in neurologically healthy subjects and drops sharply in patients with Alzheimer's disease. *Nat. Med.* **25**, 554-560 (2019). <https://doi.org/10.1038/s41591-019-0375-9>
45. Gault, N. & Szele, F. G. Immunohistochemical evidence for adult human neurogenesis in health and disease. *W.I.R.E.s Mech. Dis.* **13**, e1526 (2021). <https://doi.org/10.1002/wsbm.1526>
46. Semerci, F. & Maletic-Savatic, M. Transgenic mouse models for studying adult neurogenesis. *Front. Biol.* **11**, 151-167 (2016). <https://doi.org/10.1007/s11515-016-1405-3>
47. Kuhn, H. G., Toda, T. & Gage, F. H. Adult hippocampal neurogenesis: a coming-of-age story. *J. Neurosci.* **38**, 10401-10410 (2018). <https://doi.org/10.1523/JNEUROSCI.2144-18.2018>

48. Luskin, M. B. Restricted proliferation and migration of postnatally generated neurons derived from the forebrain subventricular zone. *Neuron* **11**, 173-189 (1993). [https://doi.org/10.1016/0896-6273\(93\)90281-U](https://doi.org/10.1016/0896-6273(93)90281-U)
49. Seri, B., Garcia-Verdugo, J. M., McEwen, B. S. & Alvarez-Buylla, A. Astrocytes give rise to new neurons in the adult mammalian hippocampus. *J. Neurosci.* **21**, 7153-7160 (2001). <https://doi.org/10.1523/JNEUROSCI.21-18-07153.2001>
50. Kriegstein, A. & Alvarez-Buylla, A. The glial nature of embryonic and adult neural stem cells. *Annu. Rev. Neurosci.* **32**, 149 (2009). <https://doi.org/10.1146/annurev.neuro.051508.135600>
51. Zhang, J. & Jiao, J. Molecular biomarkers for embryonic and adult neural stem cell and neurogenesis. *BioMed. Res. Int.* **2015** (2015). <https://doi.org/10.1155/2015/727542>
52. Codega, P. et al. Prospective identification and purification of quiescent adult neural stem cells from their in vivo niche. *Neuron* **82**, 545-559 (2014). <https://doi.org/10.1016/j.neuron.2014.02.039>
53. Babcock, K. R., Page, J. S., Fallon, J. R. & Webb, A. E. Adult hippocampal neurogenesis in aging and Alzheimer's disease. *Stem Cell Rep.* **16**, 681-693 (2021). <https://doi.org/10.1016/j.stemcr.2021.01.019>
54. Bond, A. M., Ming, G.-l. & Song, H. Adult mammalian neural stem cells and neurogenesis: five decades later. *Cell Stem Cell* **17**, 385-395 (2015). <https://doi.org/10.1016/j.stem.2015.09.003>
55. von Bohlen und Halbach, O. Immunohistological markers for proliferative events, gliogenesis, and neurogenesis within the adult hippocampus. *Cell Tissue Res.* **345**, 1-19 (2011). <https://doi.org/10.1007/s00441-011-1196-4>
56. Tozuka, Y., Fukuda, S., Namba, T., Seki, T. & Hisatsune, T. GABAergic excitation promotes neuronal differentiation in adult hippocampal progenitor cells. *Neuron* **47**, 803-815 (2005). <https://doi.org/10.1016/j.neuron.2005.08.023>
57. Dayer, A. G., Ford, A. A., Cleaver, K. M., Yassaee, M. & Cameron, H. A. Short-term and long-term survival of new neurons in the rat dentate gyrus. *J. Comp. Neurol.* **460**, 563-572 (2003). <https://doi.org/10.1002/cne.10675>
58. Pilz, G.-A. et al. Live imaging of neurogenesis in the adult mouse hippocampus. *Science* **359**, 658-662 (2018). <https://doi.org/10.1126/science.aao5056>
59. Kempermann, G., Gast, D., Kronenberg, G., Yamaguchi, M. & Gage, F. H. Early determination and long-term persistence of adult-generated new neurons in the hippocampus of mice. *Development* **130**, 391-399 (2003). <https://doi.org/10.1242/dev.00203>
60. Faulkner, R. L. et al. Development of hippocampal mossy fiber synaptic outputs by new neurons in the adult brain. *Proc. Natl. Acad. Sci. U. S. A.* **105**, 14157-14162 (2008). <https://doi.org/10.1073/pnas.0806658105>
61. Sun, G. J. et al. Seamless reconstruction of intact adult-born neurons by serial end-block imaging reveals complex axonal guidance and development in the adult hippocampus. *J. Neurosci.* **33**, 11400-11411 (2013). <https://doi.org/10.1523/JNEUROSCI.1374-13.2013>
62. Seki, T. & Arai, Y. Different polysialic acid-neural cell adhesion molecule expression patterns in distinct types of mossy fiber boutons in the adult hippocampus. *J. Comp. Neurol.* **410**, 115-125 (1999). [https://doi.org/10.1002/\(SICI\)1096-9861\(19990719\)410:1<115::AID-CNE10>3.0.CO;2-C](https://doi.org/10.1002/(SICI)1096-9861(19990719)410:1<115::AID-CNE10>3.0.CO;2-C)
63. Seki, T. & Arai, Y. Temporal and spacial relationships between PSA-NCAM-expressing, newly generated granule cells, and radial glial-like cells in the adult dentate gyrus. *J. Comp. Neurol.* **410**, 503-513 (1999). [https://doi.org/10.1002/\(SICI\)1096-9861\(19990802\)410:3<503::AID-CNE11>3.0.CO;2-H](https://doi.org/10.1002/(SICI)1096-9861(19990802)410:3<503::AID-CNE11>3.0.CO;2-H)
64. Bonfanti, L. PSA-NCAM in mammalian structural plasticity and neurogenesis. *Prog. Neurobiol.* **80**, 129-164 (2006). <https://doi.org/10.1016/j.pneurobio.2006.08.003>
65. Ambrogini, P. et al. Morpho-functional characterization of neuronal cells at different stages of maturation in granule cell layer of adult rat dentate gyrus. *Brain Res. J.* **1017**, 21-31 (2004). <https://doi.org/10.1016/j.brainres.2004.05.039>
66. Mongiat, L. A., Espósito, M. S., Lombardi, G. & Schinder, A. F. Reliable activation of immature neurons in the adult hippocampus. *PLoS One* **4**, e5320 (2009). <https://doi.org/10.1371/journal.pone.0005320>
67. Marín-Burgin, A., Mongiat, L. A., Pardi, M. B. & Schinder, A. F. Unique processing during a period of high excitation/inhibition balance in adult-born neurons. *J. Sci.* **335**, 1238-1242 (2012). <https://doi.org/10.1126/science.1214956>
68. Aimone, J. B., Wiles, J. & Gage, F. H. Potential role for adult neurogenesis in the encoding of time in new memories. *Nat. Neurosci.* **9**, 723-727 (2006). <https://doi.org/10.1038/nn1707>
69. Schmidt-Hieber, C., Jonas, P. & Bischofberger, J. Enhanced synaptic plasticity in newly generated granule cells of the adult hippocampus. *Nature* **429**, 184-187 (2004). <https://doi.org/10.1038/nature02553>
70. Kempermann, G., Kuhn, H. G. & Gage, F. H. Experience-induced neurogenesis in the senescent dentate gyrus. *J. Neurosci.* **18**, 3206-3212 (1998). <https://doi.org/10.1523/JNEUROSCI.18-09-03206>
71. Lee, S. W., Clemenson, G. D. & Gage, F. H. New neurons in an aged brain. *Behav. Brain Res.* **227**, 497-507 (2012). <https://doi.org/10.1016/j.bbr.2011.10.009>
72. Nada, M.-B., Slomianka, L., Vyssotski, A. L. & Lipp, H.-P. Early age-related changes in adult hippocampal neurogenesis in C57 mice. *Neurobiol. Aging* **31**, 151-161 (2010). <https://doi.org/10.1016/j.neurobiolaging.2008.03.002>
73. Amrein, I., Slomianka, L., Poletaeva, I. I., Bologova, N. V. & Lipp, H. P. Marked species and age-dependent differences in cell proliferation and neurogenesis in the hippocampus of wild-living rodents. *Hippocampus* **14**, 1000-1010 (2004). <https://doi.org/10.1002/hipo.20018>
74. Shors, T. J. et al. Neurogenesis in the adult is involved in the formation of trace memories. *Nature* **410**, 372-376 (2001). <https://doi.org/10.1038/35066584>
75. Imayoshi, I. et al. Roles of continuous neurogenesis in the structural and functional integrity of the adult forebrain. *J. Neurosci.* **11**, 1153-1161 (2008). <https://doi.org/10.1038/nn.2185>
76. Van Praag, H., Shubert, T., Zhao, C. & Gage, F. H. Exercise enhances learning and hippocampal neurogenesis in aged mice. *J. Neurosci.* **25**, 8680-8685 (2005). <https://doi.org/10.1523/JNEUROSCI.1731-05.2005>
77. Gould, E., Reeves, A. J., Graziano, M. S. & Gross, C. G. Neurogenesis in the neocortex of adult primates. *Science* **286**, 548-552 (1999). <https://doi.org/10.1126/science.286.5439.548>
78. Sahay, A. & Hen, R. Adult hippocampal neurogenesis in depression. *Nat. Neurosci.* **10**, 1110-1115 (2007). <https://doi.org/10.1038/nn1969>
79. Negredo, P. N., Yeo, R. W. & Brunet, A. Aging and rejuvenation of neural stem cells and their niches. *Cell Stem Cell* **27**, 202-223 (2020). <https://doi.org/10.1016/j.stem.2020.07.002>
80. Mathern, G. W. et al. Seizures decrease postnatal neurogenesis and granule cell development in the Human Fascia Dentata. *Epilepsia* **43**, 68-73 (2002). <https://doi.org/10.1046/j.1528-1157.43.s.5.28.x>

81. Mikkonen, M. et al. Remodeling of neuronal circuitries in human temporal lobe epilepsy: increased expression of highly polysialylated neural cell adhesion molecule in the hippocampus and the entorhinal cortex. *Ann. Neurol.* **44**, 923-934 (1998). <https://doi.org/10.1002/ana.410440611>
82. Gu, H., Wang, S., Messam, C. A. & Yao, Z. Distribution of nestin immunoreactivity in the normal adult human forebrain. *Brain Res.* **943**, 174-180 (2002). [https://doi.org/10.1016/S0006-8993\(02\)02615-X](https://doi.org/10.1016/S0006-8993(02)02615-X)
83. Ní Dhúill, C. M. et al. Polysialylated neural cell adhesion molecule expression in the dentate gyrus of the human hippocampal formation from infancy to old age. *J. Neurosci.* **55**, 99-106 (1999). [https://doi.org/10.1002/\(SICI\)1097-4547\(19990101\)55:1<99::AID-JNR11>3.0.CO;2-S](https://doi.org/10.1002/(SICI)1097-4547(19990101)55:1<99::AID-JNR11>3.0.CO;2-S)
84. Flor-Garcia, M. et al. Unraveling human adult hippocampal neurogenesis. *Nat.* **15**, 668-693 (2020). <https://doi.org/10.1038/s41596-019-0267-y>
85. Knoth, R. et al. Murine features of neurogenesis in the human hippocampus across the lifespan from 0 to 100 years. *PLoS One* **5**, e8809 (2010). <https://doi.org/10.1371/journal.pone.0008809>
86. Leuner, B., Kozorovitskiy, Y., Gross, C. G. & Gould, E. Diminished adult neurogenesis in the marmoset brain precedes old age. *Proc. Natl. Acad. Sci.* **104**, 17169-17173 (2007). <https://doi.org/10.1073/pnas.0708228104>
87. Aizawa, K., Ageyama, N., Yokoyama, C. & Hisatsune, T. Age-dependent alteration in hippocampal neurogenesis correlates with learning performance of macaque monkeys. *Exp. Anim.* **58**, 403-407 (2009). <https://doi.org/10.1538/expanim.58.403>
88. Ngwenya, L. B., Heyworth, N. C., Shwe, Y., Moore, T. L. & Rosene, D. L. Age-related changes in dentate gyrus cell numbers, neurogenesis, and associations with cognitive impairments in the rhesus monkey. *Front. Neurosci.* **9**, 102 (2015). <https://doi.org/10.3389/fnins.2015.00102>
89. Spalding, K. L. et al. Dynamics of hippocampal neurogenesis in adult humans. *Cell* **153**, 1219-1227 (2013). <https://doi.org/10.1016/j.cell.2013.05.002>
90. Dennis, C., Suh, L., Rodriguez, M., Kril, J. & Sutherland, G. Human adult neurogenesis across the ages: an immunohistochemical study. *Neuropathol. Appl. Neurobiol.* **42**, 621-638 (2016). <https://doi.org/10.1111/nan.12337>
91. Kempermann, G. et al. Human adult neurogenesis: evidence and remaining questions. *Cell Stem Cell* **23**, 25-30 (2018). <https://doi.org/10.1016/j.stem.2018.04.004>
92. Snyder, J. S. Recalibrating the relevance of adult neurogenesis. *Trends in Neurosci.* **42**, 164-178 (2019). <https://doi.org/10.1016/j.tins.2018.12.001>
93. Tobin, M. K. et al. Human hippocampal neurogenesis persists in aged adults and Alzheimer's disease patients. *Cell Stem Cell* **24**, 974-982.e3 (2019). <https://doi.org/10.1016/j.stem.2019.05.003>
94. Cipriani, S. et al. Hippocampal radial glial subtypes and their neurogenic potential in human fetuses and healthy and Alzheimer's disease adults. *Cereb. Cortex* **28**, 2458-2478 (2018). <https://doi.org/10.1093/cercor/bhy096>
95. Darmanis, S. et al. A survey of human brain transcriptome diversity at the single cell level. *Proc. Natl. Acad. Sci.* **112**, 7285-7290 (2015). <https://doi.org/10.1073/pnas.1507125112>
96. Thomsen, E. R. et al. Fixed single-cell transcriptomic characterization of human radial glial diversity. *Nat. Methods* **13**, 87-93 (2016). <https://doi.org/10.1038/nmeth.3629>
97. Fan, X. et al. Spatial transcriptomic survey of human embryonic cerebral cortex by single-cell RNA-seq analysis. *Cell Res.* **28**, 730-745 (2018). <https://doi.org/10.1038/s41422-018-0053-3>
98. Frey, B. N. et al. The role of hippocampus in the pathophysiology of bipolar disorder. *Behav. Pharmacol.* **18**, 419-430 (2007). <https://doi.org/10.1097/fbp.0b013e3282df3cde>
99. Hajek, T. et al. Hippocampal volumes in bipolar disorders: opposing effects of illness burden and lithium treatment. *Bipolar Disord.* **14**, 261-270 (2012). <https://doi.org/10.1111/j.1399-5618.2012.01013.x>
100. Malykhin, N. V., Carter, R., Seres, P. & Coupland, N. J. Structural changes in the hippocampus in major depressive disorder: contributions of disease and treatment. *J. Psychiatry Neurosci.* **35**, 337-343 (2010). <https://doi.org/10.1503/jpn.100002>
101. Walton, N. et al. Detection of an immature dentate gyrus feature in human schizophrenia/bipolar patients. *Transl. psychiatry* **2**, e135-e135 (2012). <https://doi.org/10.1038/tp.2012.56>
102. Reif, A. et al. Neural stem cell proliferation is decreased in schizophrenia, but not in depression. *Mol. psychiatry* **11**, 514-522 (2006). <https://doi.org/10.1038/sj.mp.4001791>
103. Lucassen, P. J., Stumpel, M. W., Wang, Q. & Aronica, E. Decreased numbers of progenitor cells but no response to antidepressant drugs in the hippocampus of elderly depressed patients. *Neuropharmacology* **58**, 940-949 (2010). <https://doi.org/10.1016/j.neuropharm.2010.01.012>
104. Sachs, G. S. Bipolar mood disorder: practical strategies for acute and maintenance phase treatment. *J. Clin. Psychopharmacol.* **16**, 32S-47S (1996). <https://doi.org/10.1097/00004714-199604001-00005>
105. Duval, F., Lebowitz, B. D. & Macher, J.-P. Treatments in depression. *Dialogues Clin. Neurosci.* (2022) **8**, 191-206 <https://doi.org/10.31887/DCNS.2006.8.2/fduval>
106. Boldrini, M. et al. Hippocampal angiogenesis and progenitor cell proliferation are increased with antidepressant use in major depression. *Biol. Psychiatry* **72**, 562-571 (2012). <https://doi.org/10.1016/j.biopsych.2012.04.024>
107. Boldrini, M. et al. Antidepressants increase neural progenitor cells in the human hippocampus. *Neuropsychopharmacology* **34**, 2376-2389 (2009). <https://doi.org/10.1038/npp.2009.75>
108. Warner-Schmidt, J. L. & Duman, R. S. Hippocampal neurogenesis: opposing effects of stress and antidepressant treatment. *Hippocampus* **16**, 239-249 (2006). <https://doi.org/10.1002/hipo.20156>
109. Malberg, J. E., Eisch, A. J., Nestler, E. J. & Duman, R. S. Chronic antidepressant treatment increases neurogenesis in adult rat hippocampus. *J. Neurosci.* **20**, 9104-9110 (2000). <https://doi.org/10.1523/JNEUROSCI.20-24-09104.2000>
110. Colle, R. et al. Smaller hippocampal volumes predict lower antidepressant response/remission rates in depressed patients: A meta-analysis. *World J. Biol. Psychiatry* **19**, 360-367 (2018). <https://doi.org/10.1080/15622975.2016.1208840>
111. Carreno, F. et al. Activation of a ventral hippocampus-medial prefrontal cortex pathway is both necessary and sufficient for an antidepressant response to ketamine. *Mol. psychiatry* **21**, 1298-1308 (2016). <https://doi.org/10.1038/mp.2015.176>
112. Jahn, H. Memory loss in Alzheimer's disease. *Dialogues Clin. Neurosci.* **15**, 445-454 (2022). <https://doi.org/10.31887/DCNS.2013.15.4/hjahn>
113. Halliday, G. Pathology and hippocampal atrophy in Alzheimer's disease. *Lancet Neurol.* **16**, 862-864 (2017). <https://doi.org/10.1016/S1474->

114. Gomez-Nicola, D. et al. Temporal dynamics of hippocampal neurogenesis in chronic neurodegeneration. *Brain* **137**, 2312-2328 (2014). <https://doi.org/10.1093/brain/awu155>
115. Lovell, M. A., Geiger, H., Van Zant, G. E., Lynn, B. C. & Markesbery, W. R. Isolation of neural precursor cells from Alzheimer's disease and aged control postmortem brain. *Neurobiol. Aging* **27**, 909-917 (2006). <https://doi.org/10.1016/j.neurobiolaging.2005.05.004>
116. Ziabreva, I. et al. Altered neurogenesis in Alzheimer's disease. *J. Psychosom. Res.* **61**, 311-316 (2006). <https://doi.org/10.1016/j.jpsychores.2006.07.017>
117. Terreros-Roncal, J. et al. Impact of neurodegenerative diseases on human adult hippocampal neurogenesis. *Science* **374**, 1106-1113 (2021). <https://doi.org/10.1126/science.abl5163>
118. Essa, H., Peyton, L., Hasan, W., León, B. E. & Choi, D.-S. Implication of Adult Hippocampal Neurogenesis in Alzheimer's Disease and Potential Therapeutic Approaches. *Cells* **11**, 286 (2022). <https://doi.org/10.3390/cells11020286>
119. Wadhwa, M. et al. Inhibiting the microglia activation improves the spatial memory and adult neurogenesis in rat hippocampus during 48 h of sleep deprivation. *J. Neuroinflammation* **14**, 1-18 (2017). <https://doi.org/10.1186/s12974-017-0998-z>
120. Lue, L.-F., Walker, D. G. & Rogers, J. Modeling microglial activation in Alzheimer's disease with human postmortem microglial cultures. *Neurobiol. Aging* **22**, 945-956 (2001). [https://doi.org/10.1016/S0197-4580\(01\)00311-6](https://doi.org/10.1016/S0197-4580(01)00311-6)
121. Kohman, R. A., Bhattacharya, T. K., Kilby, C., Bucko, P. & Rhodes, J. S. Effects of minocycline on spatial learning, hippocampal neurogenesis and microglia in aged and adult mice. *Behav. Brain Res.* **242**, 17-24 (2013). <https://doi.org/10.1016/j.bbr.2012.12.032>
122. Chakrabarti, M. et al. Molecular signaling mechanisms of natural and synthetic retinoids for inhibition of pathogenesis in Alzheimer's disease. *J. Alzheimer's Dis.* **50**, 335-352 (2016). <https://doi.org/10.3233/JAD-150450>
123. Ding, Y. et al. Retinoic acid attenuates β -amyloid deposition and rescues memory deficits in an Alzheimer's disease transgenic mouse model. *J. Neurosci.* **28**, 11622-11634 (2008). <https://doi.org/10.1523/JNEUROSCI.3153-08.2008>
124. Huang, T.-T., Zou, Y. & Corniola, R. Oxidative stress and adult neurogenesis--effects of radiation and superoxide dismutase deficiency. *Semin Cell Dev. Biol.* **23**, 738-744 (2012). <https://doi.org/10.3390/cells12010061>
125. Rego, A. C. & Oliveira, C. R. Mitochondrial dysfunction and reactive oxygen species in excitotoxicity and apoptosis: implications for the pathogenesis of neurodegenerative diseases. *Neurochem. Res.* **28**, 1563-1574 (2003). <https://doi.org/10.1023/A:1025682611389>
126. Wang, X. et al. Oxidative stress and mitochondrial dysfunction in Alzheimer's disease. *Biochim. Biophys. Acta.* **1842**, 1240-1247 (2014). <https://doi.org/10.1016/j.bbadis.2013.10.015>
127. Montiel, T., Quiroz-Baez, R., Massieu, L. & Arias, C. Role of oxidative stress on β -amyloid neurotoxicity elicited during impairment of energy metabolism in the hippocampus: protection by antioxidants. *Exp. Neurol.* **200**, 496-508 (2006). <https://doi.org/10.1016/j.expneurol.2006.02.126>
128. Traber, M. G. & Atkinson, J. Vitamin E, antioxidant and nothing more. *Free Radic. Biol. Med.* **43**, 4-15 (2007). <https://doi.org/10.1016/j.freeradbiomed.2007.03.024>
129. Devore, E. E. et al. Dietary antioxidants and long-term risk of dementia. *Arch. Neurol.* **67**, 819-825 (2010). <https://doi.org/10.1001/archneurol.2010.144>
130. Padayatty, S. J. et al. Vitamin C as an antioxidant: evaluation of its role in disease prevention. *J. Am. Coll. Nutr.* **22**, 18-35 (2003). <https://doi.org/10.1080/07315724.2003.10719272>
131. Li, F.-J., Shen, L. & Ji, H.-F. Dietary intakes of vitamin E, vitamin C, and β -carotene and risk of Alzheimer's disease: a meta-analysis. *J. Alzheimer's Dis.* **31**, 253-258 (2012). <https://doi.org/10.3233/JAD-2012-120349>
132. Murakami, K. et al. Vitamin C restores behavioral deficits and amyloid- β oligomerization without affecting plaque formation in a mouse model of Alzheimer's disease. *J. Alzheimer's Dis.* **26**, 7-18 (2011). <https://doi.org/10.3233/JAD-2011-101971>
133. Ak, T. & Gülçin, İ. Antioxidant and radical scavenging properties of curcumin. *Chem. Biol. Interact.* **174**, 27-37 (2008). <https://doi.org/10.1016/j.cbi.2008.05.003>
134. Kim, G.-Y. et al. Curcumin inhibits immunostimulatory function of dendritic cells: MAPKs and translocation of NF- κ B as potential targets. *J. Immunol.* **174**, 8116-8124 (2005). <https://doi.org/10.4049/jimmunol.174.12.8116>
135. Lim, G. P. et al. The curry spice curcumin reduces oxidative damage and amyloid pathology in an Alzheimer transgenic mouse. *J. Neurosci.* **21**, 8370-8377 (2001). <https://doi.org/10.1523/JNEUROSCI.21-21-08370.2001>
136. Hamaguchi, T., Ono, K. & Yamada, M. Curcumin and Alzheimer's disease. *C.N.S. Neurosci. Ther.* **16**, 285-297 (2010). <https://doi.org/10.1111/j.1755-5949.2010.00147.x>
137. Van Praag, H., Christie, B. R., Sejnowski, T. J. & Gage, F. H. Running enhances neurogenesis, learning, and long-term potentiation in mice. *Proc. Natl. Acad. Sci.* **96**, 13427-13431 (1999). <https://doi.org/10.1073/pnas.96.23.13427>
138. Van Praag, H., Kempermann, G. & Gage, F. H. Running increases cell proliferation and neurogenesis in the adult mouse dentate gyrus. *Nat. Neurosci.* **2**, 266-270 (1999). <https://doi.org/10.1038/6368>
139. Liu, P. Z. & Nusslock, R. Exercise-mediated neurogenesis in the hippocampus via BDNF. *Front. Neurosci.* **12**, 52 (2018). <https://doi.org/10.3389/fnins.2018.00052>
140. Choi, S. H. et al. Combined adult neurogenesis and BDNF mimic exercise effects on cognition in an Alzheimer's mouse model. *Science* **361**, eaan8821 (2018). <https://doi.org/10.1126/science.aan8821>
141. Ibrahim, M. M. & Gabr, M. T. Multitarget therapeutic strategies for Alzheimer's disease. *Neura. Regen. Res.* **14**, 437 (2019). <https://doi.org/10.4103/1673-5374.245463>
142. Neuner, S. M., Heuer, S. E., Huentelman, M. J., O'Connell, K. M. & Kaczorowski, C. C. Harnessing genetic complexity to enhance translatability of Alzheimer's disease mouse models: a path toward precision medicine. *Neuron* **101**, 399-411.e5 (2019). <https://doi.org/10.1016/j.neuron.2018.11.040>
143. Wang, F. et al. RNAscope: a novel in situ RNA analysis platform for formalin-fixed, paraffin-embedded tissues. *J. Mol. Diagn.* **14**, 22-29 (2012). <https://doi.org/10.1016/j.jmoldx.2011.08.002>

